THE TIME-COURSE OF PERCEPTUAL DECISION-MAKING: TEMPORAL AND SPATIAL DYNAMICS OF SCALP-RECORDED OSCILLATORY PHASE AND AMPLITUDE

Francisco J. Parada

Submitted to the Faculty of the University Graduate School

in partial fulfillment of the requirements for the degree

Doctor of Philosophy

in the Department of Psychological & Brain Sciences

and the Program in Neuroscience

Indiana University

September 2014

Accepted by the Graduate Faculty, Indiana University, in partial fulfillment of the requirements for the degree of Doctor of Philosophy

Doctoral Committee

Professor Thomas Busey, Ph.D.

Professor Olaf Sporns, Ph.D.

Professor Aina Puce, Ph.D.

Professor Bennett Bertenthal, Ph.D.

Professor Robert Nosofsky, Ph.D.

Date of dissertation defense:

June 19th 2014

Acknowledgments

Probable things pass in front of our eyes without us even noticing, they compose most of our daily lives. Improbable things are remembered and commented for years to come as the odd event they are. Impossible things sometimes happen; rare fruits, ripened by time, and sweetened by the wonderful flavors of ordinary day-by-day routine.

This dissertation is a very small seed of a very strange fruit.

The fruit has been ripened by time well spent with my partner Alejandra; my parents Raquel and Eduardo; my brothers Christian and José; my aunts Marcela and Teresa; my grandparents Fresia and José; my academic advisors and professors Tom, Olaf, Aina, Oriana, Jorge, Nelson, Pedro, Pancho; and all of my extended family composed of my friends. The fruit has been sweetened by the fact that I would have not been able to do anything without their support and their love. If my life were worth something, it would only be because all these wonderful people surround me.

Francisco J. Parada

THE TIME-COURSE OF PERCEPTUAL DECISION-MAKING:

TEMPORAL AND SPATIAL DYNAMICS OF SCALP-RECORDED OSCILLATORY PHASE AND AMPLITUDE

In natural conditions the brain has to actively integrate information about the current percept with information about past/present behavioral demands and cognitive states of the observer along with future outcomes related to a decision. Despite of somewhat extensive research, we still know little about the neuro-cognitive mechanisms and temporal dynamics allowing an observer to perceive an object and rapidly make a decision about it.

This dissertation is based on previous research suggesting that there must be at least two cognitive processes underlying a task such as perceptual decision-making. An early mechanism related to the perception of information and a later one related to the subsequent decision-making process. Evidence has led to the proposal of the match-and-utilization model, stating that early synchronization in the gamma band is the result of a match between the current percept and memory/attentional processes. In contrast, later synchronization would reflect the utilization/readout of the early matching process; updating or influencing future processes.

Evidence for this two-stage process, comes mainly from the classic event-related potential literature and, in lesser degree, from newer measures such as oscillatory amplitude. Moreover, the exploration of multivariate nonlinear techniques derived from the study of synchronization between and within neural systems, has been largely

neglected in the literature. Thus, explorations of a more complete electrophysiological picture than the one provided by ERP or ERSP analyses alone, can provide us more information about the relation between neural oscillations and ERP components as electrophysiological markers of cognitive events. This is important because differential roles for frequency, phase, and amplitude as different information coding strategies in neural systems have been theoretically suggested and empirically shown. The present work presents for the first time, concomitant analyses of phase and amplitude dynamics in the context of perceptual decision-making.

In this dissertation I present a parametrical task that can effectively separate the visual properties of the stimuli from the decision regarding the task at hand. Results indicate that the experimental design effectively separated stimulus properties from task demands. Additionally, I suggest distinct roles for the temporal dynamics of gamma-band oscillations. Finally, a central role for alpha oscillations is suggested.

Table of Contents

Index of Figures

Glossary

ERP:	Event-Related Potential. 1-D measure of mean potential differences from a predetermined baseline (e.g. pre-stimulus onset, button press)
ERSP:	Event-Related Spectral Power. Mean change in oscillatory amplitude power (i.e. spectral power) from baseline (e.g. pre-stimulus onset, button press)
ITPC:	Inter-Trial Phase Clustering. Event-related phase consistency across trials measured at 1 sensor. In the literature this measure has also been called inter-trial coherence [ITC], inter-trial phase-coherence [ITPC], phase-locking factor [PLF], and phase-locking
ISPC:	Inter-Site Phase Clustering. Event-related phase consistency across trials measured between 2 sensors. In the literature this measure has also been called phase-coherence, coherence, phase-locking value (PLV), and phase synchrony
ERPAC:	Event-Related Phase-amplitude Coupling. Within- and/or between-sensors measure of modulation of a target amplitude by a source phase across trials

1. Introduction

A decision is a purposeful process whose result is the transient engagement to a categorical proposition. In order to make a decision, specific sensory information must be collected from the environment and used to guide behavior. The process of mapping perceptual states onto goal-directed actions is known as perceptual decision-making (Gold & Shadlen, 2007; Smith & Ratcliff, 2004).

Our everyday lives are composed of an immeasurable number of decisions. Imagine taking a leisure walk in a park during spring on a quiet Sunday afternoon. There are no cars around and the weather is optimal. We could say that the demands of this task are low. You can allocate most of your attention into enjoying the blue sky above you and the soft breeze.

However, the situation could be very different. Imagine that you have travelled to Paris for work reasons. This is your first time in France and you do not speak French. You are staying in a hotel in a busy location, Marx Dormoy. You have an important meeting in Montmartre in a couple of hours. You start walking west on Boulebard de la Chapelle, a chaotic street full of cars, cabs, buses, and other people. You need to find the place of your meeting and keep track of time while navigating through the crowded street. Without being able to ask for directions and avoiding possible threats such as cars you realize that in contrast to taking a leisure walk on the park, this is a very demanding task. Attentional resources must be allocated to task-relevant information such as street

names[1]. You must also keep track of important task-irrelevant information, such as cars and other people. All of these processes have to be orchestrated in such a manner that useful task-relevant information will be available to adaptively coordinate behavior in time: Should you cross the street now? Should you turn left in the next intersection?

During adaptive goal-directed behavior, perceptual and cognitive states are flexibly mapped onto motor plans (Gold & Shadlen, 2007). Historically, psychologists have studied these processes using reaction times (Cartwright & Festinger, 1943). Reaction times are a compound measure including multiple factors such as stimulus processing, memory retrieval and encoding, attention allocation/relocation, decision-making, response selection, and response execution (Donkin, Brown, & Heathcote, 2009; Smith & Ratcliff, 2004). Cognitive electrophysiology can add new vistas and insights into the processes leading towards perceptual decisions. Cognitive electrophysiology can help "unpack" reaction time and provide an insight onto the temporal dynamics and neurobiological mechanisms underlying decisions. The goal of this dissertation is to implement a systematic semi-exploratory approach to study the time-course of perceptual decision-making using electroencephalogram (EEG) in healthy human population.

1.1 Mapping perceptual states onto behavior

Adaptive goal-directed behavior is characterized by flexibility; it is the trademark of behavior of every single living species (Allen & Bekoff, 1997; Maturana & Varela, 1984; F. J. Varela, Thompson, & Rosch, 1991). Behavioral flexibility emerges from the dynamic integration of multiple cognitive processes in tight functional coupling with the

[1] Which will be hard to encode because they are written in French

environment (Maturana & Varela, 1984; F. J. Varela et al., 1991). Thus, every single autonomous agent has to (i) sense the environment with a sampling rate appropriate to the scale of its environment[2], (ii) process the information provided by the senses at a rate appropriate to the sampling rate of the senses, (iii) integrate the processed information at a rate appropriate to the autonomous agent's spontaneous ongoing activity, and (iv) generate adequate sensorimotor adjustments at a rate appropriate to the scale of its environment (Baars & Franklin, 2007; Freeman, 2002; Halgren, Boujon, Clarke, Wang, & Chauvel, 2002; Maturana & Varela, 1984; F. J. Varela et al., 1991). Cognition emerges from these different timescales. Furthermore, the interaction between timescales can be described as cycles. These cycles are reflected in the periodicity of brain functioning (see 2. Exploring Cognitive Dynamics Using Scalp-Recorded Neural Signals).

Thus, I think moment-to-moment sensorimotor adjustments defining decision-making emerge from processes operating at different timescales. This is observed in the characteristic flexibility of behavior. Therefore, for an autonomous agent the interpretation of a certain environmental event as described by its senses will depend not only on the nature of the event, but also on the agent's current behavioral and cognitive states (Maturana & Varela, 1984; F. J. Varela et al., 1991). In other words, depending on the state of the system and the current behavioral demands, the exact same sensory input can be utilized to adjust different sensorimotor patterns or update different cognitive representations.

[2] Environments can be defined at different scales: microscopic, mesoscopic, or macroscopic. At each scale a different number of interacting entities will be found. These can range from particles to cells to organisms to other agents. Each scale will have its own intrinsic dynamics that are most probably nested and functionally engaged by local-to-global and global-to-local causation (Kelso, 1995) between each other but rarely encounter one another in a direct manner

Neurobiological models explaining the implementation of such flexibility can be summarized by two ideas: First, a "central controller" anatomically localized in anterior brain regions[3] using top-down influences selectively bias the acquisition and processing of information in a task-dependent manner (Corbetta & Shulman, 2002; E. K. Miller & Cohen, 2001). Second, recurrent and transient feedback and feedforward loops integrate sensory information with previous task-relevant knowledge (Bar, 2003; Engel, Fries, & Singer, 2001)[4].

In this dissertation, I will base my work on two existing models of information acquisition and utilization in the brain; the memory match and utilization model (C. S. Herrmann, Munk, & Engel, 2004) and the top-down facilitation model (Bar, 2003). These two models, although complementary have not encountered a converging point at empirical and/or theoretical levels. I will use these models in the same context and moreover link them to perceptual judgments with the purpose of exploring the time-course of perceptual decision-making.

1.2 Flexible perceptual decisions

As mentioned earlier, in natural conditions, the brain has to actively integrate information about the current percept (e.g. physical properties of the stimuli) with

[3] Usually the prefrontal and posterior parietal cortices (Corbetta & Shulman, 2002; E. K. Miller & Cohen, 2001)

[4] I find myself conceptually closer to the second kind of models; understanding decision-making not only as a neurobiological but also as systemic process (Bertalanffy, 1968; Maturana & Varela, 1984; F. J. Varela et al., 1991). Therefore, I think that the flexible mapping of perceptual states onto adaptive behavior mostly depends on the temporal dynamics within and between widely distributed neuronal populations. More specifically, I think that neural activity at different timescales flexibly regulates the interaction within and between neuronal populations underlying perceptual decision-making

information about past/present behavioral demands and cognitive states of the observer (e.g. instruction or task at hand) along with future outcomes related to the decision.

Despite of the somewhat extensive amount of research on the subject, we still know little about the neuro-cognitive mechanisms and their temporal dynamics that allow an observer to perceive an object and rapidly make a decision about it (Gold & Shadlen, 2007; Smith & Ratcliff, 2004). Previous literature suggests that there must be at least two cognitive processes underlying tasks such as perceptual decision-making: an early process related to the perception of information and a later one related to the subsequent decision-making process (Busch, Herrmann, Muller, Lenz, & Gruber, 2006; Busch, Schadow, Frund, & Herrmann, 2006; C. S. Herrmann, Lenz, Junge, Busch, & Maess, 2004; C. S. Herrmann, Munk, et al., 2004; Philiastides, Ratcliff, & Sajda, 2006; Philiastides & Sajda, 2007; VanRullen & Thorpe, 2001). Evidence from this two-stage process can be found in different EEG studies of healthy human participants.

1.2.1 The time-course of perception

An early negative ERP component peaking around 170 ms post-stimulus onset has been linked to perception of the object of relevance for the decision. Importantly, the N1 ERP component has been found weakly associated with the prediction of task errors (Philiastides et al., 2006), thus relegating this component to be a correlate of sensory evidence gathering (Philiastides et al., 2006; Schyns, Gosselin, & Smith, 2009; VanRullen & Thorpe, 2001).

Later in time, a positive ERP component peaking after 200 ms after stimulus onset strongly correlated with the difficulty of the decision to be made by participants at

the trial-by-trial level (Philiastides et al., 2006) as well as in the grand-average responses (VanRullen & Thorpe, 2001). Therefore, a P3 ERP component has been posed as a putative signature of the link between sensory evidence gathering occurring earlier (~170 ms) and the participant's later decision (~300 ms).

Importantly, in this context, P3 could be an electrophysiological marker of the accumulation of: prior cognitive states, current perceptual evidence, and/or future decision-related outcomes. Particularly, these outcomes can either reflect the actual decision or announce the commitment to a particular decision-to-be-made. However, the ERP signal alone cannot give us a complete idea of its functional nature. This is due to how ERPs are computed. Due to the process of averaging, any signal that is not time-locked to the event of interest will be lost in the average. Moreover, most ERP researchers filter their signals with a 30 or 40 Hz low-pass filter. This means that any signal in the gamma range (>30 Hz) will be regarded as noise and discarded. Thus, ERP measure is an important, nevertheless, limited measure of brain activity (see Event Related Potentials (ERP)).

1.2.2 The matching and utilization model (MUM)

Herrmann and colleagues posed a model of information match and utilization (MUM) based on empirical findings (C. S. Herrmann, Munk, et al., 2004). This model suggests that neural oscillations in the gamma band (>30 Hz), measured by event-related spectral perturbation (ERSP), reflect a twofold mechanism of perception (Figure 1). Early gamma-band response (GBR), peaking around 100 ms post-stimulus onset, might be a signature of the comparison and matching between incoming sensory information and a

memory-stored representation (Busch, Herrmann, et al., 2006; Busch, Schadow, et al., 2006). Later in time, around 300 ms post-stimulus onset, another GBR could be a signature of the usage of the result of the first operation (~100 ms) to store new items, evoke old stored representations, and/or integrate information in large-scale networks (C. S. Herrmann, Munk, et al., 2004).

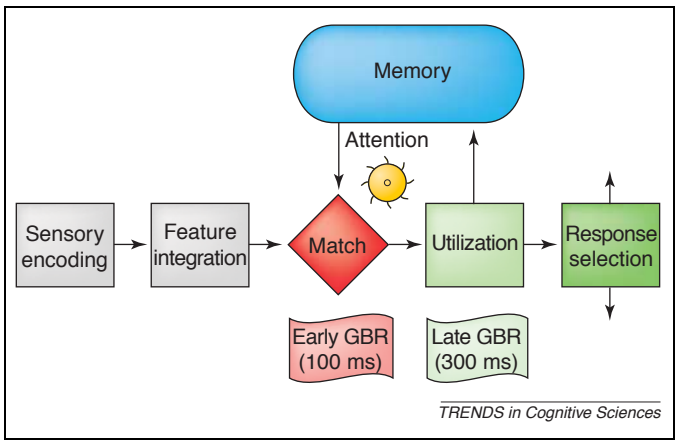

Figure 1 – Schematic representation of the memory match and utilization model (MUM). After sensory encoding and feature integration processes occurring early in visual perception a "matching" process occur. Information stored in memory is matched against the current percept. This matching process is reflected by an "early" high-frequency spectral component in the gamma band (early GBR) occurring at ~100 ms. In the period comprised after the matching, attentional processes are allocated/relocated and items are stored in memory as needed. Furthermore, a "utilization" process occurs around 300 ms. The "utilization" is evidenced by a "late" high-frequency spectral component in the gamma band (late GBR) occurring at ~300 ms. The "utilization refers to the usage of the preceding processes in order to adjust behavior. Taken from (C. S. Herrmann, Munk, et al., 2004)

Previous research has not approached the functional or physiological relation between gamma-band activity and ERP components in the context of visual information acquisition/utilization. Furthermore, the MUM model makes no reference to ERPs. However, it has been shown that visual ERP components may result from changes in phase and amplitude dynamics across different scalp locations and at different

frequencies in a highly task-dependent fashion[5] (Makeig, Debener, Onton, & Delorme, 2004; Makeig et al., 2002). Moreover, it has been shown that phase dynamics code for more information than power alone, suggesting that phase-related measures could be a complementary, and sometimes a more accurate reflection of brain function (Schyns, Thut, & Gross, 2011; F. Varela, Lachaux, Rodriguez, & Martinerie, 2001). However, the MUM model does not address the role of phase dynamics in perception. Importantly no study has explored concomitant phase and amplitude dynamics in the context of information acquisition/utilization for decisions. To the best of my knowledge, the presented work is the first study to concomitantly explore the functional role of phase and amplitude dynamics in the context of perceptual decision-making.

1.2.3 The top-down facilitation model (TDF) of visual recognition

Similar to the match and utilization model (C. S. Herrmann, Munk, et al., 2004), Bar (Bar, 2003, 2004, 2007, 2009; Bar et al., 2006) has posed a model proposing that early visual processing rapidly transmits coarse information about the world to frontal areas[6], allowing the brain to use past experiences and learned statistical regularities of the world to generate "hypotheses" on what the object might be or how it could be used (Bar, 2009). In this model (Figure 2), orbitofrontal cortex (OFC) would be functionally connected to the occipital cortex, back-projecting information about the identity/usage of the objects of current perception via top-down facilitation (Bar et al., 2006).

[5] Central and lateral posterior α along with frontal midline theta (4 – 8 Hz) rhythms in visual selective attention tasks

[6] Specifically to orbito-frontal cortex, OFC

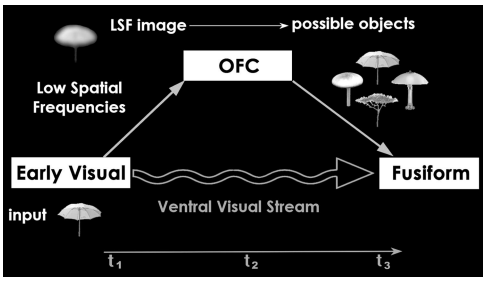

Figure 2 – Top-down facilitation model. Feedback and feedforward projections between occipital and frontal areas would facilitate perception in a flexible context-dependent manner. Taken from (Bar et al., 2006)

To the best of my knowledge, the work by Bar and colleagues (2006) has been the only one to deal with temporal dynamics in the context of the top-down facilitation model (TDF) of visual recognition. Moreover, although complementary, MUM (C. S. Herrmann, Munk, et al., 2004) and the TDF model of visual recognition (Bar, 2003) have been considered as separate and have not been empirically or theoretically related to one another yet.

1.2.4 Linking models

Considering the lack of uniformity and theoretical congruency of the aforementioned models, linking this literature together in the context of perceptual decision-making is not straightforward. Neither of these two models has been related to ERP components in the context of acquisition/utilization of information. Moreover, ERP components in general have been linked to a plethora of other processes that go far beyond simple sensory information acquisition (e.g. processing of emotional face expressions, Blau, Maurer, Tottenham, & McCandliss, 2007). Likewise, evoked and induced gamma-band oscillatory activity has been experimentally associated to a wide

range of cognitive and neural processing, sprouting several functional interpretations that range from a specific perceptual binding mechanism to a more general signature of local computation (Fries, 2009; Merker, 2013; Tallon-Baudry & Bertrand, 1999; Uhlhaas, Pipa, Neuenschwander, Wibral, & Singer, 2011). Hence, interpreting changes in measures of neural activity in the light of certain cognitive processes is not a simple task. To facilitate interpretation and analyses, a linear model along with a systematic analysis approach is used in this dissertation (see 2.4 Linear Modeling of EEG Measures and Analyzing Temporal Dynamics with a Systematic Approach).

Changes in neural activity can be found in studies where specific experimental manipulations are implemented, yet no behavioral effects are seen. Drawing meaningful interpretations from data obtained from experiments as such is not a straightforward task either (e.g. Wilkinson & Halligan, 2003). However, this is not something that only happens in decision-related experimental paradigms. Scientists have been challenged to understand the meaning of neural signals in cognition in language research (e.g. Grossman et al., 2002), social neuroscience (e.g. Keightley et al., 2003), visual perception (e.g. Weiss, Marshall, Zilles, & Fink, 2003), memory research (e.g. Suzuki et al., 2002), and many other fields of cognitive neuroscience.

In this dissertation, I will implement a dual-task parametric design in order to separate stimuli properties from the task at hand. Furthermore, I will make use of a multi-linear regression, which will allow me to benefit from my experimental paradigm and link neural measures to the experimental manipulation and behavior (see 2.4 Linear Modeling of EEG Measures). Furthermore, several linear and non-linear measures of

brain activity will be implemented. In the following sections I will describe and discuss them in the context of this dissertation.

2. Exploring Cognitive Dynamics Using Scalp-Recorded Neural Signals

Natural phenomena are recursive, systematic, and essential for the known universe; periodicity is a natural law (Carroll, 2012). Functional periodicity[7] is an essential property in all long-term sustained systems (Suh, 2004). Furthermore, the impact of periodic phenomena on life on Earth can be seen at all scales. From the wax and wane of daylight determining circadian rhythms to the periodicity of menstrual cycles allowing sexual reproduction.

The nervous system is not different. Recurrent, periodic events are seen at all scales (Buzsáki, 2006; Fries, 2009; Gazzaniga, Ivry, & Mangun, 2013; Llinas, Ribary, Contreras, & Pedroarena, 1998; VanRullen, Busch, Drewes, & Dubois, 2011; F. Varela et al., 2001). Neurons communicate via electrochemical pulses. These pulses generate changes in the membrane potential of individual nerve cells. Membrane dynamics cause the opening and closing of membrane channels; flux of ions in and out of nerve cells is possible. Collectively from these events, dynamical variations in electrical voltages emerge. Thus, induced electrical dynamics unfold over extended temporospatial scales. Over time, the net effect of each individual neuronal spike and synapsis organized as neuronal populations gives way to the emergence of short-lived neural oscillations with characteristic frequency, phase, and amplitude (Buzsáki, 2006).

[7] Along with stable equilibrium

Recent evidence indicates that frequency, phase, and amplitude extracted from neurophysiological signals have different roles as putative information coding strategies in neural systems (Akam & Kullmann, 2010; Canolty & Knight, 2010; Fries, 2005; Makeig et al., 2004; F. Varela et al., 2001). Thus, neural communication mechanisms such as synchronization and phase coupling have recently become particularly active topics of research[8].

Scientists observe direct evidence of these complex dynamics using a wide variety of methods ranging from patch-clamp to local-field potentials (LFP) to electroencephalogram (EEG). Each one of these methods provides a small window of observation to the multidimensional space were brain dynamics unfold (Figure 3). Therefore, recorded brain signals at different spatial scales are direct observations of specific known neurobiological events (Buzsáki, 2006; Fries, 2009; Gazzaniga et al., 2013; Llinas et al., 1998; VanRullen et al., 2011; F. Varela et al., 2001).

Due to the non-linearity of neural events, their dependence on their own historicity, and the existence of feedback and feedforward loops, brain dynamics are regarded as complex (Buzsáki, 2006; Llinas et al., 1998; Maturana & Varela, 1984; Tononi, Edelman, & Sporns, 1998). Understanding complex brain dynamics requires the systematic study of the multiple operational dimensions where they unfold.

[8] Phase coupling refers to correlations between a source phase and a target oscillatory amplitude or phase separated in frequency (e.g. theta phase coupled to gamma amplitude). Whereas synchronization refers to a particular kind of phase-coupling dynamic in which separate oscillators maintain a constant phase relationship that can be measured at the level of amplitude and/or phase. Studying oscillatory brain dynamics may lead to understand how neural activity underlying the flexible nature of cognition and behavior emerges from neural ensembles or brain networks based on a relatively static structure. Furthermore exploring temporospatial connectivity dynamics using measures derived from both information (Paninski, 2003) and graph theory (O. Sporns, Chialvo, Kaiser, & Hilgetag, 2004) promises to be a fruitful approach for future research.

Over the last 25 years of cognitive electrophysiological research, a plethora of neural measures have been used in order to model and mine brain dynamics (M. X. Cohen, 2011; M. X. Cohen & Gulbinaite, 2014). In this dissertation I relied on linear and non-linear measures of brain functioning. In the following sections I will describe and discuss neural measures of temporal, spatial, and spectral dynamics of electrophysiological signals. I will start with the study of temporal dynamics (see

2.1 Neural Dynamics in the Time Domain), followed by the study of temporal and spectral dynamics (see 2.2 Neural Dynamics in the Time-Frequency Domain). Finally, I will address the study of EEG connectivity (see 2.3 Functional Connectivity Dynamics in the Time-Frequency Domain).

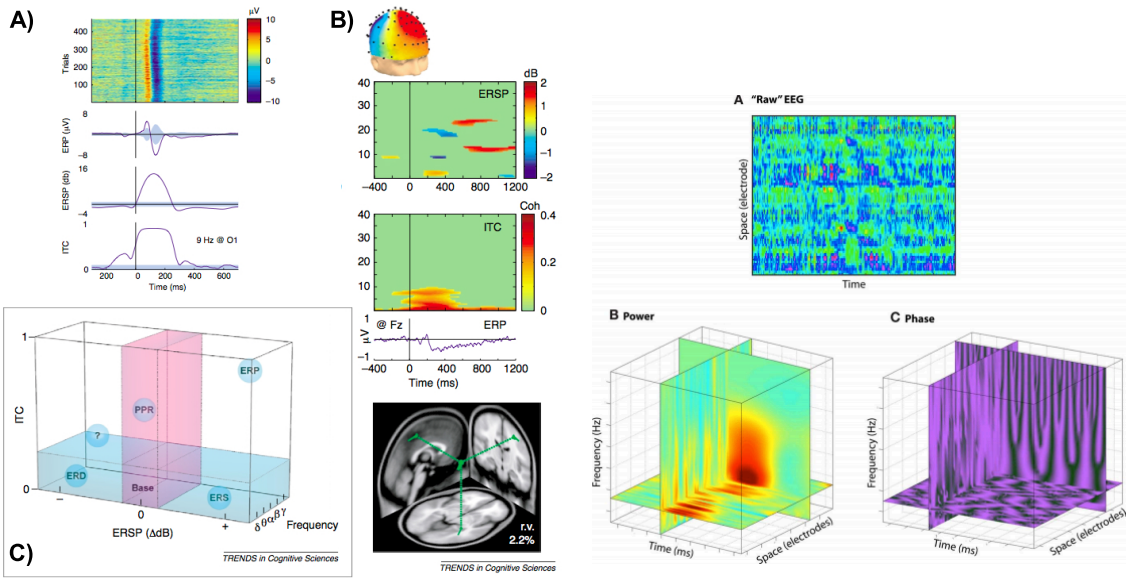

Figure 3 – Some of the dimensions of brain functioning that can be modeled using cognitive electrophysiological methods (taken from (Makeig et al., 2004) and (M. X. Cohen, 2011))

2.1 Neural Dynamics in the Time Domain

Using M/EEG, neuroscientists can measure fast, complex signals of long-range and local neural network activity. Due to these signals' multidimensionality (Figure 3), they can be used for testing hypotheses drawn from psychological and/or physiological processes. Several measures, such as microstates (Lehmann, 1971) and ERP-images (Makeig et al., 2004), have been developed in order to quantify scalp-recorded temporal dynamics. Reviewing all the relevant time-domain M/EEG analyses is beyond the scope of this dissertation. Therefore, I will focus on the event-related potential (ERP) technique; the most common analysis applied to M/EEG signals.

I will proceed to describe and discuss ERP. I will furthermore briefly discuss the physiological basis of its generation and interpretation. Finally, I will highlight its advantages and limitations as a measure of temporal brain dynamics in cognitive neuroscience research.

2.1.1 Event-Related Potentials (ERP)

ERP is the most frequently used technique for modeling scalp-recorded brain dynamics. Its success is partially due to its simplicity in computation and interpretation. ERP is widely interpreted as capturing signals evoked by sensory stimulation (Kok, 1997). It is commonly derived from the post-stimulus average across a sufficient number of condition trials. ERPs provide an account of phase-locked mean amplitude changes from baseline in μV with millisecond precision. Figure 4 depicts ERPs in contrast to the original EEG single trials that originated it. Summing all voltages at each time-point per

channel and diving by the number of trials produces an ERP waveform. ERP's robustness can be evidenced in Figure 4.

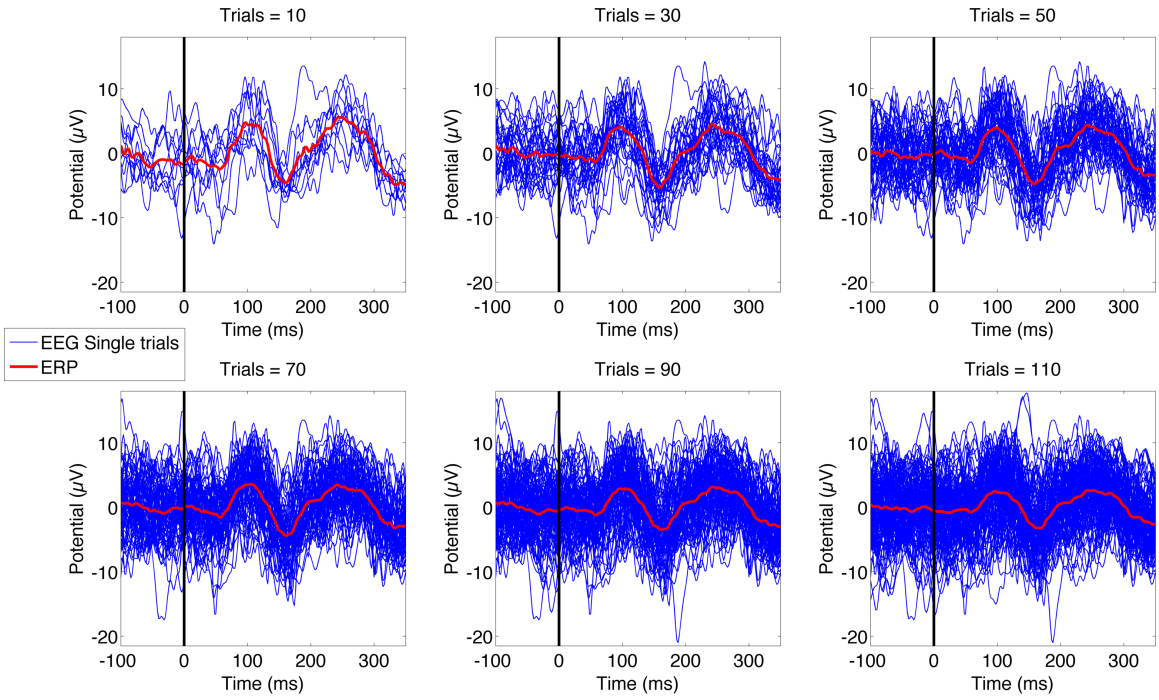

Figure 4 – ERP (red line) superimposed over an increasing number of trials (10 - 110) of ongoing EEG activity (blue lines) that originated it. Trials come from channel PO8 from a randomly selected subject. Vertical black continuous line at 0 ms represents event onset. Pre-stimulus ERP signal (red) is mostly flat, while 'evoked components' P1 (~100 ms), N1 (~170 ms), and P2 (~250 ms) can be seen in the post-stimulus ERP signal even with 10 trials (top left panel), demonstrating the robustness of the ERP measure

Generative Mechanisms and Physiological Basis of ERPs

ERP is the most widely used technique in cognitive electrophysiology. Nevertheless, its physiological basis is still an issue of ongoing debate (Makeig et al., 2004). The classic generative model of ERP assumes that ongoing EEG activity is uncorrelated noise (Figure 4, pre-stimulus blue lines). When some external event is

perceived (Figure 4, indicated by vertical black line), signals reflecting neuronal activation are evoked (Figure 4, post-stimulus red line). It is commonly thought that each evoked signal has fixed polarity and more-or-less consistent latency (Jervis, Nichols, Johnson, Allen, & Hudson, 1983). Linear summation of the signal of interest and ongoing noise occurs at the scalp (Nunez & Srinivasan, 2006); therefore, averaging techniques must be used in order to increase the signal-to-noise ratio. Once multiple trials of M/EEG activity are averaged, an ERP emerges (e.g. 100 trials used to compute ERP in Figure 4). This model of ERP generation is known in the literature as "additive" or "evoked".

In contrast to the "additive" model, an alternative physiological generative mechanism of ERPs does not consider ongoing EEG activity as noise. The "phase-reset" model assumes that ERPs are generated by a transient re-organization of the phase of ongoing EEG activity (Brandt, Jansen, & Carbonari, 1991). In other words, the ongoing oscillatory phase of the EEG would "collapse" and reset after sensory stimulation or cognitive events. Figure 5 depicts the relationship between ongoing phase and ERPs. Blue lines show the phase angle in radians of 4 Hz EEG signals for 30 randomly selected trials from channel PO8. Each blue vector in the polar plots (Figure 5 top panels) represents the phase angle of 1 trial at a particular time point. During pre-stimulus time points phase angles are somewhat uniformly distributed across the polar space (-54 ms. Figure 5, top left panel), whilst a clear clustering tendency can be seen for both post-stimulus time-points (160 and 242 ms. Figure 5, top middle and right panels). Moreover, phase angles relatively clustered near the polar axis (0 rad, around $\pi/2$ and $-\pi/2$) temporally correlate with positive ERP potentials (e.g. P1 and P2), while phase angles clustered in the opposite side of the polar space (180 rad, around π and $-\pi$) correlate with negative

potentials (e.g. N1). The close relationship between phase and ERPs has led to the idea that generating ERPs is mostly caused by the transient resetting of phase (Makeig et al., 2002).

Despite long discussions and research efforts the neurophysiological mechanisms that underlie ERP generation are still unknown (Brandt et al., 1991; Jervis et al., 1983; Makeig et al., 2004; Min et al., 2007). No modern analysis technique is capable of quantifying the amount of influence phase resetting or additive responses have on ERP generation (Makeig et al., 2004). Simulations support parsimonious approaches, where ERPs might be generated by complex additive and non-linear effects (David, Kilner, & Friston, 2006) or sudden transient changes at different frequencies (Burgess, 2012). Thus, parsimonious approaches suggest that a combination of both phase resetting and additive power might be the answer to such fundamental, yet, overlooked question (Makeig et al., 2004; Min et al., 2007).

The mystery surrounding ERP generation is one of its main disadvantages. ERPs provide a weak ground for interpreting obtained results into plausible neurophysiological mechanisms. In fact, most ERP articles discuss the role of functional brain networks in diverse perceptual and/or cognitive phenomena even though ERPs cannot readily test such interactions[9]. The disconnection between ERPs and neurophysiological mechanisms can be seen in its relation to the single EEG trials that generate them (Figure 6). Figure 6, panel A shows an ERP computed with the same 30 trials used to generate Figure 5. Pre-stimulus onset ongoing brain activity is far from being 'flat' as normally described by the

[9] I will provide no citation of articles on which 'network activity' is discussed while only measuring ERP. Nevertheless a simple scholar search would suffice

pre-stimulus ERP baseline (red line, Figure 6 panel A). In contrast, single-trial EEG signals are highly active throughout the trial (blue lines, Figure 6 panel A). Vertical red dashed lines indicate the maxima and minima of typical ERP components for this trial subset (Figure 6, P1=98 ms, N1=160 ms, P2=242 ms). It can be seen how the ERP measure (Figure 6, red line) is somewhat disconnected from the EEG signals (Figure 6, blue lines). The ERP is a rough descriptor of the peaks/troughs occurring in single trial data; their complexity poorly translates into the ERP. Hence, it can be said that the ERP is not necessarily defined by the single-trial EEG (Makeig et al., 2004).

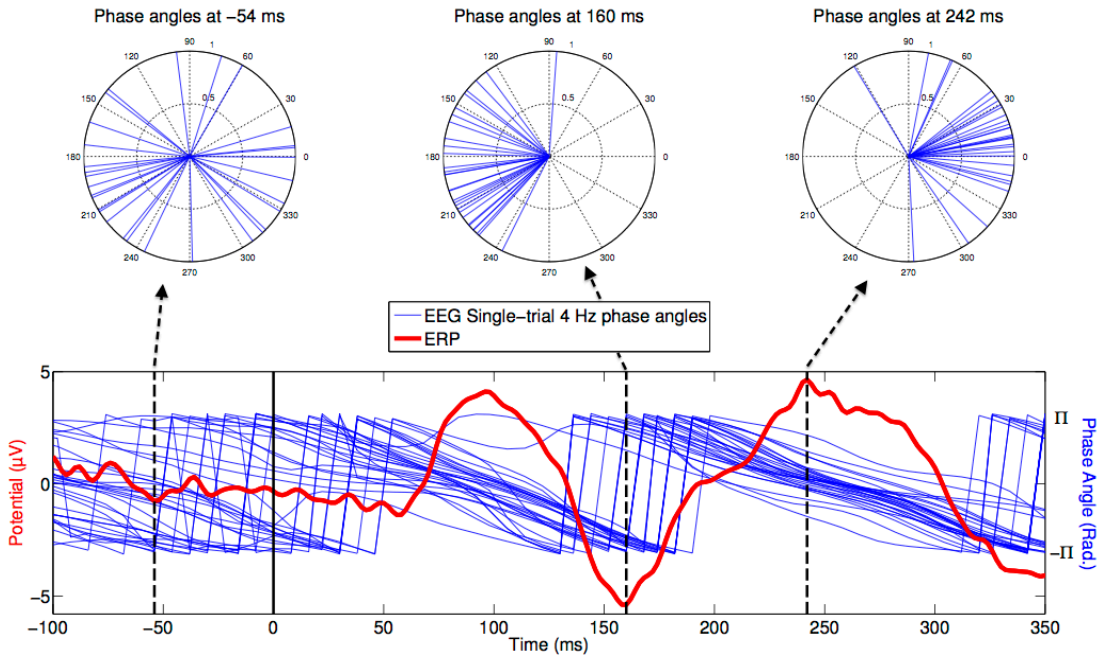

Figure 5 – The relation between ERP and ongoing oscillatory phase. 30 EEG trials were used to compute an ERP (red line, lower panel). The spectral components of the same 30 trials were extracted using wavelet decomposition (see Methods). Phase angles (blue lines, lower panel) were calculated from the complex wavelet output. Phase angles at 4 Hz are shown in radians. Phase angle distributions for individual trials are represented as blue vectors on polar plots (top panels) for a pre-stimulus onset point (-54 ms, top left panel), for the N1 (160 ms, top middle panel) and P2 (242, top right panel) ERP components minima and maxima, respectively

Figure 6, panel B shows 10 simulated EEG trials created using noise in addition to a 6 Hz sine wave and a 10 Hz signal, representing an "evoked response" (M. X. Cohen, 2011)[10]. Left column plots show simulated EEG single trials where no analyses are needed in order to identify the simulated "event-related" non-time locked response occurring between ~1000 and ~1500 ms. Middle panels depict simulated ERPs using the number of single trials indicated on the left panels. It can be clearly seen how after only 5 trials the ERP is almost flat. In contrast, by computing the mean alpha power the simulated "event-related" response is quantified. This simple simulation indicates that other measures (e.g. power) might be better at describing single trial activity, and therefore might better relate to neural mechanisms[11]. I will go over some of these measures in the next section (Modeling Dynamics in the Time-Frequency Domain).

In summary, this simple exercise clearly shows that in the averaging process, the richness of single trials is collapsed into a single statistic that can sometimes miss task-related brain activity (Figure 6). Furthermore, it is argued that due to its simplicity and its unclear generation, ERP hardly relates to fundamental neuronal mechanisms for information processing and communication. Such mechanisms (e.g. interregional synchronization, cross-frequency coupling) have been described across a wide range of species and experimental paradigms and promise to be of great relevance for future research (Buzsaki & Draguhn, 2004; Canolty & Knight, 2010; Fries, 2005; F. Varela et al., 2001).

---

[10] Simulated data provided by Dr. Michael X. Cohen

[11] As an alternative to ERP, power-based measures better describe single trial EEG activity as shown in Figure 6, panel B. For example, Friston (1997) suggested that transient spatiotemporal cross-frequency power interactions might be a good descriptor of distinct neural populations involved in information integration

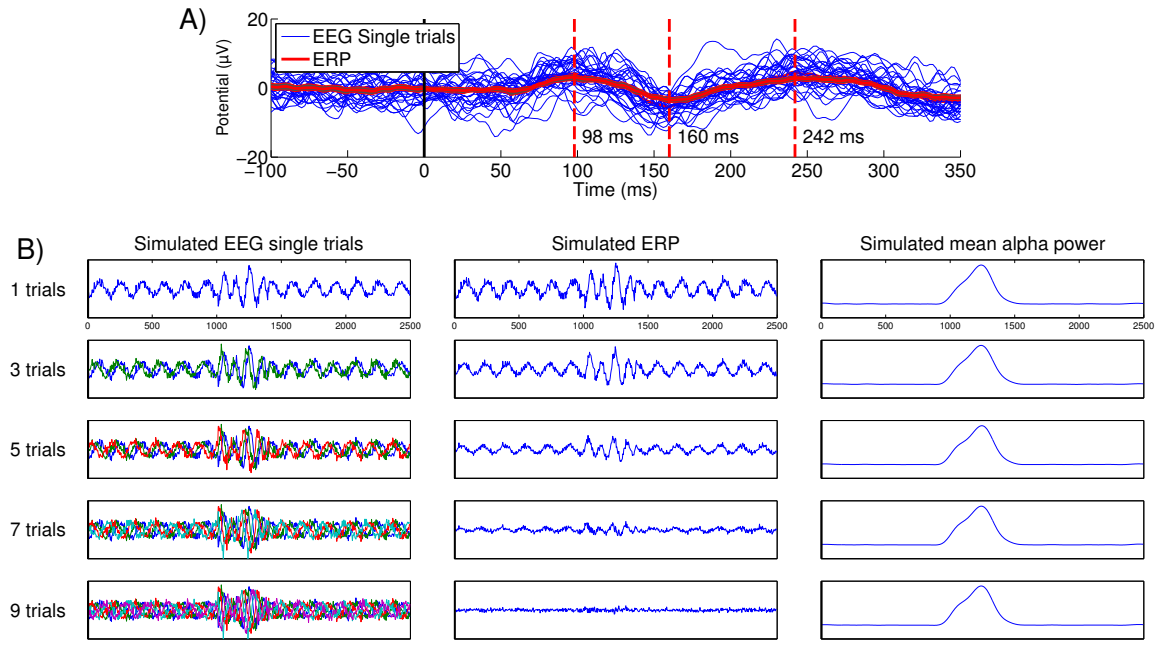

Figure 6 – The disconnection between ERP peaks and troughs and single EEG trials. A) 30 randomly selected single EEG trials (blue lines) from channel PO8 (same as in Figure 5) were averaged in order to produce an ERP (red line). Vertical red dashed lines signal the maxima and minima of each ERP component (P1=98 ms, N1=158 ms, P2=242 ms). The ERP (red line) is a poor descriptor of the single EEG trial activity (blue lines). Black continuous line signals stimulus onset. B) 9 trials of simulated EEG data (left column) were used in order to compute ERPs (middle column) and simulated mean alpha-band power (right column). An "event-related" 10 Hz response can be identified in individual trials (left column). Nevertheless, these responses are lost in the ERP (middle column). In contrast, the estimation of alpha power recovers the "event-related" activity (right column)

Simplicity, a Double-Edged Sword

ERP's simplicity is both one of its greatest strengths and main disadvantages. ERPs main advantage is its simple and fast computation. The straightforward nature of ERPs has positioned them as the most widely used measure in cognitive electrophysiology research. Modern computers can perform single-subject grand-averages of large arrays of M/EEG electrodes in a matter of seconds, while subject-level analyses will only take a couple of minutes. ERPs are thus an excellent way to inspect the

integrity of the collected data. Therefore, before proceeding to more complex analyses, it is advisable to first compute ERPs for each subject/condition.

Another advantage is that ERP computation practically has no assumptions. More specifically, ERP analysis is not influenced by the philosophical/theoretical position of the researcher. No direct impacts will be seen in the results if a researcher cannot decide whether ERPs are generated by addition of evoked activity or by the resetting of ongoing oscillatory phase. Furthermore, results will not be affected if the researcher has never even wondered about ERP generation and its physiological meaning[12].

An additional advantage of simplicity is that virtually no parameters have to be optimized in order to compute ERPs. The calculations involved are so simple that no real understanding of the M/EEG signal and/or the processes involved in ERP computation are needed in order to effectively calculate ERPs from M/EEG signals.

Temporal Precision of ERPs

In addition to the advantages of simplicity, ERP's major strength relies on its high temporal precision and accuracy. This is because ERP computation, by definition, should involve minimal data processing. Thus, if computed correctly, the estimation of electrical activity that ERP provides at the millisecond level is very precise. Nevertheless, a limitation emerges from a common mistake made by ERP researchers. An important distinction is that time-domain averaging of EEG signals is itself a low-pass filter; non-phase locked activity (usually above 15 Hz) gets lost in the averaging process (e.g. Figure 6). Grand-average ERPs across subjects provides further filtering. Nevertheless, most

[12] Nevertheless, the lack of insight about these topics may lead to poor experimental designs, weak hypotheses, and to inappropriate interpretation of results

classic ERP studies report in their method sections additional cut-off filter frequencies between 25 and 40 Hz. These filters are implemented in order to temporally smooth the signals and get clear peaks and troughs for statistical testing.

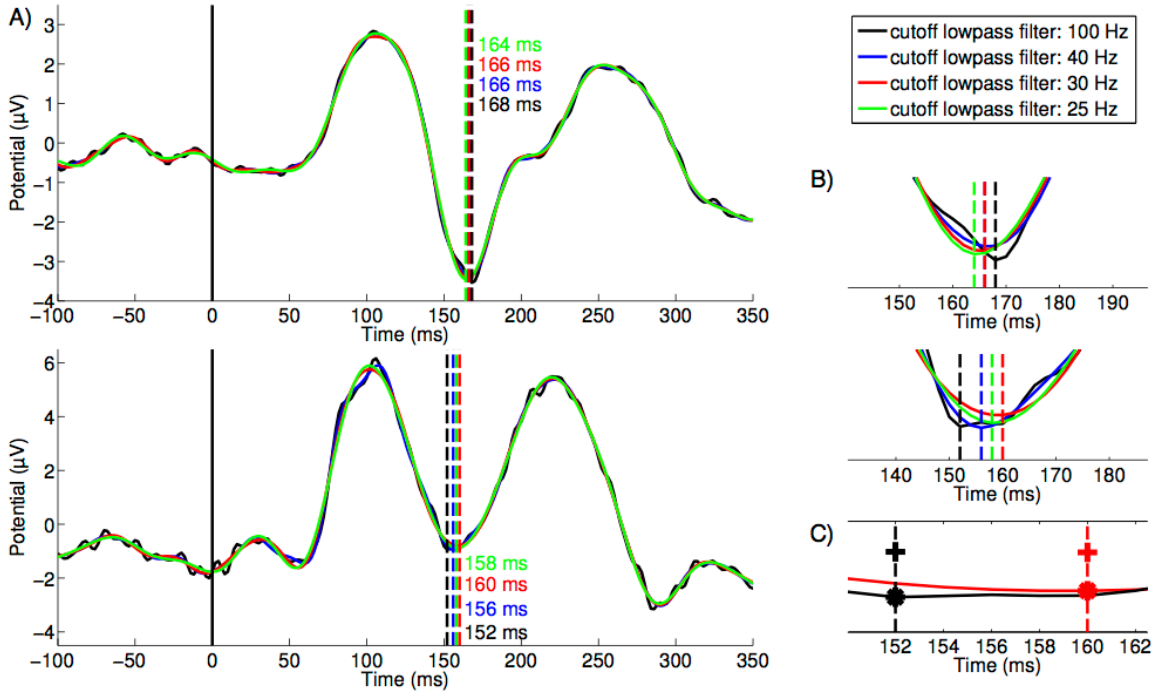

Figure 7 – The impact of low-pass filtering. ERP waveforms were calculated using data from channel PO8 taken from 2 randomly selected subjects (subjects X and Y). 4 different low-pass filter cut-offs: 100 (black), 40 (blue), 30 (red), and 25 (green) Hz were used. A) ERP waveforms computed using 300 randomly selected trials per subject. Top panel shows ERP for subject X. Vertical black continuous line at 0 ms represents event onset. Colored vertical dashed lines indicate N1 ERP trough minima. Resulting ERP trough minima suffer temporal shifts ranging from 2 up to 8 ms for these subjects, depending on filter parameters. B) Detail at N1 trough for both subjects shown in panel A better display temporal shifts of ERP trough minima due to filtering. C) The impact of filtering on different methods for computing "ERP peaks". Dots indicate trough values according to N1 minima for both 100 (black) and 30 Hz (red), difference is 0.14 μV. Crosses indicate trough values according to the integration of data points across a 50 ms window centered at the N1 minima for both 100 (black) and 30 Hz (red), difference is 0.01 μV. Amplitude values are not dramatically affected by filtering while latency suffers time shifts.

Figure 7 is an exercise showing how detrimental data filtering can be for the estimation of the precise timing of brain dynamics. The same EEG signals were filtered

using 4 different filter parameters. The resulting ERPs display temporal shifts. Importantly, the variability of the shifts is not linear or monotonic. As can be seen in Figure 7 panel A, when a wide filter was applied to subject X's data (100 Hz, black) the N1 trough minima is 168 ms. In contrast, when a 30 or 40 Hz low-pass filter cut-off is applied (red, blue), a 2 ms shift is obtained in comparison to 100 Hz low-pass (black). In contrast, different filter cut-off frequencies made a noticeable impact in subject Y's data (Figure 7, lower panel). The wider filter (100 Hz, black) shows the earliest N1 trough (152 ms), while using a 30 Hz low-pass filter (red) delayed the same trough by 8 ms.

A common 'ERP peak' analysis procedure sets a pre-defined "search window" and finds the extreme value inside such window. For this simple exercise, I will define my window as extending for 50 ms starting at 130 ms post-stimulus onset, a period of time that contains the N1 ERP component for both subjects. If we find the minimum μV value and its latency within the pre-defined window, the resulting values are -0.93 μV at 152 ms using a 100 Hz low-pass filter and -0.79 μV at 160 ms using a 30 Hz low-pass filter (Figure 7, panel C).

Another common strategy to compute 'ERP peaks', just like the previously described strategy, defines a pre-defined "search window" and finds the 'peak' (extreme μV value). However, the average of values over a new window centered on the 'peak' is considered as the actual "ERP peak measure". For example, if we compute the 'N1 peak' for subject Y using a 50 ms window centered on its minima and integrate values inside the window, the resulting μV values are 0.08 μV at 152 ms using a 100 Hz low-pass filter and -0.07 μV at 160 ms using a 30 Hz low-pass filter (Figure 7, panel C).

Two things can be learned from the simple exercise shown in Figure 7. First, ERP amplitude values are not dramatically affected by filtering, but latency suffers time shifts that may undermine the study of the time-course of perceptual or cognitive processes. Second, when measuring ERP components 'peaks', the integration of values over a window is a much more robust method against filter-based distortions: the difference between ERP amplitudes when using different low-pass filters was only .01 μV (Figure 7, panel C).

In summary, high temporal precision is one of the greatest strengths of the ERP measure. It was shown how filtering EEG signals in order to temporally smooth ERPs and remove unwanted 'noise' produces temporal shifts while amplitude remains virtually unaffected. One could argue that as long as filtering parameters and 'peak' measuring parameters are kept constant, no problems should arise when analyzing 'ERP peaks' after filtering. This reasoning is at the heart of most ERP studies published to date. Notwithstanding its validity, this logic must be critically examined because there is no clear rationale behind centering ERP analysis only on peaks and troughs. Thus, I think we must question the very reason why researchers filter EEG signals for ERP analysis in the first place.

Analyzing Temporal Dynamics with a Systematic Approach

Temporal precision is a key feature of the ERP measure. ERPs can be used as a powerful and computationally inexpensive tool for analyzing the time-course of perceptual and cognitive processes. Nevertheless, most ERP articles do not exploit this relevant feature. Researchers commonly discard most of the ERP time series in order to

focus their analysis on specific peaks and troughs, an approach known as "peak analysis". ERP 'peaks' are the main variable used in virtually thousands of research articles. As discussed above, researchers have acquired the tradition of temporally "smoothing" ERPs by eliminating unwanted high-frequency 'noise' in order to obtain ERP component peak amplitude and its latency (Figure 7). These 'peaks' are then used for null hypothesis significance testing (NHST).

Peaks and troughs are by far the most commonly quantified, analyzed, and reported ERP feature. However, no clear reason exists for studying ERP peaks and troughs while discarding all other data points in the time series. Most ERP researchers conceptually correlate the 'ERP peak' to a relevant functional brain event. In contrast, it could be argued that different time points in the ERP waveform could be equally important as the peaks and troughs.

Let me re-draw Figure 5 with polar representations using different time points. Thus, Figure 8 shows single-trial phase angle distributions at four different time points (-54, 120, 160, and 200 ms). In comparison to pre-stimulus onset phase angle distributions (-54 ms, top left panel) post-stimulus oscillatory phases are roughly clustered around specific phase angles (Figure 8). From this extremely simple exercise it can be said that it is unclear what makes ERP 'peaks' special as opposed to activity in-between peaks. Furthermore, to the best of my knowledge, there is no evidence to argue that an ERP 'peak' is a descriptor or counterpart of a "functional brain component" as commonly believed by ERP researchers. In the literature, this point has been made clear in several occasions (e.g. Kutas & Federmeier, 2011; Luck, 2005; Rousselet & Pernet, 2011; Rousselet, Pernet, Bennett, & Sekuler, 2008; Schyns, Petro, & Smith, 2007; Vanrullen,

2011). Nevertheless, for some reason this important conceptual remark has not percolated to the wide number of ERP researchers, perpetuating the sole use and interpretation of 'peaks' in ERP studies.

Once researchers measure a 'peak' they can obtain its latency (e.g. Figure 7). Most published articles that have quantified the ERP measure using peak analysis consider 'peak' amplitude and its latency as independent sources of information. To the best of my knowledge, there is no evidence to argue for such independence. In a study by Schyns et al. (2007) subjects were provided with specific spatial frequency information for a facial expression classification task. Participants used sparse samples of information in order to categorize facial expression images. Using reverse correlation between the partial information provided by the stimuli and the categorization output from participants, and the single-trial EEG signals, they concluded that processes for accumulating information start 50 ms prior to the N1 peak, occurring at 170 ms post-stimulus onset (Schyns et al., 2007). Importantly, their analysis showed that participants categorizing facial expressions stopped integrating information at the N1 peak (170 ms).

This study provides relevant evidence linking ERP peak latency to the speed of information accumulation, further indicating that ERP peaks might be describe the termination of a perceptual or cognitive process and not the cognitive process itself. Moreover, this study shows that differences in ERP peak latency necessarily imply an amplitude difference starting before the measured ERP peak (in this case, 50 ms prior ERP peak). This also indicates that latency and amplitude are rather confounded, far from being independent sources of information as commonly believed by ERP researchers. Evidence supporting these findings has been found using parametric approaches of

single-trial EEG analysis (Rousselet, Husk, Bennett, & Sekuler, 2008; Rousselet, Pernet, et al., 2008). Such evidence further supports the idea that neural activity described by ERP peaks might not be more important than activity described by other time points in the ERP waveform.

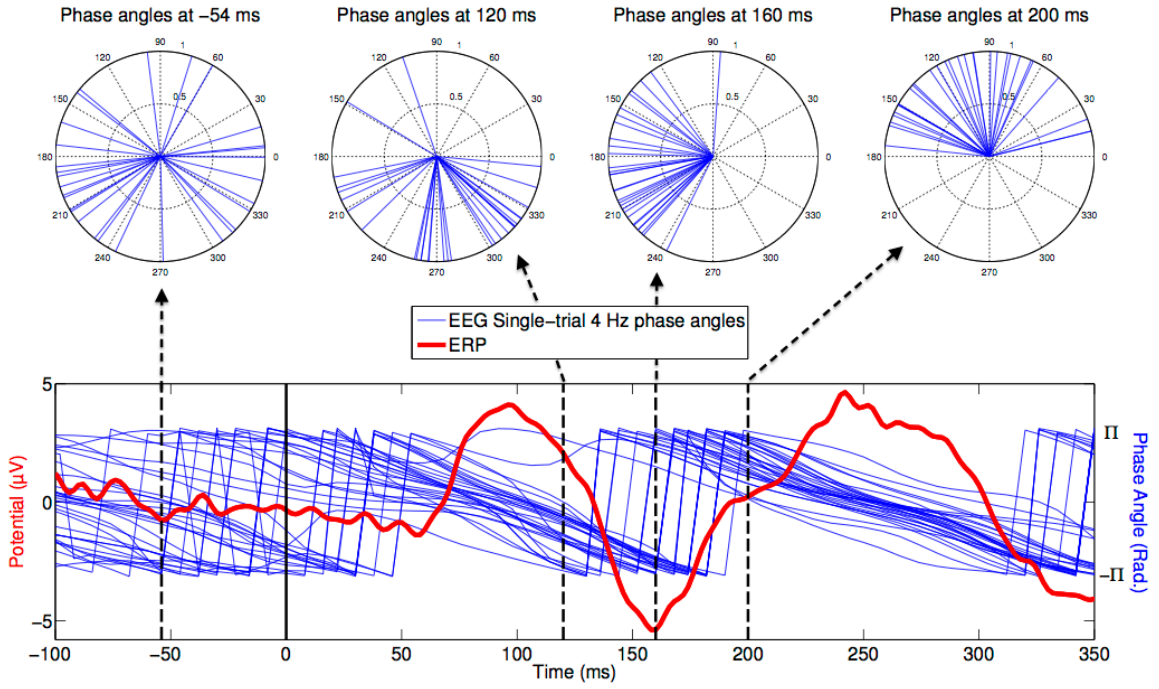

Figure 8 – Same 30 trials used to generate Figure 5 were used to generate an ERP (red) and phase angles (blue) were obtained using wavelet transform (see Methods). Polar representations of 3 different time points (-54, 120, 160, 200 ms) are shown. In contrast to pre-stimulus onset (-54 ms) whose phase angles are evenly distributed, rather a "phase preference" can be seen for post-stimulus activity (~270 at 140 ms, ~180 at 160 ms and ~120 at 200 ms)

Therefore, instead of measuring peaks or troughs inside pre-defined analysis windows, a consistent and systematic approach was applied to examine the temporal dynamics of brain activity. In contrast to the classic "peak analysis" approach, a suggested viable alternative is to analyze all the time-points in a time-series in order to

reveal the complete time course of effects (Maris & Oostenveld, 2007; Pernet, Chauveau, Gaspar, & Rousselet, 2011; Rousselet, Husk, et al., 2008; Rousselet & Pernet, 2011; Rousselet, Pernet, et al., 2008; Vanrullen, 2011).

An counterargument can be made to continue using the classic peak analysis approach in current and future ERP studies regardless of the implementation of new analysis techniques (e.g. Wilcox & Keselman, 2003). The first part of the argument would suggest that current and new studies could benefit from the historicity of the ERP measure. An extensive and impressive body of work on the ERP measure has been published in multiple scientific journals, spanning more than five decades. Peak analysis of ERPs has been so widely used that multiple studies can be found for virtually all kinds of clinical and healthy populations performing all sorts of cognitive tasks. Following this part of the argument, the contextualization and interpretation of current ERP studies could rely on the 'classic literature'. The second part of the argument is based on the fact that a large number of theoretical interpretations of ERP effects have been published over the years. These could provide a good playground for the development and testing of hypothesis-driven studies of cognition. However, this argument fails to acknowledge that the lack of a consistent experimental, analytic, and statistical framework on the majority of these "classic studies" renders them as practically unusable in order to compare results across studies (Ioannidis, 2005; Rousselet & Pernet, 2011). Therefore, just like with any other technique, ERPs peaks must be used rigorously, interpreted with healthy skepticism, and by any means taken by a default "gold standard" in cognitive electrophysiology research.

In this dissertation, no peak analysis will be performed in ERPs. Moreover, all measures will be analyzed as time series using modern statistical procedures. This approach will be further described and discussed in sections 2.4 Linear Modeling of EEG Measures, 2.5 Non-Parametric Permutation Testing, and 3.6 Statistical Testing.

Summary

The event-related potential (ERP) is the most widely used measure of temporal brain dynamics in cognitive electrophysiology. Although the neural mechanisms that generate ERPs remain unknown, two main theories have been broadly discussed in the literature using modeling and experimental approaches. The "additive" and the "phase reset" models of ERP generation try to link neural dynamics to ERPs. Though, due to the nature of ERP, it might be impossible to pinpoint the mechanisms that produce the signals at the scalp. Thus, parsimonious approaches have been postulated suggesting mixed generation mechanisms (Makeig et al., 2004).

ERP is a great research tool for studying the time-course of brain dynamics. Its temporal precision can resolve neural events within the millisecond range. However traditional approaches misuse this striking feature of ERPs by focusing analyses on pre-defined time windows. A systematic approach where all time points conforming the ERP waveform are analyzed has been suggested as a reliable alternative to peak analysis (Maris & Oostenveld, 2007; Pernet et al., 2011; Rousselet, Husk, et al., 2008; Rousselet & Pernet, 2011; Rousselet, Pernet, et al., 2008; Vanrullen, 2011).

Finally, it is argued that ERPs are somewhat disconnected from the single-trial EEG activity that generates them. EEG activity at the single-trial level reflects the

summation of excitatory and inhibitory postsynaptic potentials of large ensembles of neurons at the scalp. The dynamic interaction between excitatory and inhibitory neurons produces rhythmic excitability fluctuations observed as "ripples" at different temporal and spatial scales (F. Varela et al., 2001). Over the last 20 years, research has provided evidence indicating that short-lived brain oscillations play a key role in information processing and communication in cortical networks (Canolty & Knight, 2010; Engel et al., 2001; Uhlhaas et al., 2009; F. Varela et al., 2001). Only exploring temporal dynamics seems to overlook the complexity conveyed by M/EEG signals. Furthermore, the present experimental manipulation allowed me to separate activity linked to task demands from physical stimulus properties. I therefore expect effects quantified by oscillatory activity (Fries, 2005; Uhlhaas et al., 2009; Uhlhaas et al., 2011; F. Varela et al., 2001). A natural extension to the study of neural activity is to study their dynamics in the time-frequency domain.

2.2 Neural Dynamics in the Time-Frequency Domain

Although neural network models can be built from simple components using logical states (Hopfield, 1982) or graded responses (Hopfield & Tank, 1986), real-world neural networks need inhibitory forces in order to counterbalance the effect of sole excitation (Freeman, 2000). From the complex hierarchical nature of the cerebral cortex, self-organized networks are built from excitatory and inhibitory components giving way to the emergence of complex phenomena such as feedback and feedforward inhibition (Buzsaki, 1984). The regulatory properties of these complex neural networks have been shown to influence spike timing with precision in the submillisecond range (Pouille &

Scanziani, 2001). Thus, it has been proposed that maximum functional complexity in neural systems can be reached through the intricate organization of inhibitory and excitatory cells (Buzsáki, 2006). Periodic patterns of activation emerging from such complex organization generate brain oscillations occurring at different temporospatial levels (F. Varela et al., 2001). Neuronal oscillations often vary with behavioral and cognitive experimental manipulations.

In the following sections I will proceed to describe and discuss time-frequency measures used in this dissertation. At a global level, all time-frequency measures have three major advantages over measures that can only model time-domain brain dynamics. First, most time-frequency measures can be directly related to neurophysiological mechanisms. The mechanisms responsible for generating brain oscillations are fairly well understood at the cellular and network level. Importantly, the functional role of oscillatory network dynamics in high-level processes remains unknown. However, quantifying oscillatory activity in cognitive electrophysiology can help establish direct links between well-known neural mechanisms and cognition.

Furthermore, a second advantage is that neural oscillations can be studied using multiple populations, scales, species, and methods. Results obtained using time-frequency measures can be interpreted in the light of recent modeling, *in vitro*, and *in vivo* findings elucidating physiological mechanism underlying the generation of neuronal oscillations (Buzsáki & Wang, 2012; Fries, 2009; Tiesinga & Sejnowski, 2009; Wang, 2010). Therefore, the oscillatory framework can easily serve as a bridge linking literature from different fields of life science to multiple species, scales, and methods.

Working under the oscillatory framework implies the belief that neural systems operate over a multi-dimensional domain. Consequently, M/EEG data captures only a small fraction of that multidimensional space where brain dynamics emerge. Therefore time-frequency measures of brain activity are probably the most appropriate approach to analyze M/EEG signals since they allow a larger portion of the dynamics embedded in raw data to be modeled. Not only the time and frequency dimensions are taken into account but also power, phase, and space. Furthermore, time-frequency approaches have the ability to model brain signals' complex dynamics at the single-trial level. As shown in Figure 6, time-frequency measures can reveal task-relevant M/EEG dynamics that time-domain measures cannot.

At the global level, all time-frequency-based measures share two distinguishable limitations. First, temporal resolution is decreased when computing time-frequency decompositions. This is not a specific property to M/EEG data, but an intrinsic property of signal processing in general. Thus all time-frequency-based approaches have a lower temporal resolution than unfiltered time-domain measures (see 3. Methods).

The second limitation relies on the complexity of time-frequency analysis. Compared to ERP, time-frequency-based measures have several key parameters that need to be optimized for each dataset. Theoretical or empirical approaches can be used in order to find the optimal parameters for a given M/EEG dataset (Christoph S Herrmann, Crigutsch, & Busch, 2005). On one hand, research questions might demand investigating certain frequencies or certain time-points, defining the parameters to be used. On the other hand, exploratory analyses might want to use a more open range of times and frequencies to be explored. Thus, the number of frequencies used in order to characterize

a frequency range[13], the spacing between those frequencies[14], the wavelet length[15], the number of cycles for the Gaussian tapper[16], and other parameters will have an impact on the results. Poorly chosen parameters will result in deficient estimations of the analytic signal and ultimately the measure of interest. The fact that many parameters have to be optimized according to the nature of the data renders the existence of ready-to-use "off-the-shelf" time-frequency measures virtually impossible.

Just like how the number of parameters that must be set increases with more complex time-frequency-based methods, so too do the number of comparisons that must be made. Thus, researchers not only have to perform tests over time, but over frequency as well. Typical time-frequency studies have between 20 and 50 different frequencies sampled across 200 and 600 time-points per trial, per channel, per condition, per subject. Researchers will easily find themselves working with 5-dimensional matrices when performing time-frequency-based analyses. The complexity of statistical procedures and their corresponding corrections for multiple comparisons will increase considerably. Fortunately, robust non-parametric statistical methods have been developed for this problem (e.g. Maris & Oostenveld, 2007; Pernet et al., 2011). Yet again, none of these methods can be used "off the shelf".

The results of a simple exercise are shown in Figure 9. Optimized parameters were used in order to calculate the analytic signal of 200 randomly selected trials from PO8

[13] If a research group wants to test the effects of manipulation X over alpha-band oscillations, should they use a 10 Hz wavelet? Should they use wavelets from 8 to 12 Hz? Should they use an even wider range of frequencies?
[14] Should the researchers linearly or logarithmically space their frequencies?
[15] Should the researchers define their wavelet using a time-range of 1, 2, 3, or more seconds?
[16] Should the researchers use fewer or should they use more cycles per wavelet?

from a randomly selected subject using wavelet convolution (see 3. Methods). Figure 9, top right panel shows clear event-related spectral components across different frequency bands and spanning multiple time-points. Most notably, a low-frequency power increment is visible starting at ~200 ms (maximally visible at ~150 ms post-stimulus onset) and extending up until the end of the chosen window. This increment spans between ~4 and ~10 Hz, where a power decrement between ~10 and ~20 Hz can be observed after the ~150 ms post-stimulus onset. If we select a particular frequency (e.g. ~40 Hz), we can see its time-course (Figure 9, top left panel).

In contrast, suboptimal parameters were used in order to calculate the analytic signal of the same data sample using wavelet convolution. From this suboptimal analysis, clear event-related spectral components can also be recovered. Most notably, a power increment between ~10 and ~20 Hz starting at ~200 ms and extending up until the end of the chosen window (Figure 9, bottom left panel). The time-course of ~40 Hz for the suboptimal analysis is also shown (Figure 9, bottom right panel). In most situations sub-optimal parameters will lead to missing effects more than generating misleading results. However, if the researcher is not aware that the parameters used are suboptimal, results can be incorrectly interpreted.

It has been seen that time-frequency-based analyses have clear advantages and limitations. Nevertheless they pose a powerful tool for exploring neural time series data. In the following sections I will describe and discuss the time-frequency measures used in this dissertation. Reviewing all existing power- and phase-based time-frequency measures is beyond the scope of this dissertation. The following review has the sole purpose of contextualizing the applied measures.

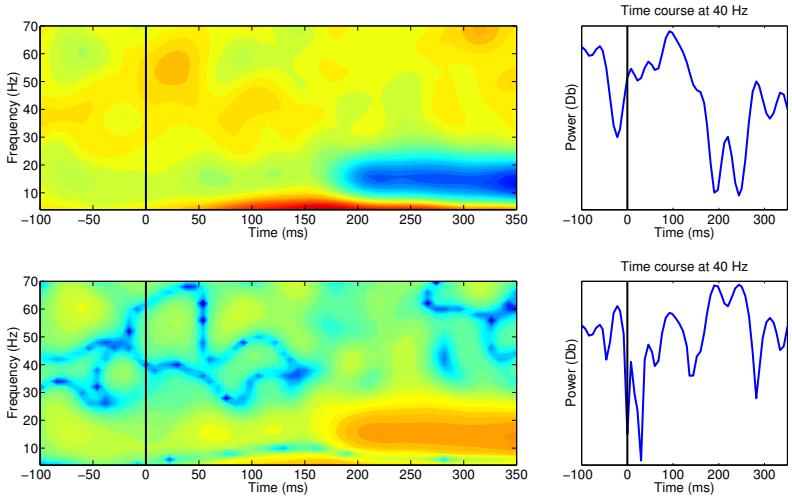

Figure 9 – The effect of different parameters on spectral power computation. Different parameters were used to perform wavelet convolution on 200 randomly selected trials from channel PO8 from a randomly selected subject. Top panels show power computed with optimized parameters (left) and corresponding power time-course at ~40 Hz (right). Bottom panels show power computed with suboptimal wavelet parameters (left) and corresponding power time-course at ~40 Hz (right). Vertical black lines signal stimulus onset. Each plot is auto-scaled

2.2.1 Event-Related Spectral Power (ERSP)

Estimates of task-related time-varying frequency-band-specific power can be calculated from M/EEG data. Several methods, mostly based on convolution, can be used in order to extract spectral power from analytic signals, among them Hilbert and Fast Fourier Transforms. When used with optimal parameters, these different approaches lead to very similar results (Bruns, 2004; Le Van Quyen et al., 2001). In this dissertation, wavelet convolution was used in order to obtain the spectral components of EEG data (see 3. Methods). The squared magnitude of the complex output of convolution provides a trial-by-trial measure of phase-locked, non-phase-locked, and ongoing background neural activity known as total spectral power. Total spectral power quantifies the amount of energy at a given time-frequency point. When computed across all available time-

points and frequencies, a time-frequency representation of total spectral power can be obtained (Figure 10, bottom right panel).

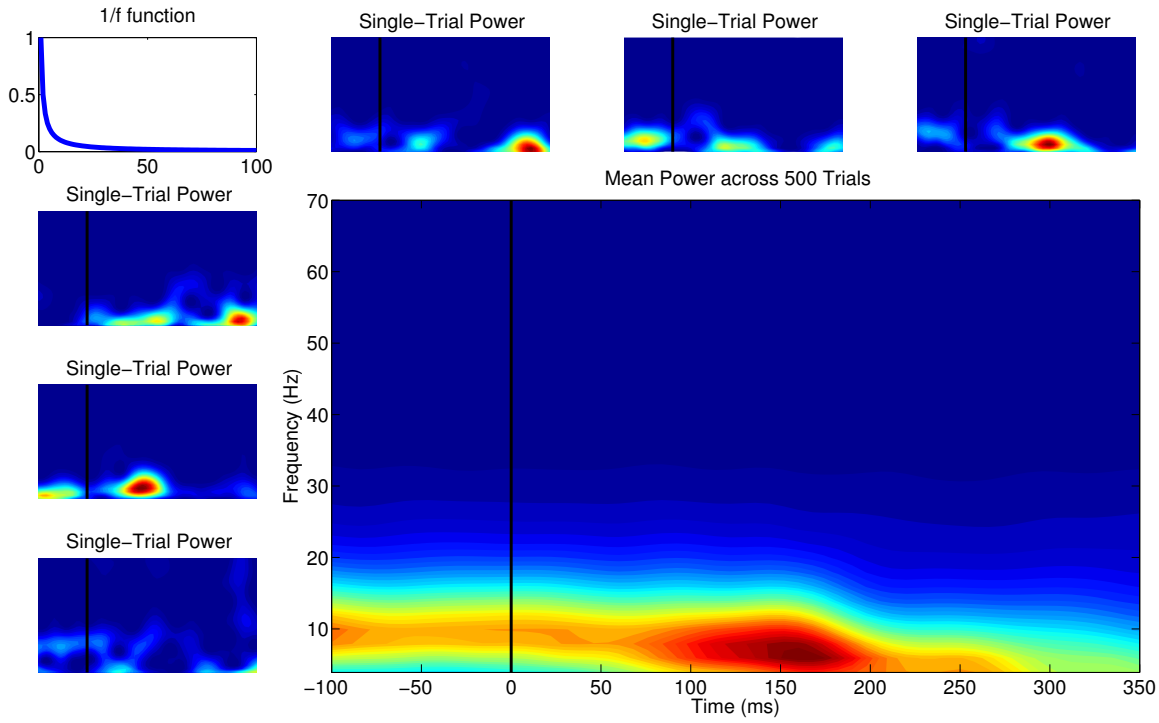

Figure 10 – Time-frequency representations of total raw power estimation of EEG activity (phase-locked, non-phase-locked, and ongoing background activity). Top left panel shows a 1/f function that characterizes EEG power. Wavelet convolution was used in order to compute total raw power (see Methods). Total raw power estimation from 6 randomly selected trials is shown. Bottom right panel depicts grand-average of total raw power estimation across 500 trials. Plots are in the same scale

Spectral power measures in general, can be found in the literature as "synchronization", "event-related synchronization" (ERS), "event-related desynchronization" (ERD), "time-frequency representations" (TFR), and "event-related spectral perturbation" (ERSP). All of these names refer to spectral power. Throughout this dissertation I will use "theory-free" measure names (M. X. Cohen & Gulbinaite, 2014). For example, the names "ERS" and "ERD" can be extremely misleading since

they may refer not only to synchronization or desynchronization either within and between neuronal populations or within and between electrodes. Moreover, denominating an augmentation in power at a given time-frequency point as "synchronization" refers to a neurobiological mechanism underlying such power increment which is far from the actual mathematical technique of data analysis. Furthermore, synchronization can be described in amplitude and/or phase and within and/or between frequencies (Canolty & Knight, 2010). I have chosen to use names that best describe the analysis, rather than the putative underlying neurobiological mechanisms (M. X. Cohen & Gulbinaite, 2014). Therefore, I will refer to changes in spectral power elicited by an event as event-related spectral power (ERSP).

Figure 10 shows 2-dimensional time-frequency total raw power plots. Adjacent small plots depict total raw power from randomly selected trials from channel PO8 from a randomly selected subject. Each trial has a different activity profile. Some trials contain high pre-stimulus onset total raw power (e.g. bottom left), while some others contain little activation overall. The grand-average of total raw power across 500 randomly selected trials from channel PO8 from a randomly selected subject is shown in the bottom right panel of Figure 10. As you might have realized, although this is a grand-average plot, it is very difficult to interpret visually. Total raw power magnitude in low frequency bands (below 15 Hz) is so much larger than in high frequency bands (above 15 Hz) that it is hard to really appreciate the time-frequency dynamics of raw power. This problem comes from the nature of the relationship between power and frequency. EEG power decreases as a function of frequency increments, following a 'power law', where EEG time-

frequency power is a power[17] function of frequency. Since EEG spectral power follows a $1/f$ phenomenon (Nunez & Srinivasan, 2006), power at higher frequencies is lower than the power at lower frequencies (Figure 10 top left panel).

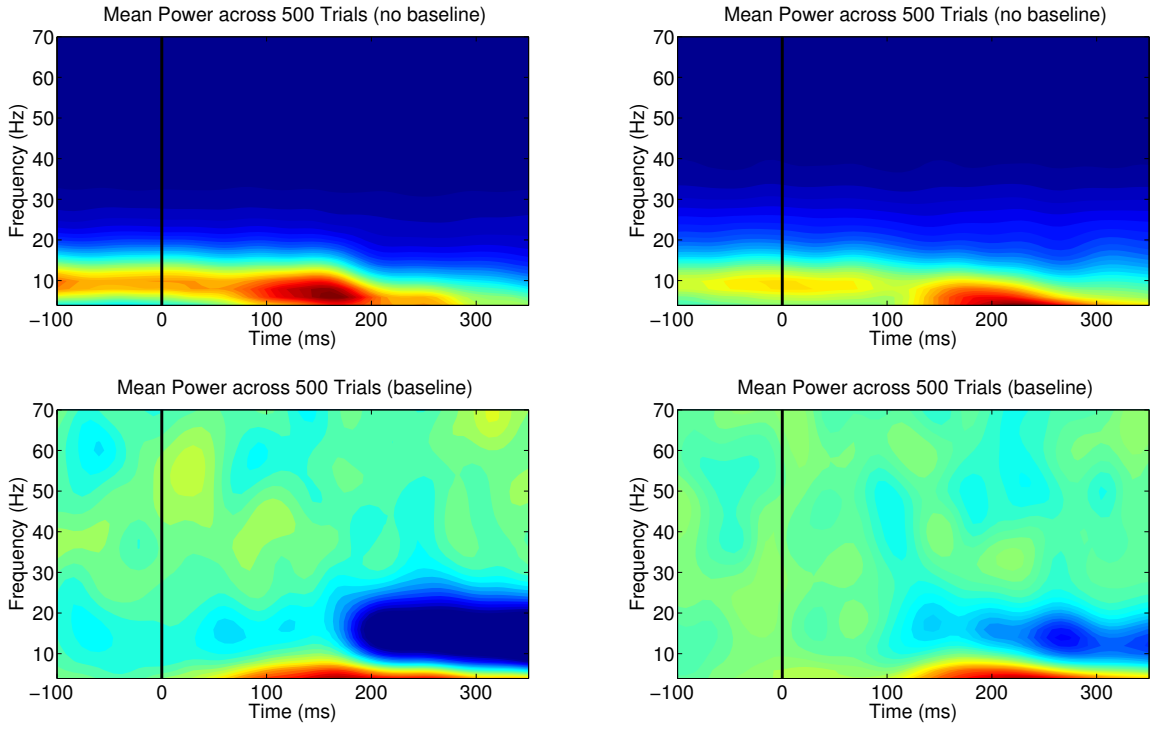

Figure 11 – Time-frequency representations of total power estimations of EEG activity. Wavelet convolution was used to extract the spectral components of 500 trials from channel PO8 from 2 randomly selected subjects (see Methods). Top row shows total raw power (phase-locked, non-phase-locked, and ongoing background activity). In contrast, bottom row shows total ERSP. All plots are in the same scale

Limitations with visualizing and quantifying EEG raw power can be reduced by baseline normalizations (Grandchamp & Delorme, 2011). Baseline procedures allow data to be transformed from different frequencies, channels, and subjects into the same scale. Moreover, baseline correction untangles 'uninformative' ongoing background activity

[17] Importantly, "power" here denotes the mathematical operation of raising a number to a power of another number. Not to the squared magnitude of a complex number as in spectral "power"

from event-related power variations (for a counter argument to this point see He, Zempel, Snyder, & Raichle, 2010; and VanRullen et al., 2011). Thus, from raw spectral power, the ERSP measure can be used to quantify task-dependent mean power deviations from baseline (Makeig et al., 2004). Figure 11 shows a comparison between total raw power of data from 2 subjects form channel PO8 and total ERSP. Just like in Figure 10 bottom right panel, top panels in Figure 11 cannot be easily understood. In contrast, bottom panels depicting total ERSP can be interpreted more easily as representing event-related mean changes in total spectral power from baseline in decibels (Figure 11).

Spectral Power: Total, Phase-Locked, and Non-Phase-Locked

Importantly, time-frequency representations in Figure 10 and Figure 11 were made using total spectral power. Top panels of Figure 11 depict total spectral power with no baseline correction. Therefore, the data utilized to generate these images contain phase-locked, non-phase-locked, and ongoing background activity. Lower panels in Figure 11 depict total ERSP representing event-related phase-locked and non-phase-locked activity. Task-unrelated ongoing background activity was removed using single-trial-based baseline correction (see 3. Methods). Total ERSP is the most commonly used measure of spectral power in the cognitive electrophysiology literature and is obtained by averaging single-trial total spectral power values. All power-based analyses in this dissertation were made using total spectral power. Therefore, the term "ERSP" refers to baseline-corrected total spectral power (see 3. Methods).

Nevertheless, two variants of ERSP can be found in the literature as well[18]. Figure 12 compares three power-based measures. First, a measure of non-phase-locked spectral power, known as "induced" power (Tallon-Baudry, Bertrand, Delpuech, & Pernier, 1996). Although several ways to compute this measure have been suggested (e.g. Klimesch, Russegger, Doppelmayr, & Pachinger, 1998) there is general agreement in the main idea as to how to compute it. The logic is simple, if phase-locked activity produces ERPs, subtracting the ERP at each trial and then computing time-frequency decomposition on the 'ERP-free' single trials should leave behind only non-phase-locked activity. Moreover, if baseline correction procedures are applied, only event-related non-phase-locked activity should remain. The second variant of ERSP is a measure of phase-locked spectral power or "evoked" activity, which is obtained by subtracting non-phase-locked spectral power from the total representation. Thus, activity that is not phase-locked to the onset of the stimulus (time=0) will not be represented. More variants for the computation of this measure have been suggested. However, they all rely in the same principle stated above (e.g. Busch, Herrmann, et al., 2006; Christoph S Herrmann et al., 2005; Min et al., 2007).

The main argument for computing phase-locked and non-phase-locked ERSP separately is that in combination they can be used in order to assess the contribution of "induced" and "evoked" activity at a given task (Gruber & Muller, 2002). However, it is not known if the neurophysiological events that generate phase-locked activity are different from the ones that generate non-phase-locked power (David et al., 2006).

[18] Technically, a third variant could be mentioned. The "ERP power" measure can be computed by calculating time-frequency decomposition on the ERP. Nevertheless, I do not consider this measure as being relevant and will not be further discussed

Furthermore, it is not certain if a clear separation of phase-locked and non-phase-locked activity can be effectively achieved by simple subtraction; this latter argument is a recurrent discussion topic in time-series analysis boards (e.g. Delorme & Makeig, 2014).

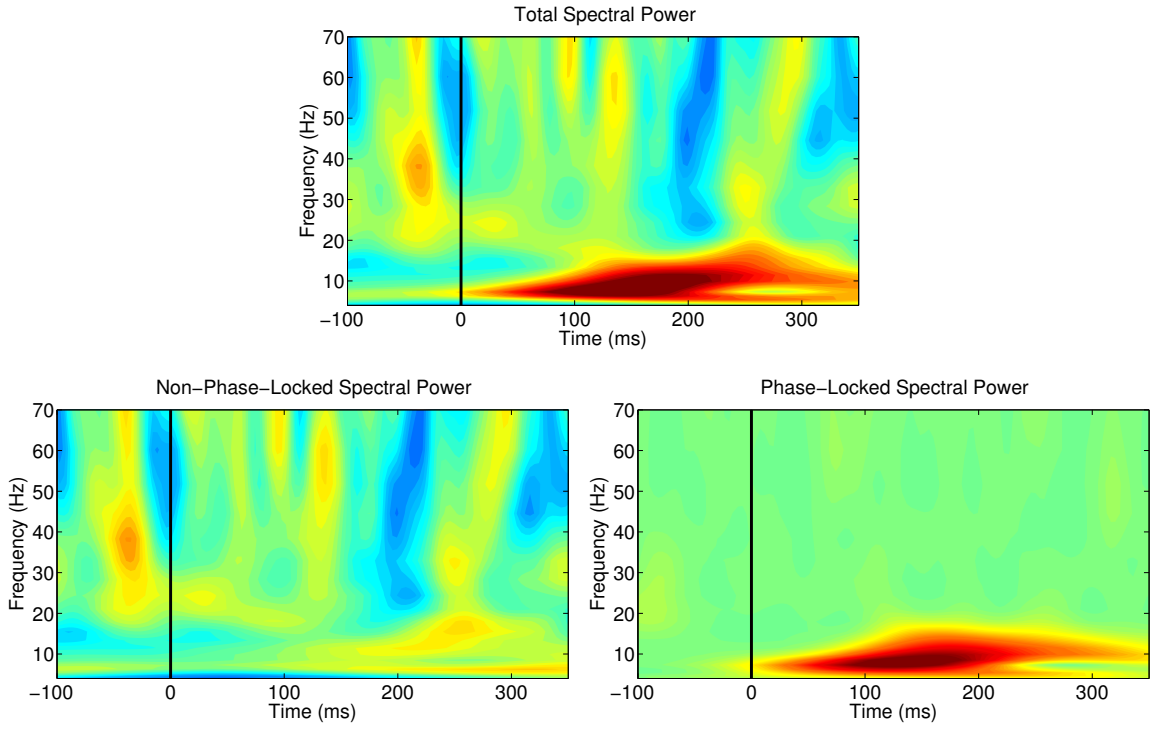

Figure 12 – Time-frequency representations of event-related spectral power measures. Top panel depicts total spectral power, the measure used for power-based analyses in this dissertation. Bottom left panel depicts non-phase-locked spectral power. Bottom right panel depicts phase-locked spectral power. All plots are in the same scale

Figure 12 depicts total, non-phase-locked, and phase-locked spectral power computed using 100 trials from a randomly selected subject from channel Pz. Figure 12, top panel shows clear spectral features in the event-related total power time-frequency representation. Most notably a power increment in low-frequency ranges (~4 to ~10 Hz) extending maximally from ~100 to ~200 ms and a high-frequency range (~20 to >70 Hz) power decrease at ~200 ms. Bottom right panel in Figure 12 shows non-phase-locked

activity. Clear spectral features can be seen in the "induced" time-frequency representation. Most notably a high-frequency range (~20 to >70 Hz) power decrease at ~200 ms. Likewise, clear spectral features can be seen in the "induced" time-frequency representation most notably a low-frequency range (~4 to ~10 Hz) power increment extending maximally from ~100 to ~200 ms (Figure 12, bottom right panel). By plotting the three variants of ERSP we can clearly see that event-related total spectral power captures both "evoked" and "induced" activity. In this dissertation I have decided to use the total power measure (top panel Figure 12) because it does not assume any paradigm of physiological generation and involves no arbitrary data alterations. Therefore, all power-based results and discussions will be using total spectral power.

Functional Interpretation of Spectral Power-Based Measures

The amplitude of EEG signals is the most widely measured aspect of scalp-recorded neurophysiological dynamics. The current EEG literature is mostly based in amplitude-dependent measures of EEG signals, primarily ERP and in a much lesser degree ERSP. However, the functional interpretation of amplitude-based measures of brain function is still vague and a matter of debate due to the lack of understanding of the generation of amplitude changes.

EEG amplitude variations are a function of current dipole magnitudes emerging from linearly summated synaptic potentials at the scalp, produced by cortico-cortical and thalamo-cortical neural networks (Buzsáki, 2006; Nunez & Srinivasan, 2006; Tenke, Schroeder, Arezzo, & Vaughan, 1993; Whittingstall & Logothetis, 2009). Thus, it is widely accepted that scalp-recorded amplitude changes reflect differences in transient

synchronization of neural activity across relatively large patches of cortex (Buzsáki, 2006; Makeig et al., 2002; F. Varela et al., 2001). Nevertheless, changes in amplitude dynamics may occur without increments or decrements of synchronization. For example, (Hughes et al., 2004) used *in vitro* thalamic recordings to show that alpha oscillations can be modulated by antiphase subpopulations. Importantly, amplitude changes were independent of the number of active neurons in the network. When manipulating the number of active neurons entrained to the oscillation, the amplitude of the recorded signals varied. In contrast, when the number of active neurons remained fixed, amplitude modulations were seen due to phase relationships between subpopulations (Hughes et al., 2004). These results indicate that amplitude changes can be obtained by changing the number of members involved in the neural assembly and by phase dynamics alone. These results have been confirmed by computational modeling (Cosandier-Rimele, Merlet, Badier, Chauvel, & Wendling, 2008). Furthermore, these ideas were tested using concomitant local-field potential (LFP) and EEG recordings in behaving nonhuman primates (Musall, von Pfostl, Rauch, Logothetis, & Whittingstall, 2014). Musall et al. (2014) found that EEG power is a direct function of the linear summation of LFP power and phase synchronization. Moreover phase synchronization alone can trigger changes in EEG amplitude. Finally, it has also been shown that significant changes in phase synchrony can be quantified with no repercussions on spectral power (J. M. Palva, Palva, & Kaila, 2005).

Summary

Power-based measures of brain function are good measure of trial-by-trial neural activity as recorded by M/EEG. In this dissertation I used a measure of total event-related mean spectral power deviations from baseline. ERSP not only provides a quantification of neural signals that are phase-locked to the stimulus onset but it can also measure non-phase-locked "induced" activity (Figure 12). Thus, as understood in this dissertation, ERSP provides a measure of event-related total spectral power.

It is thought that fluctuations in spectral power reflect synchronization changes in neural populations contributing to the EEG signal. Empirical research and computational modeling indicates that the main interpretation of EEG power as an indicator of neural synchronization is not erroneous but incomplete. Thus, functional interpretations regarding neural mechanisms of cognition relying solely on spectral power-based measures should be cautiously made. Recent evidence demonstrates that in order to uncover the neural mechanisms underlying cognition it is necessary to go beyond power-based measures EEG signals.

2.2.2 Inter-Trial Phase Clustering (ITPC)

The output of convolution not only can be used to extract spectral power from the analytic signal. Other information can be also obtained from the convolved M/EEG signal. Thus, from the analytic signal we can extract linear measures of EEG activity (e.g. ERSP) and

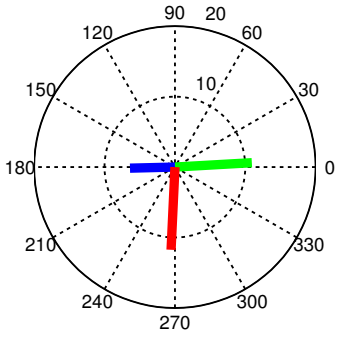

Figure 13 – Polar plane with vectors of diverse magnitude and phase angle distributions

also non-linear measures of oscillatory activity. Figure 13 depicts a polar plane representing three different time-points at a given frequency[19]. The length of each vector represents the magnitude of the selected time-frequency point whereas the phase angle is indicated by the vector angle relative to the positive real axis. Phase angles provide researchers with information about the timing of activity in specific frequency bands. Phase synchronization of neuronal oscillations has been suggested as an important mechanism for neural communication (Fries, 2005; F. Varela et al., 2001). Importantly, phase dynamics can be used as a trial-based measure of such neurobiological mechanism (VanRullen et al., 2011). Finally, due to the ambiguous relation between spectral power and synchronization, power-based measures can be better informed by phase-based metrics of neural activity. Further providing a link between frequency band-specific M/EEG activity and its putative interpretation as a signature of local and/or inter-regional synchronization.

Measuring Phase-based Neural Dynamics

The most intuitive way to measure the degree of phase angle consistency at a given time-frequency point would be to average phase angles across trials, just like it would be done in order to compute ERP or ERSP. Nevertheless this procedure is wrong.

Top left panel in Figure 14 shows 2 phase angles at the same time-frequency point (blue and green vectors), which are fairly close to each other (near the polar axis at 0). The *average vector* (black) clearly captures this relationship. In contrast, *averaging values in radians* fails at describing the relationship between these 2 phase angles (red

[19] Not from real data

vector at 180º). This simple exercise shows how this seemingly correct procedure bears a wrong description of the relationship between phase angles across trials. Lower panel in Figure 14 shows 30 trials (blue lines, same as in Figure 6) and their average in radians (red line) over time. Despite its apparent exactitude, mean phase angle (red line, bottom panel Figure 14) is not an adequate descriptor of phase-based dynamics across trials. Unwary researchers may fall in this trap.

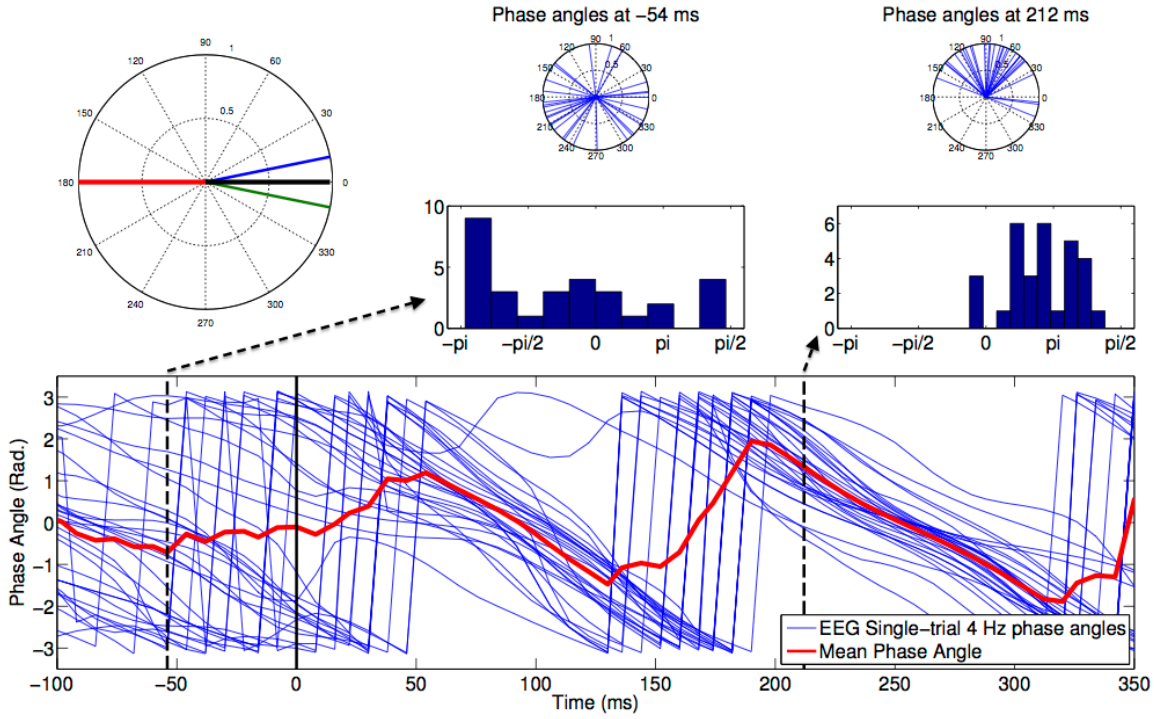

Figure 14 – Estimating inter-trial phase clustering (ITPC). Top left polar plane shows the incorrect way of quantifying phase angle clustering, 2 random phase angles (green, blue vectors) are near the polar axis (0) as represented by the average vector (black vector). The average vector in radians (red vector. 180º, π) does not represent the 2 data vectors (green, blue vector). Lower panel represents the phase angles of 30 trials (blue lines) and their average in radians (red line). Top middle and right panels depict phase angle distributions on polar plane and as histograms at -54 ms (pre-stimulus onset) and at 212 ms (post-stimulus onset). Clear clustering of phase angles can be seen post-stimulus

In contrast, the ITPC measure can effectively quantify the degree of phase angle consistency across trials. First introduced as phase-locking factor (PLF, Tallon-Baudry et al., 1996), this measure is also known as "phase-resetting", "phase-locking", 'inter-trial coherence" (ITC), "cross-trial phase coherence", and many others. I prefer using the term "inter-trial phase clustering" because it implies no functional interpretation of the measure (M. X. Cohen & Gulbinaite, 2014). The use of the word "clustering" is a description of what the measure is actually quantifying with no putative functional interpretations referring to coherence or resetting of ongoing phase.

Similarly to Figure 5 and Figure 8, top middle and right panels of Figure 14 depict phase angle distributions at different time-points. Polar plots and histograms show that pre-stimulus (-54 ms) phase angles are not clustered (top middle panel) whilst post-stimulus (212 ms) phase angles show clear consistency across trials (top right panel). The very simple exercise in Figure 14 shows that computing the average vector (not the phase angle average in radians) provides a good measure of the degree of the distribution of phase angles across trials.

The further the distance between phase angles at a given time-frequency point across trials, the smaller the average vector length will be. Top right panel in Figure 15 exemplifies this concept. Unit-length vectors were arbitrarily generated (blue, green). On the one hand, blue vectors are rather far from each other; the length of their average vector is ~0.17. On the other hand green vectors are close to each other; the length of their average vector is ~0.75. If these were phase angles taken from convolved M/EEG data from 2 different conditions (blue vs. green) at a particular time-frequency point (e.g. 4 Hz at 200 ms post-stimulus onset), the length of the red average vectors would

represent their ITPC values (Figure 15, top right panel). The direction of the average vectors (red) is interpreted as the "preferred" phase over all considered trials. So, depending on the experimental questions, both ITPC strength (average vector length) and preferred phase angle (average vector direction) could be quantified (VanRullen et al., 2011).

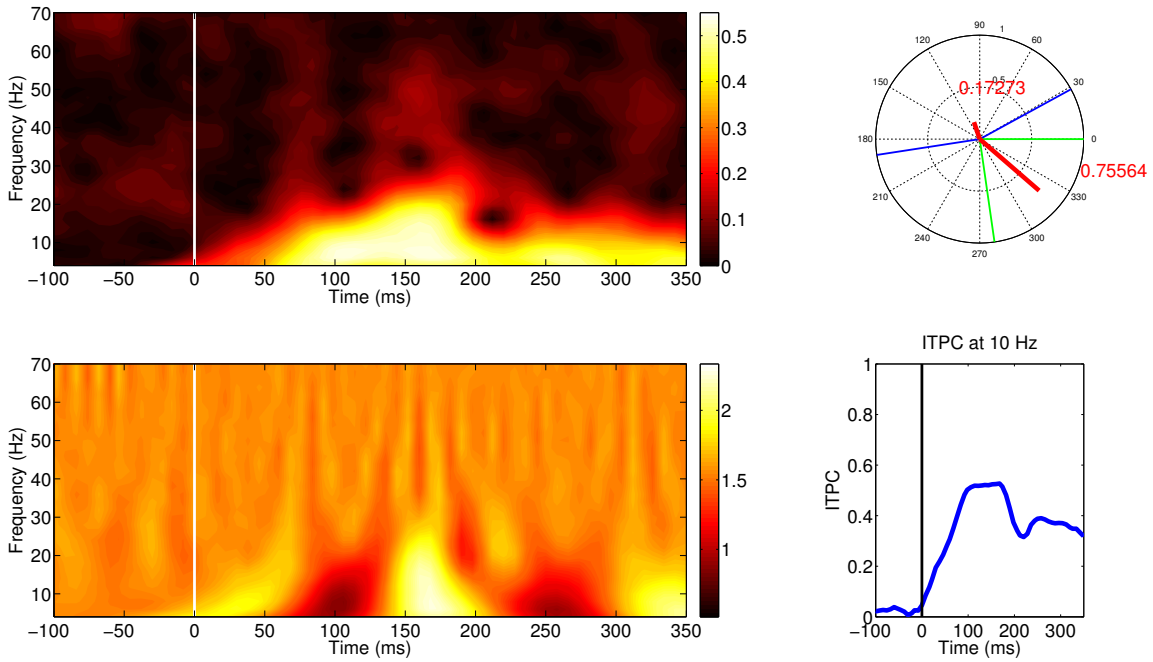

Figure 15 – Estimating the degree of clustering across vectors. Top right panel shows examples of arbitrary unit-length vectors (blue, green) and the length of their average vectors (red vectors, values) as a descriptor of their proximity. Bottom right panel depicts ITPC for all time-points at 10 Hz. Top left panel shows ITPC calculated for all time-frequency points over 70 trials in channel PO8 for a randomly selected subject. Bottom left panel shows ITPC calculated with a formula error. Left panels data is auto-scaled

Moreover, an ITPC time-course can be computed using all time-points at a given frequency. Bottom right panel in Figure 15 shows the time-course of ITPC for all time-points at a given frequency (~10 Hz). When using real data, is preferable to calculate

ITPC for all available time-frequency points, generating a time-frequency representation of ITPC (top left panel Figure 15).

Importantly, ITPC is bounded from 0 to 1. Evenly distributed phase angles across the polar plane result in ITPC with value of 0. In contrast, two identical signals have perfect synchrony; ITPC will be 1. Therefore, ITPC cannot be negative nor can go beyond 1. Bottom left panel in Figure 15 depicts an incorrect computation of ITPC, where the *average of the absolute values* was taken resulting in numbers larger than 1.

Functional Interpretation of ITPC

In contrast to other phase-based measures of brain activity such as coherence (Carter, 1987), ITPC is mostly independent from spectral power (J.-P. Lachaux, E. Rodriguez, J. Martinerie, & F. J. Varela, 1999). ITPC thus deserves a functional interpretation that is different from that given to power-based measures[20]. Furthermore, as suggested earlier, ITPC is an adequate companion metric to power-based measures of brain function.

As discussed earlier, the computation of ITPC uses phase angle information obtained from the analytic signal of neurophysiological data. Mathematically, ITPC provides a measure of the clustering of the timing of band-specific neural activity across trials. Thus, the phase of frequency-band specific activity can be quantified. An increasing amount of empirical evidence indicates that phase synchronization in cortical networks reveals the timing of population-level dynamics; thus playing a central role in the functional coordination of neural communication and processing (Fries, 2005; J. M. Palva et al., 2005; Uhlhaas et al., 2009; VanRullen et al., 2011; F. Varela et al., 2001).

[20] This argument also applies to other phase-based measures of brain function (e.g. Stam et al. 2007; Vinck et al 2012; Lobier et al. 2014)

Oscillatory phase indicates the signal's position within an oscillation cycle (F. Varela et al., 2001). ITPC can be thus interpreted as providing an account of the functional state of the underlying neural networks generating the measured signal. In other words, if high phase-consistency is measured across trials for a given cognitive act or perceptual state it can be argued that the underlying neural populations are engaged in similar or potentially the same functional configurations. Recurrent functional network organization can be thus indicative of relevant neurobiological events, such as the maximization of information processing (F. Varela et al., 2001). The influence of oscillatory phase on neural processing has been known for a long time using *in vitro* recordings (Calvin & Stevens, 1967). More recently, *in vivo* recordings have shown that oscillatory phase determines neuronal firing (Fries, Neuenschwander, Engel, Goebel, & Singer, 2001) and that it is a robust indicator of neuronal activation (Vinck et al., 2010). Finally, it has been shown that transient synchronization of large populations of neurons, as the ones measured by phase-based M/EEG metrics, is less metabolically demanding (Buzsaki & Draguhn, 2004) an important evolutionary constrain for a neurobiological mechanisms supporting cognition.

Summary

In order to quantify the amount of phase consistency across trials at specific time-frequency points, I used the ITPC measure. Phase-based measures are an excellent companion metric to descriptors based on spectral power. Phase-based synchronization has been suggested as an important mechanism for the integration and computation of information in neural systems (Fries, 2005). Moreover, it has been argued that is at the

level of large-scale network activity where phase synchronization can be a key mechanism underlying top-down and bottom-up processes (F. Varela et al., 2001). Thus, ITPC can be conceptualized as a measure of recurrent functional states among neural networks underlying a given cognitive act.

The cognitive electrophysiology literature is full of highly interesting theoretical questions and fantastic experimental manipulations. However, only superficial analyses are often performed on such rich datasets. Therefore, in order to better provide an account of the neurobiological mechanisms underlying cognition, it is of prime importance that cognitive electrophysiologists concomitantly quantify the phase and power of neurophysiological signals.

2.3 Functional Connectivity Dynamics in the Time-Frequency Domain

In the previous sections I have described and discussed measures of brain activity that are particularly concerned with local activity. ERPs are a very robust measure with excellent temporal resolution. Moreover, they are simple and inexpensive to compute, making them an accessible, 'bread and butter' measure. In contrast, time-frequency domain measures such as ERSP and ITPC provide a better opportunity to link findings across species, levels, and methods. Although their temporal resolution gets decreased when compared to that of ERPs, time-frequency domain measures provide a rich description of temporal brain dynamics.

Gray, Konig, Engel, and Singer (1989) showed that high-frequency activity in the beta and gamma ranges (20 – 80 Hz) reflects an alignment in the action potentials generated by cortical neurons. Since that milestone, it has become widely accepted that

synchrony within these frequency bands plays an important role in establishing functional integration between distributed neural sources.

Thus, in order to better asses the functional role of oscillatory brain activity in cognition, electrophysiologists must consider not only exploring single-sensor time-frequency activity. Thus connectivity analyses promise to be of great use for the future of cognitive electrophysiology. Functional connectivity measures will be understood in this dissertation as any quantification of more than one signal at a time. This is, as operationalized in this dissertation, functional connectivity measures will quantify:

i. *Time-frequency domain signals measured at different sensors*. This kind of connectivity refers to correlations quantified by power- or phase-based measures of brain function between different electrodes (Friston, 1997; F. Varela et al., 2001). Thus, theory-driven or exploratory analyses of within- or between-frequency power or phase connectivity can be performed (i.e. power-power, phase-phase, and phase-amplitude coupling). The main goal behind this kind of analysis is to test relations between a particular time-frequency point measured at a sensor and the same time-frequency point measured at a different sensor (see inter-site phase clustering, section 2.4.1). The logic behind this kind of analysis relies on (i) the concept of inter-regional neural synchronization as a mechanism for the functional integration and computation of information within and between neural networks (Fries, 2005; Uhlhaas et al., 2009; F. Varela et al., 2001) and (ii) the concept of oscillatory activity as a multiplexing mechanism for the processing and communication of information (see cross-frequency coupling, section 2.4.2)

(Akam & Kullmann, 2010; Canolty & Knight, 2010). This latter point makes this type of connectivity analysis the most compatible with analyses performed in the time-frequency domain (e.g. ERSP and ITPC, sections 2.3.1 and 2.3.2). Nevertheless, a disadvantage is that the number of statistical tests that have to be made increases exponentially. Take into account that in time-frequency domain analyses, statistical tests have to be performed at each time-frequency point per electrode (see 3. Methods). When analyzing functional connectivity in the time frequency domain, statistical tests have to be performed at each time-frequency point for each pair of electrodes. Thus, mass-bivariate approaches increase the possibility of finding false-positives due to the increased number of comparisons needed. In this dissertation an approach based on multi-linear regression was used in order to address this issue (see 3. Methods). Several alternative methods can be applied in order to deal with the increased dimensionality intrinsic to these analyses. Reviewing and discussing them is outside the scope of this dissertation (for alternative methods see Maris, van Vugt, & Kahana, 2011; Morup, Hansen, & Arnfred, 2008).

ii. *Multiple signals in the time-frequency domain from multiple sensors*. Connectivity can be measured using more straightforward methods. For example a single global measure of connectivity can be computed by averaging power- or phase-based measures computed intra- and inter-electrode. Another possible measure is to use a measure called "global field power" or "global field amplitude", computing using the standard deviation across electrodes (Lehmann

& Skrandies, 1980; Rousselet, Husk, et al., 2008). Simple connectivity techniques such as global means or global field amplitude (Lehmann & Skrandies, 1980; Rousselet, Husk, et al., 2008) can provide several advantages. First, when no specific hypothesis can be made due to experimental design constrains or lack of theoretical background[21], the aggregation of multiple signals from multiple sensors can be used to provide a global description of the data. These global descriptions, although rough and unspecific can be used as a first exploratory step towards the formulation of hypotheses. Moreover, global measures are a simple way to reduce the intrinsic increased dimensionality of connectivity analyses, avoiding an inflated and inconvenient number of multiple comparisons. Even though their simple nature obscures possible physiological interpretations, global measures are a suitable, simple, and safe "first pass" measure for connectivity analysis. Since the analyses in this dissertation were based on multi-linear regression (see 3. Methods) I did not use global measures; this type of connectivity analysis will not be further discussed.

iii. *Two different time-frequency domain signals measured at the same sensor*. This type of connectivity analysis is based on a variation of ITPC and ERSP (sections 2.3.1 and 2.3.2). These measures assume that frequency band-specific activity quantified at a sensor carries independent information. The logic behind this assumption relies in the hypothesis that the functional role of oscillations is to serve as a multiplexing mechanism for information transmission and processing

[21] This might be the case in some understudied topics

within and between neural networks (see cross-frequency coupling, section 2.4.2). Thus, different frequency points measured at a single electrode are tested for correlations across time. Hypothesis-driven and exploratory analyses can be carried out between phase (i.e. phase-phase coupling) or power measures (i.e. power-power coupling). Moreover, a very popular approach has been to test for relations between low-frequency phase and high-frequency amplitude. This kind of cross-frequency method is known as phase-amplitude coupling and has been, by far, the most studied type of cross-frequency connectivity analysis (Canolty & Knight, 2010). In this dissertation, phase-amplitude coupling was used a measure of same-sensor connectivity.

In summary, functional connectivity measures in the time-frequency domain can be based on power and/or phase and may use a wide variety of linear and non-linear methods (for a review of linear methods see Makeig et al., 2004; for a review of non-linear methods see Pereda, Quiroga, & Bhattacharya, 2005). As all metrics in neuroscience, functional connectivity measures have clear advantages and disadvantages. In the following sections, I will discuss the main properties of the connectivity measures I used in this dissertation. Importantly, it is impossible to define a "correct" or "best" functional connectivity measure. Even in controlled situations (e.g. modeled data, EEG/fMRI data) it has been shown that no measure of functional connectivity will outperform all other ones in every domain (David, Cosmelli, & Friston, 2004; Wendling, Ansari-Asl, Bartolomei, & Senhadji, 2009). Thus, experimental designs, hypothesis to be tested, and details of the data should be taken into account when choosing a particular

functional connectivity measure. In this dissertation I followed two simple rules to choose my connectivity metrics:

i. *Choose metrics that have been previously used in the literature*. Since this dissertation presents a mixture of hypothesis-driven and exploratory analyses. Connectivity analyses are mostly of exploratory nature, since these kinds of analyses have been neglected from literature. Thus, using previously used connectivity measures was the safer choice

ii. *Choose metrics that can be easily linked to well understood neurobiological mechanisms*. A big risk of performing exploratory analysis is to end up with unintelligible results. In this dissertation, the present experimental design was carefully made (see 3. Methods). The stimuli were explicitly controlled in order to answer a specific question. Therefore, this dataset is appropriate for exploratory data analyses. However, since no many precursor studies to ours exists nowadays, using connectivity measures that can be link to well understood neurobiological mechanisms was the safe choice

Thus, in this dissertation, two connectivity measures were used. The following sections will describe and discuss Inter-Site Phase Clustering (ISPC) and Cross Frequency Coupling (CFC).

2.3.1 Inter-Site Phase Clustering (ISPC)

Like many time-frequency measures, ISPC can be found in the literature with a plethora of names. “Phase-locking value”, “phase synchronization”, “phase-locking statistic”, and “phase coherence”, are terms often used in the literature to refer to the clustering of phase angle differences between electrodes in polar space. Therefore, following the “theory-free” measure-naming strategy that I am adopting in this dissertation, the term Inter-Site Phase Clustering (ISPC) will be preferred (M. X. Cohen & Gulbinaite, 2014).

In this dissertation I chose phase-based connectivity analyses because they are a natural complementary extension to inter-trial phase clustering (ITPC). As shown in Equation 12 and Equation 13, ISPC is the spatial version of ITPC. Therefore, much of what was said about ITPC in section 2.3.2 can be applied to inter-site phase clustering (ISPC). Thus, like ITPC, functional interpretation of phase-based connectivity metrics is straightforward. The main logic behind quantifying phase-based connectivity is that high-level cognitive processes such as decision-making, relies on the dynamic recruitment of distant neural populations (O. Sporns et al., 2004; F. Varela et al., 2001). Thus, when large-scale functional networks become active, oscillatory activity emerging from them can be described as synchronized at specific time-frequency points. Importantly, as mentioned earlier, phase synchrony has been suggested as an important mechanism for functional information integration and computation in neural networks using *in vitro*, *in vivo*, and computational models (Fries, 2005, 2009; F. Varela et al., 2001).

The fact that phase-based connectivity analysis can be easily interpreted in a plausible neurobiological framework has positioned them as widely used measures of functional connectivity[22]. Thus like ITPC, one of the main advantages of inter-areal phase connectivity metrics relies on its functional interpretation. Furthermore, phase-based measures have been used in a wide range of species and levels (e.g. Fries, Neuenschwander, et al., 2001; Schroeder & Lakatos, 2009b; F. Varela et al., 2001; Vinck et al., 2010). Therefore, results obtained with M/EEG signals can be linked to network dynamics at different temporospatial levels and species.

It was mentioned before that the main assumption of ITPC is that event-related changes in connectivity will produce a re-alignment of the distribution of phase angles across trials at specific time-frequency points (J.-P. Lachaux et al., 1999). Such assumption adds a strong constraint to phase-based connectivity measures; there must be inter-areal consistency of phase-angle differences across trials. Thus, another advantage of computing an inter-areal phase angle consistency measure is that it provides strong evidence for task-related changes in connectivity.

A further advantage is that just like ITPC, ISPC is computed at each time point. This means that apart from the wavelet-related temporal smoothing (see 3.5 EEG data analysis), no further loss in temporal resolution exists. In contrast to ITPC that is bounded from 0 to 1 indicating homogeneous phase distribution across the complex polar plane or clustering at a "preferred phase", ISPC quantifies the amount of phase angle clustering

[22] This statement is certainly true for invasive recordings using humans and animal models. Sadly, the cognitive electrophysiology literature still lags far behind is this kind of analyses.

differences between channels across trials. Moreover, baseline normalization procedures are needed in ISPC. Therefore, there is no such bound.

Left and right columns in Figure 16 compare uninformative single-trial phase angles from 2 different channels (PO8, left. O2, right). No real differences can be described between phase angles at the single-trial level. The average difference between single trials provides a better account of the consistency of phase angles between these 2 channels.

Top middle panel in Figure 16 depicts the mean phase angle differences between channels PO8 and O2 (topographic map). Nevertheless, in order to quantify the amount of event-related phase consistency across trials between different sensors, it is necessary to adjust for pre-stimulus phase angle consistency. Thus, as mentioned before in order to compute ISPC baseline normalization is required. Bottom middle panel in Figure 16 depicts ISPC between channels PO8 and O2 (topographic map). ISPC quantifies the amount of event-related phase angle consistency that cannot be seen in the mean phase angle differences. An important discussion point is that mean phase angle differences (top middle panel Figure 16) describes ongoing EEG phase activity while ISPC removes it. Although, baseline-subtracted measures of phase-based are usually recommended as a measure (M. X. Cohen & Cavanagh, 2011; J.-P. Lachaux et al., 1999), other metrics can be used in other to test for phase consistency of ongoing oscillations (e.g. Phase Bifurcation Index. See Busch, Dubois, & VanRullen, 2009). Since no hypothesis-driven questions about ongoing oscillatory phase were made in this dissertation, ISPC will be the preferred phase-based connectivity metric.

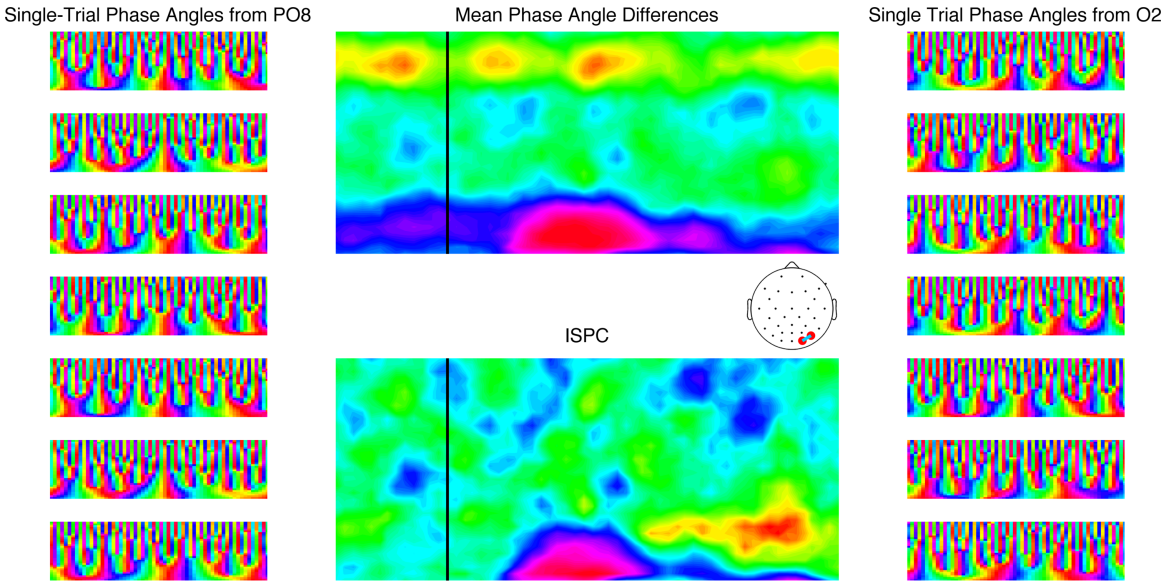

Figure 16 – The effect of baseline correction on ISPC. Left and right columns display time-frequency representations of phase angles single trials (bounded π, -π). Middle column shows time-frequency representations of the mean phase angle differences between both channels (top) and the inter-site phase clustering (ISPC) between both channels (bottom). Mean phase angle, by definition, has no baseline procedures while ISPC, by definition, is baseline-corrected

The main disadvantage of phase-based measures of connectivity is that it is very difficult to provide compelling evidence for any interpretations based on signal directionality. Although some techniques such as Granger "causality" have been developed in order to address this question (Oostenveld, Fries, Maris, & Schoffelen, 2011; Seth, 2010), skepticism still exists about the possible usage of such techniques in cognitive electrophysiology. Furthermore, newer metrics based on information theory have been recently suggested as a good approach to resolve this issue (Lobier, Siebenhuhner, Palva, & Palva, 2014). In this dissertation I attempted no directionality analyses using phase-based connectivity. Therefore this issue will not be further discussed.

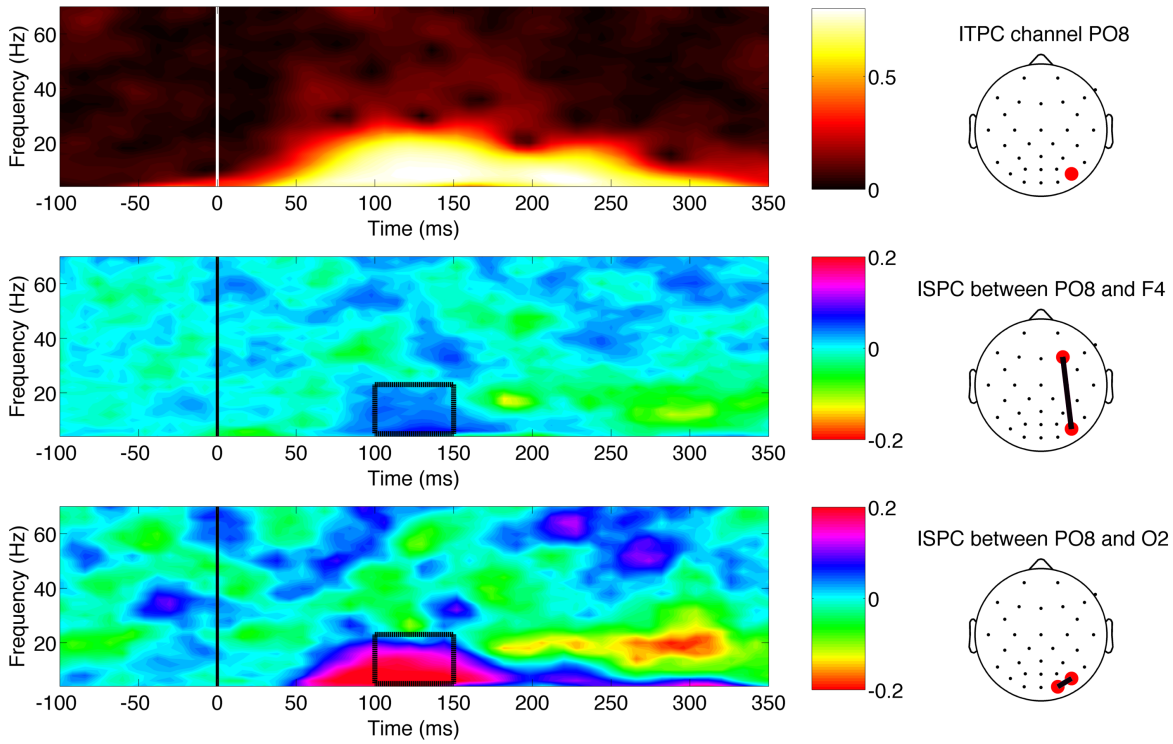

Figure 17 – Comparison between inter-trial phase clustering (ITPC) and inter-site phase clustering (ISPC). Top left panel depicts a time-frequency representation of ITPC for channel PO8 (red dot in headmap). Middle panel depicts a time-frequency representation of ISPC between closely located channels PO8 and O2 (red dots in headmap). Middle panel depicts a time-frequency representation of ISPC between spatially apart channels PO8 and F4 (red dots in headmap). Color-coded lines indicating strength of connection between channels as quantified by ISPC can be seen in both ISPC headmaps (middle and bottom right). Black square signals the time-frequency points used to compute headmap

Another relevant disadvantage is the potential confound posed by volume conduction. Spurious connectivity results can be obtained due to volume-conducted signals. It is well known that active brain networks would generate large electromagnetic fields. Such spatially large fields will be measured by more than 1 M/EEG sensor. Thus, highly autocorrelated data will be measured at the electrode level. Middle and bottom panels of Figure 17 compare the amount of phase clustering between contiguous and distant electrodes. Data from one randomly selected subject was used. Middle and bottom panels depict ISPC across trials between PO8 and two different electrodes. First, I

computed ISPC across trials between the posterior channel PO8 and the anterior channel F4. The results are shown in the middle panel in Figure 17. It is not expected to find much similarity between such distant channels. Thus, the amount of phase clustering across the randomly selected trials (N=100) is low (in the range of ~0.1). Further, I calculated the amount of phase clustering across trials between the posterior channel PO8 and the contiguously located channel O2. Figure 17 (bottom panel) shows a time-frequency representation of ISPC for contiguous electrodes. It is expected to find a large amount of phase clustering from this simple exercise. Even when calculated using only 100 trials, ISPC is much higher between contiguous electrodes than between distant ones (in the range of >0.2). This simple exercise demonstrates the effect of autocorrelations at the sensor level when computing ISPC.

There is no evidence for robustness and congruency of results between phase-based connectivity measures. The primary reason for the lack of literature in the subject is that non-linear measures of temporal brain dynamics are not commonly used in cognitive electrophysiology. A comparison between ISPC and 3 different phase-lag-based measures (i.e. phase-lag index (PLI. Stam, Nolte, & Daffertshofer, 2007), weighted phase-lag index and de-biased weighted phase-lag index (wPLI, dwPLI. Vinck, Oostenveld, van Wingerden, Battaglia, & Pennartz, 2011)) was performed in order to explore the functional role of phase-based inter-areal connectivity. Results show that although slight differences exist, possible due to volume conduction, phase-lag measures show more robustness. However, ISPC results are congruent with the phase-lag (Parada, Moravec, Emerick, & Busey, in preparation). Our results further suggest that the exploration of zero phase-lag cortical brain dynamics is a phenomenon worth studying

(Uhlhaas et al., 2009). In this dissertation ISPC was used since it is the natural extension to ITPC. Therefore phase-lag measures will not be further discussed.

Figure 17 also illustrates the differences between ITPC and ISPC. Data from channel PO8 was used in order to quantify the degree of phase angle clustering at a single channel. ITPC describes phase angles broadly clustered in time and frequency, extending from ~50 to ~300 ms in time and encompassing theta, alpha, and beta ranges in frequency. Moreover, maximal clustering in the alpha range occurs at two different time-points, first between ~100 and ~150 ms and then between ~200 and ~250 ms. In contrast, ISPC provides an insight into phase dynamics across electrodes, revealing similar features as ITPC (e.g. low frequency phase consistency between ~150 and 200 ms), time-frequency-specific features (e.g. ~20 Hz beta phase clustering before 200 ms).

2.3.2 Cross-Frequency Coupling (CFC)

Cross-frequency coupling is a non-linear method that allows cognitive electrophysiologists to quantify the statistical relationship of brain activity between different frequency bands. Such relationships can be described between power spectrums; as the power of one signal fluctuates in time, so does the power of the other in a correlated way. This type of interaction is known as amplitude-amplitude or power-power coupling (Friston, 1997). Another way computing CFC is by correlating their phase dynamics. Thus, the phase of one signal modulates the phase of the other. This kind of interaction is known as phase-phase coupling, *n:m* phase-locking, and *n:m* phase synchrony (J. M. Palva et al., 2005; Tass et al., 1998). A third kind of interaction involves the phase of one signal modulating the power of another. It is physiologically assumed

that slow frequencies drive faster ones, although the reverse interaction could also happen theoretically (Canolty & Knight 2010). This type of interaction is known in the literature as phase-amplitude coupling (PAC).

Different methods have been suggested for the calculation of cross-frequency interactions. For example, Penny, Duzel, Miller, and Ojemann (2008) proposed a method that uses the general linear model to test if variance in phase explains variance in power. Another approach is based on the generation of phase bins and testing the uniformity of power distribution across those bins (Tort, Komorowski, Eichenbaum, & Kopell, 2010). The biggest disadvantage of these and other methods is that it requires the integration of data points across a pre-defined window. Furthermore, in order to improve estimation stability signal-to-noise ratio has to be improved. Therefore, large windows are recommended in order to perform CFC analyses. Unfortunately, event-related processes in EEG change in the order of milliseconds. Therefore, these approaches are not the most optimal for the quantification of event-related cross-frequency coupling.

In this dissertation I implemented the event-related phase-amplitude coupling (ERPAC) measure as described by Voytek, D'Esposito, Crone, and Knight (2013). This method uses circular-linear correlation, linearizing the oscillatory phase (non-linear by default) into its *sin* and *cos* components. In order to perform this operation the CircStat MATLAB toolbox was used (Berens, 2009). Once the phase of a given low frequency has been linearized, correlation can be tested with a high-frequency power (linear by default). Importantly, this procedure allows the estimation of phase-amplitude coupling in a data point-by-data point basis; allowing the exploration of transient changes related to events.

As a measure of connectivity, cross-frequency coupling can be computed within a single channel in order to infer local organization at the sensor level. Moreover, the lower frequency signal can be selected from one channel whilst the high frequency signal can be selected from a different sensor; thus testing for long-range cross-frequency connectivity. The logic behind testing for nested oscillations is based on the concept of multiplexing. Multiplexing is the process of combining multiple signals of information into a single channel for its transmission. Importantly, the different signals can be independently recovered from the multiplexed channel; serving as a mechanism for selective communication in telecommunication systems (Weinstein & Ebert, 1971). In neuroscience, the concept of multiplexing has been often used as a putative mechanism of information representation. Thus, multiplexed neural coding has been suggested as the neural mechanism underlying a plethora of cognitive functions; from the binding of object features (Singer, 1999) to the emergence of consciousness (Doesburg, Green, McDonald, & Ward, 2009). Thus, cross-frequency interactions have been of interest for neuroscientists due to its physiological plausibility. The tight relationship between nested oscillations as a neurobiological mechanism for information communication and processing is its main advantage. CFC has been reported using a variety of species and methods (Canolty & Knight, 2010), including the human cortex (Canolty et al., 2006). Recently, Canolty et al. (2006) recorded 64-channel electrocorticogram (ECoG) from human subjects. Distinct cognitive, sensory, and motor tasks were performed. Results showed high gamma (80 – 150 Hz) functionally coupled with theta phase (4 – 8 Hz) for the first time in human cortical recordings. Remarkably, this CFC was task-dependent and significantly present in most electrodes in different cortical areas. This supports

earlier reports of CFC in different species and brain regions, leading to the idea that phase-amplitude interactions might play a vital role in linking functional systems across time and space scales.

Importantly, there is evidence that low-frequency oscillatory phase facilitates cortical computation through the dynamic coordination of spike timing (Buzsaki & Draguhn, 2004; Womelsdorf & Fries, 2007). Moreover, it has been shown that phase-amplitude CFC can suppress and facilitate cortical processing. For example the phase of theta can enhance spike transmission between synchronized brain regions, which triggers an increment in gamma-band amplitude and a corresponding processing of information (Womelsdorf and Fries 2007). Further, inhibition could be easily exerted over synchronized populations by phase-resetting active networks, hence destroying the time-locked interaction. Thus, it might well be the case that the phase of low-frequency oscillations enslaves the power of high-frequency ones in order to facilitate information processing (Schroeder & Lakatos, 2009a). These and other results (reviewed in Canolty & Knight, 2010) support the idea that slow frequencies can be dynamically entrained by external and endogenous processes in order to become an action-oriented predictive system (Schroeder & Lakatos, 2009b). Thus, recently, CFC analyses of connectivity have been increased interest in neuroscience. However, not many studies have explored the functional role of CFC in cognition using non-invasive methods.

As most connectivity measures, the main disadvantage of CFC is the increased number of multiple comparisons to be performed, which can be in the order of hundreds per channel, per time point. Consider that in order to test for theta-gamma phase-amplitude coupling, tests have to be performed for the selected theta range and power at

all subsequent frequencies (e.g. 20 to 100 Hz) at all channels and time points. Thus, the search space for CFC is extremely large and requires appropriate statistical and multiple comparison correction methods, which are not commonly used in the cognitive electrophysiology literature (see 3.6 Statistical Testing).

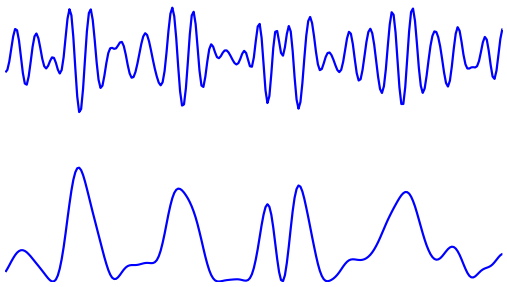

Figure 18 – Putative cross-frequency interaction at the single trial level. Top panel depicts the time-course of low-pass filtered EEG signal at 25 Hz. Bottom panel shows power at 25 Hz. Clear power 'bursts' can be seen suggesting that 25 Hz power might interact with a lower frequency signal. Cross-frequency coupling test the robustness of these interactions across trials

A second disadvantage is the lack of previous findings in the cognitive electrophysiology literature, which makes it really hard to interpret current results if no specific manipulations have been made by the experimenter. Thus, for now and in the near future, the success of exploratory CFC analyses in cognitive electrophysiology will mainly rely on the quality of experimental designs. In this dissertation we have carefully crafted an experimental paradigm that allows me to ask specific questions (see 3. Methods). Moreover, by using multi-linear regression I have implemented a data-driven dimensionality reduction (see 3. Methods). Therefore, exploratory analyses can be safely performed on these data.

Cross-frequency interactions can be anecdotally seen in band-passed data. Figure 18 depicts a 25 Hz low-pass filtered single EEG trial (top panel). In the filtered signal small 'bursts' of power can be seen where the amplitude of the signal increases rhythmically. Furthermore, power at 25 Hz was extracted from the filtered signal (bottom

panel). When power is computed, the suspicion of cross-frequency interactions becomes even stronger. The bottom waveform in Figure 18 depicts clear rhythmic bursts of power. Remember that this waveform was created from a randomly selected EEG trial. Thus, cross-frequency interactions can be (anecdotally) seen even at the single trial level. Several approaches can be employed in order to test for nested oscillations. Since the search space is so big[23] and limited evidence is available for the generation of specific hypotheses, a mixed hypothesis-driven and exploratory approach has been primarily used (M. X. Cohen, 2008). This mixed approach uses a priori-defined low frequency oscillation while the rest of the high frequency space is used to search for relations. Generally, the low frequency is set a priori while high frequencies are explored, however there are no restrictions to arbitrarily choose a high frequency in order to explore the low frequency space (M. X. Cohen, 2008). Top left panel in Figure 19 shows the result of semi-exploratory CFC approach. Theta phase at 6 Hz was chosen while a wide range of frequencies (16 to 70 Hz) was used for power in order to compute phase-amplitude coupling. This semi-exploratory analysis suggests that for this arbitrarily chosen group of trials (N=200), for this particular subject, in channel PO8, for a pre-defined window (170 to 470 ms post-stimulus onset), gamma power (~30 Hz and >55 Hz) is coupled to theta at 6 Hz (Figure 19, top left panel).

In contrast, a completely hypothesis-driven approach could be taken, where 2 specific frequency bands are tested for correlations. Bottom left panel in Figure 19 depicts the results of hypothesis-driven CFC. The phase of theta at 6 Hz and the power of gamma at 30 Hz were arbitrarily chosen in order to compute CFC over time points. This strategy

[23] Usually in the order of subject x frequency x frequency x electrode x condition x time

has several advantages, most importantly increased statistical power. Potentially, hypothesis driven CFC can be calculated over a pre-defined window (e.g. 260 – 380 ms) and no corrections for multiple comparisons would have to be performed. However, in bottom left panel of Figure 19, hypothesis-driven CFC was computed over time points. Thus, a time-series of cross-frequency interaction can be obtained for the 2 frequencies of interest. The main disadvantage of this approach is that it might miss significant interactions among other frequencies. Moreover, this approach cannot resolve if the cross-frequency effect is specific to the 2 selected frequencies or corresponds to a more wide broadband effect.

Furthermore, a completely exploratory approach can be used where all frequencies are tested for correlations using all other frequencies at specific time-windows or over time. The obvious disadvantage of this approach is the inflated amount of statistical tests to be performed. Potentially, statistical tests would be performed over frequencies and over time, which can rise to the order of hundreds per electrode. Right panels in Figure 19 depict a frequency-frequency representation of cross-frequency interactions computed over a pre-defined window (e.g. 260 – 380 ms). Inset rectangles in Figure 19 present top left panel CFC in context of time (bottom left panel) and frequency (top right panel). This simple exercise shows that the exploratory approach allows uncovering other relationships that both hypothesis-driven and mixed approaches would have missed.

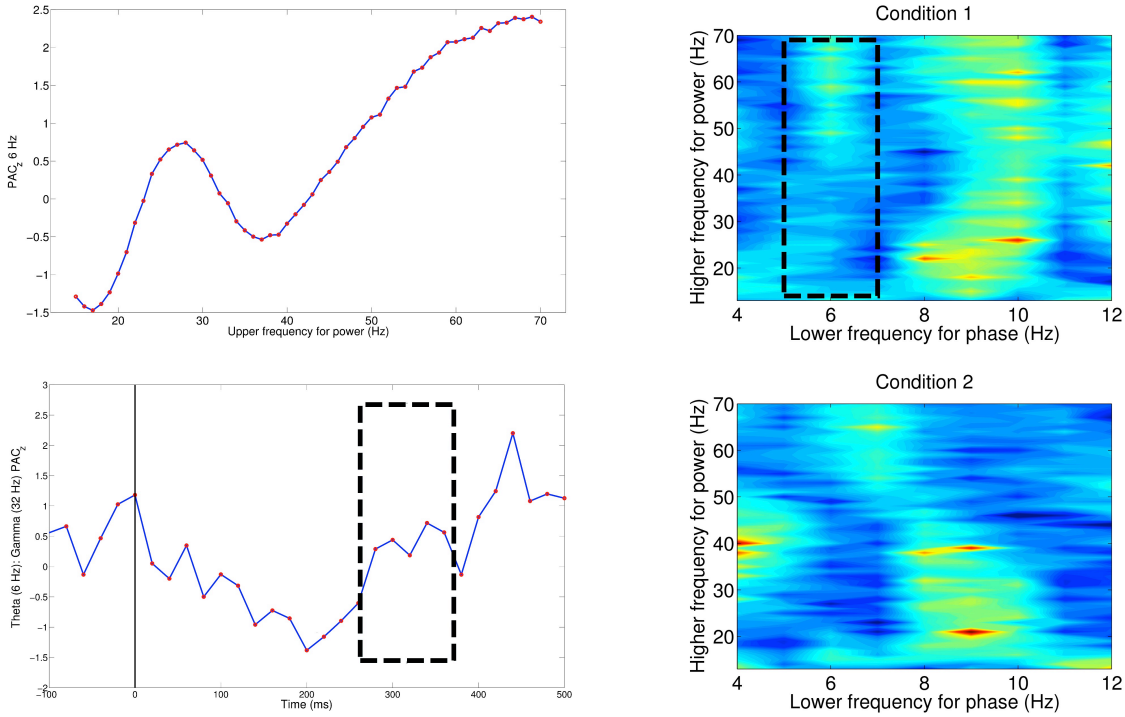

Figure 19 – Example of the 3 different approaches to compute cross-frequency coupling. Data from 200 trials from channel PO8 from 1 randomly selected subject was used in order to compute phase-amplitude cross-frequency coupling (CFC). Top left panel depicts the results of mixed CFC approach (see text) computed over a pre-defined time window (260 – 380 ms). PAC between a pre-defined low frequency phase (6 hz) and a wide range of high-frequency power (16 – 70 Hz) was computed. Bottom left panel depicts the results of hypothesis-driven CFC approach (see text) computed over time. A pre-defined low-frequency phase (6 Hz) and a pre-defined high-frequency power (30 Hz) were chosen to compute PAC. Right panels depict the results of exploratory CFC approach (see text) computed over a pre-defined time window (260 – 380 ms). PAC was computed between a range of low-frequency phase (4 – 12 Hz) and a wide range of high-frequency power (16 – 70 Hz) for 2 different conditions. Inset rectangles indicate where the results presented in top left panel fit in context of time (bottom left panel) and frequency (top right panel)

Currently, CFC analyses are so novel in the cognitive electrophysiology literature that very few previous studies can be found (in some cases, none) so as to draw strong hypotheses. Thus for now most studies will benefit from exploratory and mixed approaches more than hypothesis-driven. It is of utter importance to use appropriate statistical methods in order to use the exploratory and mixed CFC approaches. In this

dissertation I chose to use a semi-exploratory approach (see 3.5.1 Analysis of linear measures).

2.4 Linear Modeling of EEG Measures

The cognitive electrophysiology literature is mostly composed of studies based on simple categorical designs quantifying brain activity using ERPs at the group level. Thus, hundreds of studies can be simply summarized: at some point between 100 and 300 ms the peak or trough of an ERP component for a condition differs from the peak or trough measured on the opposite condition. Although this approach has been clearly useful (Luck, 2005), modern statistical approaches and increased computation power have allowed neuroscientists to implement more appropriate analysis routines, providing a relevant opportunity to improve cognitive electrophysiology as a field (Litvak et al., 2011; Makeig et al., 2004; Maris & Oostenveld, 2007; Rousselet & Pernet, 2011; Wilcox & Keselman, 2003).

Accumulating evidence suggests that exploring time series can provide insights to interesting dynamics related to information processing. Such dynamics are lost when analyses are confined to peaks, troughs, and/or pre-defined windows. For example, VanRullen and Thorpe (2001) used a dual-task design and quantified the time-course of perceptual decision-making. Analyzing the time course of ERPs allowed them to dissociate early activity related to the processing of low-level characteristics of the stimuli while separating activity independent of low-level visual processing, probably linked to decision-making (VanRullen & Thorpe, 2001). Philiastides et al. (2006) quantified the content of information associated to perceptual classification carried by

single-trial ERP time series in a categorization task. Using logistic regression they uncovered temporal dynamics of perceptual categorization at the single-trial level, separating components linked to perception and decision (Philiastides et al., 2006). Similarly, van Rijsbergen and Schyns (2009) used reverse correlation between stimuli and ERP waveforms in order to uncover the temporal evolution of face processing of facial emotion perception. By focusing on time series, they demonstrated that time frames prior to and after the N170 peak are more strongly associated with information processing than the actual N170 peak (van Rijsbergen & Schyns, 2009).

More recently, a similar approach based on information theory was used in order to determine the amount of information encoded by the temporal dynamics of power, phase, and frequency in a facial expression of emotion categorization task (Schyns et al., 2011). These examples demonstrate that temporal dynamics underlying information processing (Philiastides et al., 2006; VanRullen & Thorpe, 2001), accumulation (Philiastides et al., 2006; Schyns et al., 2007), and/or multiplexing (Schyns et al.,

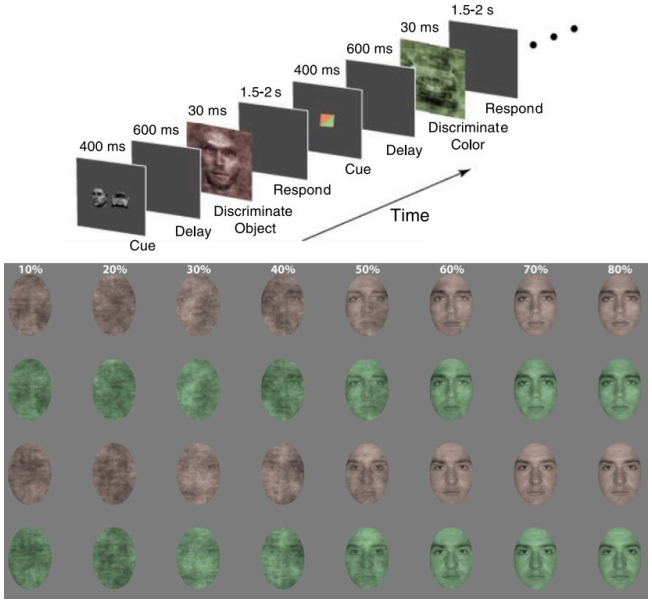

Figure 20 – Top: Schematic representation of experiment 2 in Philiastides et al. (2006). Different decisions (color/category) were made using the same evidence provided by face and car images with 2 different levels of phase coherence (30, 45%). Bottom: Stimuli used in Rousselet et al. (2011). Different decisions (color/identity) were made using 8 different levels of phase coherence (10-80%)

2011) can be examined when using appropriate analyses and experimental methods. Moreover, it has been argued that in order to uncover electrophysiological mechanisms of information processing and transmission, a single-trial analysis approach in combination with parametric and/or dual-task designs should be used (Schyns, 2010; Schyns et al., 2009; Vanrullen, 2011). Therefore, these more rigorous experimental techniques should be preferred by cognitive electrophysiologists in order to dissociate low-level stimulus-driven activity from flexible task-related activation.

In this dissertation, I have implemented a parametric, two-interval, dual-task design that allows dissociating physical stimuli from task requirements. Participants had to make block-wise similarity and discrimination judgments using the same perceptual evidence (see Figure 27 and Figure 28). Manipulating the diagnostic quality of the presented stimuli allowed me to quantify how task demands affect perceptual decision-making. Further, by analyzing time series I was able to quantify when the effects of task demands on perceptual decision-making take place. Previous studies have demonstrated how brain signals are sensitive to different physical stimuli/task (Philiastides et al., 2006; Rousselet, Husk, et al., 2008; Schyns et al., 2007; Schyns et al., 2011; van Rijsbergen & Schyns, 2009). However, very few have focused on quantifying task-related neural activity in the time domain correlated to the perception of the same information (Goffaux, Jemel, Jacques, Rossion, & Schyns, 2003; Philiastides et al., 2006; Rousselet, Gaspar, Wieczorek, & Pernet, 2011; VanRullen & Thorpe, 2001). Moreover, to the best of my knowledge no study has done so in the time-frequency domain.

In order to present the approach taken in this dissertation, let me consider 2 experiments, which were of great influence (Philiastides et al., 2006; Rousselet et al.,

2011). First, in experiment 2 of Philiastides et al. (2006), participants were provided with two stimuli categories (car or face) and used 2 levels of phase coherence (30% and 45%). Task requirements demanded judgments about stimuli's color (green vs. red) or category (car vs. face see Figure 20 top). Among other very relevant findings, the clever manipulation in Philiastides et al. (2006) allowed them to quantify the time course of events linked to perception and decision-making (Philiastides et al., 2006). Second, the manipulation made by Rousselet et al. (2011) implied a dual-decision task based on color (green vs. red) and identity (face 1 vs. face 2). Participants made judgments using 8 different levels of phase coherence (10 – 80%, see Figure 20 bottom). The parametric manipulation of noise allowed them to separately quantify the time course of noise sensitivity and task effects (Rousselet et al., 2011).

These 2 examples (Philiastides et al., 2006; Rousselet et al., 2011) exploit the manipulation of stimuli phase coherence in order to control for task difficulty. Phase coherence has been shown to contain most of the information pertaining object identity (Gaspar & Rousselet, 2009); ERP modulations are therefore expected when manipulating phase coherence. The monotonic relationship between ERP components and phase coherence levels indeed demonstrates this point in Rousselet et al. (2011) and in experiment 1 by Philiastides et al. (2006) (Figure 21). In this dissertation I did not rely on amplitude spectra and explored the neural correlates of judgments based on more subtle stimuli features that might not necessarily elicit ERP differences (Figure 21). I separated task demands and task difficulty from the physical properties of the stimuli by using composite images with equated amplitude spectra mixed in 7 different levels (see Figure 27). Thus, I predicted that no differences would be seen in the ERP measure. I

furthermore predict that measures of brain activity in the time-frequency domain would be a more appropriate descriptor of the neural dynamics underlying perceptual decision-making for the carefully crafted used experimental design.

Furthermore, the present parametric dual-task experimental design allowed me to implement a single-trial approach and express linear measures in terms of sensitivity to stimulus information ($\beta_{w3}\upsilon$), task demands ($\beta_{w1}T1$, $\beta_{w2}T2$), and behavioral outcome ($\beta_{w4}RT$). Thus, I implemented multi-linear regression at the level of single trials per subject represented in Equation 6 and Equation 7 (S. J. Kiebel & Friston, 2004a, 2004b; Litvak et al., 2011; Pernet et al., 2011). Specific factors of the present experimental design were considered and included in the linear model for ERP, ERSP, and ERPAC (see 3.5.1 Analysis of linear measures):

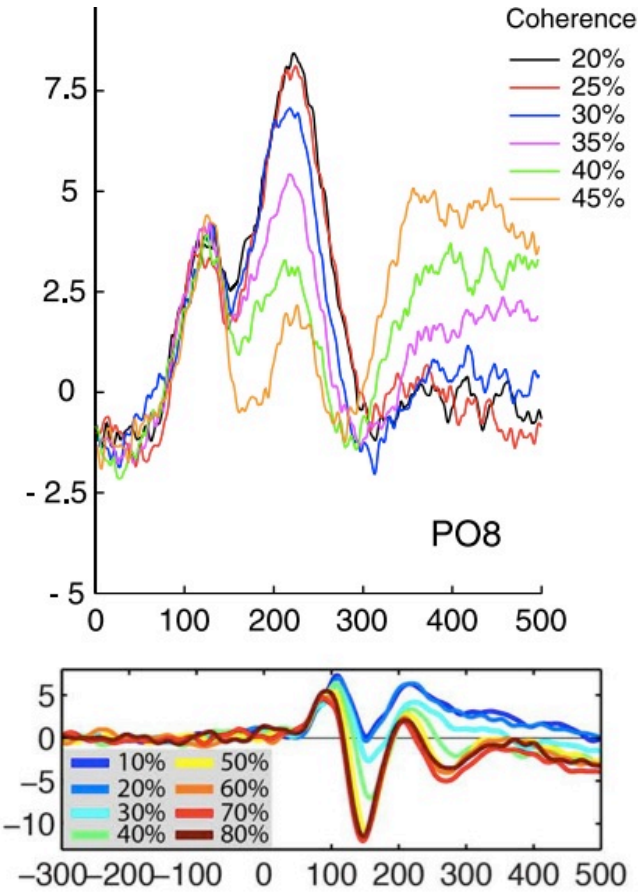

Figure 21 – Many studies confound task difficulty and stimulus properties as evidenced by the monotonic relationship of phase coherence levels as quantified by ERPs. Top: ERPs from Philiastides et al. (2006). Bottom: ERPs from Rousselet et al. (2011)

1. Sensitivity to Stimulus Properties: In order to determine if linear measures were sensitive to stimulus information (i.e. mixture level) in the context of each task, trials were tagged according to Parameter 2 – Test Face Difference and were included in the linear model as 1 regression coefficient ($\beta_{w3}\upsilon$). Using this predictor I thus expect to estimate the effect of stimulus properties over linear measures of brain activity

2. Sensitivity to Task Demands: In order to determine if linear measures were sensitive to different task demands (i.e. similarity vs. discrimination), trials belonging to each decision were separately included in the linear model as 2 regression coefficients ($\beta_{w1}T1$ and $\beta_{w2}T2$). I thus expect to uncover the effects of task demands in linear measures of brain activity. Importantly, this is the only analysis performed using non-linear measures

3. Sensitivity to Behavioral Outcome: In order to determine if linear measures were sensitive to the trial-by-trial behavioral outcome of each subject, I used the time of each button press associated with participants' responses on each trial. Thus, reaction times (RT) were included in the linear model as a single regression coefficient ($\beta_{w4}RT$). I thus expect to uncover EEG features associated with the trial-by-trial variation of participants' response

4. Sensitivity to Stimulus Difficulty: I defined "stimulus difficulty" as the effects of stimulus properties (Parameter 2) over task demands (i.e. similarity vs. discrimination). For task 1 (more car/more face), a "hard" trial would use zero and near-zero values from Parameter 2 while an "easy" trial would use extreme values from Parameter 2. In contrast, for task 2 (same/different), a "hard" trial would use near-zero values from Parameter 2 while an "easy" trial would use extreme and zero values from Parameter 2. Beta weights associated with stimulus information ($\beta_{w3}\upsilon$) were combined with beta weights associated with task demands ($\beta_{w1}T1$, $\beta_{w2}T2$) using Equation 8. I think the combination of task- and stimulus-related regressors provides an appropriate estimation of stimulus information over task demands (βw_{SIT}) as quantified by linear measures

Thus, for the ERP, ERSP, and ERPAC measures, my results will be based on the analysis of the time course of the different regression coefficients described above (see 3.5.1 Analysis of linear measures).

Each regression coefficient will be expressed per measure, per subject, per channel. In order to decrease the search space of electrodes and prevent type I errors, I used the coefficient of determination known as R^2. Furthermore, the usage of R^2 as a dimensionality reduction technique allowed me to prevent circular inferences (aka "double dipping") (Kriegeskorte, Simmons, Bellgowan, & Baker, 2009).

Coefficients of determination (R^2) are a measure of goodness of fit of data points to a statistical model, a linear model in the case of this dissertation (see 3.5 EEG data

analysis, Figure 22). The use of R^2 has been neglected in the field of cognitive electrophysiology. In contrast this approach has been successfully applied by other research groups using different kinds of data (e.g. Logothetis, Pauls, Augath, Trinath, & Oeltermann, 2001). The left panel in Figure 22 depicts the time course of R^2 computed using 200 trials from all electrodes from a randomly selected subject. Right panel in Figure 22 depicts a topographical representation of interpolated R2 values.

As depicted in Figure 22, R^2 allowed me to identify electrodes that were maximally associated with variations in neural activity across trials as modeled by the 3 factors described above (represented as a design matrix in Figure 33). A maximal R^2 value was obtained per subject, per measure; providing a way to optimize the identification of the electrode with best fitness to each regression coefficient. The time course of those electrodes were used in order to establish statistical significance. Theoretically, the time course of each R^2 function can be used in replacement of the actual neural measure of interest (e.g. ERP). However, since this approach has not been explored enough in the literature I decided to use R^2 as a dimensionality reduction technique and not as the main dependent variable of this dissertation. Therefore, the linearly modeled beta weights associated with ERP, ERSP, and ERPAC from the measure-wise R^2–optimized electrode were used for statistical testing (see 3.5.1 Analysis of linear measures).

In summary, the present dual-task parametric design allowed me to implement single-trial linear modeling in order to determine the effects of stimulus information ($\beta_{w3}\upsilon$), task demands ($\beta_{w1}T1$, $\beta_{w2}T2$), and behavioral outcome ($\beta_{w4}RT$) on perceptual decision-making as quantified by ERP, ERSP, and ERPAC. Linear modeling of neural time series allowed me to independently explore the relationship between single-trial

brain activity and task demands while accounting for the effects of stimuli information, task, and reaction time (see 3.5.1 Analysis of linear measures). Furthermore, this analysis allowed me to better take into account within-subject variance and eliminating any effects due to small sample bias (S. J. Kiebel & Friston, 2004a, 2004b; Litvak et al., 2011; Pernet et al., 2011; Wilcox, 2005a).

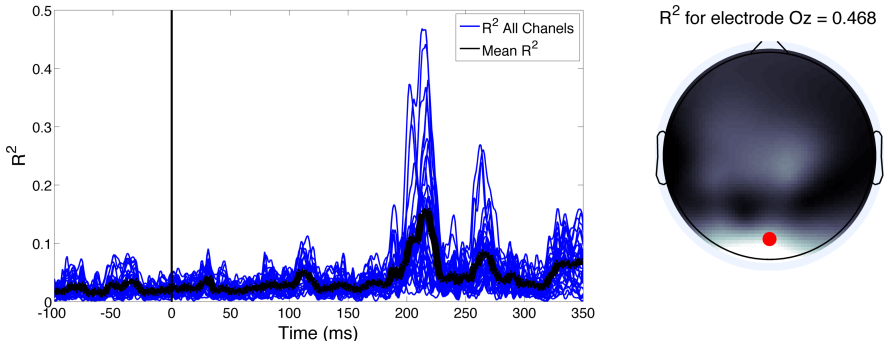

Figure 22 – Time course of R^2 values (left) and topographical representation of interpolated R2 displaying the highest-valued R^2 (right) for the ERSP measure computed using a randomly chosen set of trials (N=200) from one subject. Red dot indicates the electrode with the highest R^2 value, in this case, electrode Oz

Moreover, I used the coefficient of determination (R^2) as a dimensionality reduction technique in order to identify electrodes that were most sensitive to variations in neural activity, thus reducing type I errors. I used data recorded at R^2–optimized electrodes in order to test for statistically significant results at the group level (see 3.6 Statistical Testing). Modern statistical methods were implemented in order to detect differences in neural activity (Maris & Oostenveld, 2007; Wilcox, 2005b; Wilcox & Keselman, 2003). The following section will describe and discuss the statistical methods implemented in this dissertation.

2.5 Non-Parametric Permutation Testing

Statistical methods in psychology have been recently under attack (Cumming, 2013; Lambdin, 2012; Masicampo & Lalande, 2012; Nosek, Spies, & Motyl, 2012; Nuzzo, 2014). Most psychology studies blindly and rigidly use archaic non-appropriate methods in order to establish statistical significance. The most common statistical method in cognitive electrophysiology is the *N*-way analysis of variance *F* test (*N*-way ANOVA) as implemented in a software package originally called Statistical Package for the Social Sciences, nowadays known as SPSS (SPSS Inc.). It has been demonstrated several times that the *F* test has very good statistical power relative to other methods when the required assumptions are met (Tomarken & Serlin, 1986). However, it has been shown that when assumptions are violated, the *F* test power can very low, leading to increased probability of reporting false positives even when large samples are used (Cumming, 2013; Wilcox, 2005a). This fact poses a particularly dangerous problem for cognitive electrophysiology; our samples are usually small[24] (<30 subjects) and our data are naturally multidimensional. Furthermore, our data can easily violate the assumptions of ANOVA (Cumming, 2013; Wilcox, 2005a). Open-source toolboxes for the analysis of neurophysiological signals are nowadays available (Delorme & Makeig, 2004; Oostenveld et al., 2011; Pernet et al., 2011; Worsley et al., 1996). These and other toolboxes provide a wide range of functions that can be used in order to implement 21st century statistical analyses to neural time series data. In this dissertation I primarily relied on functions from EEGLAB (Delorme & Makeig, 2004), LIMO (Pernet et al., 2011),

[24] Although these problems can be seen with samples as big as 2000 or 1000 participants (Nuzzo, 2014; Nosek et al. 2012)

FieldTrip (Oostenveld et al., 2011), MES (Hentschke & Stüttgen, 2011), Statistics and Image Processing toolboxes (The MathWorks, Inc.).

An exhaustive discussion about statistical methods in cognitive electrophysiology is beyond the scope of this dissertation. Nevertheless, in order to justify the selection of the implemented methods (3.6 Statistical Testing) I will discuss and describe some features and characteristics of M/EEG data that should be a matter of interest for cognitive electrophysiologists when implementing statistical procedures.

Losing power

In statistics textbooks, readers are often warned about the dangers that extreme values, data distribution, and within/between subjects variation pose to the power of parametric statistical tests (Cumming, 2013; Wilcox, 2005a). In order to illustrate these 3 potential dangers for null-hypothesis testing in cognitive electrophysiology I created a new dataset composed of channel PO8 for 30 new subjects, which I will refer to as "resampled subjects". Each resampled subject was generated by randomly selecting 544 trials from the original dataset regardless of subject or condition (N=12, see 3.1 Participants).

In order to make this exercise I will use the ERP measure because of its computational simplicity and its widespread usage in the field. Thus, I run peak-analysis of the N170 integrating values over a window that comprised 140 and 200 ms using 30 resampled subjects. As in most ERP studies, the null hypothesis for this "resampled experiment" was such that there was no statistically significant differences between the

N170 elicited by "resampled condition 1" and the N170 elicited by "resampled condition 2". No real differences should exist between these resampled conditions.

Figure 23 shows 4 histograms (panel A) and 3 ERP plots (panels B, and C). Histograms were constructed with 50 bins (Freedman & Diaconis, 1981) using data from 2 randomly selected resampled subjects at 2 different time points, 170 and 200 ms (black lines, Figure 23 panel B). Red vertical lines in each histogram indicate the center of distribution (0, zero). Panel B depicts the average ERPs for 6 of the 30 resampled subjects plotted in different colors. However, 2 ERPs are plotted in black lines. Data from these 2 resampled subjects was used to generate histograms in panel A and are plotted independently in panel C. From Figure 23 I can describe that:

i. A non-trivial number of trials follow at the extremes of each distribution (Figure 23, panel A). These extreme values are commonly known as "outliers". M/EEG data, by nature, contain a not negligible number of outliers. The commonality of outliers and strategies on how to handle them are a recurrent discussion topics in statistical methods that go beyond cognitive electrophysiology (Cumming, 2013; Wilcox, 2005a)

ii. The distribution of values, although separated only by 30 ms (i.e. 15 data points), differs considerably. Whilst the distribution of trials at 170 ms tends to be following a relatively Gaussian shape[25] for one of the resampled subjects (panel A Figure 23, top left), for other resampled subject a strong negative

[25] Although it can be argued that some of these distributions could be described as bi- or multimodal

skew can be seen (panel A Figure 23, bottom left). At 200 ms the distribution of values radically changes, being skewed for both resampled subjects with opposite direction (panel A Figure 23, right). In general, asymmetry within and between individual subjects' measurements have raised strong concerns among statisticians (Cressie & Whitford, 1986; Wilcox, 2005a, 2005b; Wilcox & Keselman, 2003). Although in M/EEG data, asymmetrical distributions are expected, the implementation of single-trial analysis (Gaspar, Rousselet, & Pernet, 2011), normality tests (Mantel & Brown, 1974), and/or data transformations (Wilcox, 2005a) are rare practices among cognitive electrophysiologists and psychologists alike

iii. ERPs in panel B differ from one resampled subject to another. These variations are a product of the existence of outliers influencing the distribution of values (Figure 23, panel A), making some ERP features very unreliable at the single-subject level. For example, P1 for green, red, and yellow resample subjects is almost non-existent whereas for blue and one of the black resampled subjects P1 is very similar (Figure 23, panel B). The same can be said for all other ERP components, which are widely popular in the literature (i.e. N170, P250, etc.). Moreover, peaks and troughs can have large room for variation, whereas the transition between them can be very reliable, as shown by confidence intervals (C.I.) (Figure 23, panel C). Thus, when comparing subjects or groups using parametric tests, like the *F* ANOVA, it is assumed

that a common variance exists (Wilcox, 2005a, 2005b). Power gets affected when this assumption is violated

Strategies to overcome the 3 problems encountered in this toy dataset (Figure 23) have been developed over the years. Normality tests and data transformation techniques have been suggested as good diagnostics and solutions, however it is has been argued that they do not possess the power to actually detect problems and that they do not solve the issue presented by outliers (Wilcox, 2005b). Using trimmed means as appropriate estimators have been suggested as a possible solution (Wilcox, 2005b). Furthermore, Bayesian statistics have been also suggested as a viable alternative to null-hypothesis testing (Kruschke, 2010).

The aforementioned strategies are not commonly used in cognitive electrophysiology. Scientists often draw conclusions without verifying their data, a common practice in psychology and social sciences (Lambdin, 2012). Thus, in order to test for significance in this resampled experiment, I did not correct for any of the raised concerns.

I run a group-level *t*-test and, as expected, no statistical differences were found in this resampled experiment. However, in order to test the robustness of these results, I run this exercise 300 times. Thus, 299 new resampled experiments where made, containing 30 new resampled subjects each time. ERPs were computed for each one of these new resampled subjects and the peak of the N170 component was quantified. Figure 24 top and middle panels show the results of the original resampled experiment and the following 299 replications. Top panel displays p-values. Following the bulk of the ERP literature a

non-significant p-value was considered to be greater than 0.05; this threshold is represented by horizontal red lines (top panel). Just for reference a second horizontal red line was added indicating significance threshold of 0.01 (top panel). Blue asterisks in the top panel represent non-significant p-values (>0.05) while significant p-values (<0.05) are plotted as red dots. It can be clearly seen how p-values are widely spread acquiring ranging from ~0.01 to >0.25. The middle panel in Figure 24 shows confidence intervals for each resampled experiment. Furthermore, p-values and confidence intervals for resampled experiments number 100 to 150 are plotted for more detail in the bottom panel (Figure 24).

If one considers the results displayed in the bottom panel of Figure 24, it can be seen that about 10% of the results suggest that there is a significant difference between N170 from the resampled conditions. How can a cognitive electrophysiologist know if the obtained results are robustly significant and would be replicated? As clearly shown in the bottom panel of Figure 24, p-values represented as blue asterisks and red dots are not very informative since they range from <0.01 to 1, a phenomenon that has been described as "the dance of the p-values" (Cumming, 2013). Relying on p-values to establish significance has been critically examined many times (Cumming, 2013; Lambdin, 2012; Masicampo & Lalande, 2012; Nosek et al., 2012; Nuzzo, 2014) and has been described as "not empirical" and compared to "sorcery" (Lambdin, 2012). In contrast, confidence intervals allow scientists to understand the size and the relative importance of the effects (Cumming, 2013). In the bottom panel of Figure 24, even in the cases where I obtained a significant N170 effect, the confidence interval is so spread and close to zero that its

message can only be interpreted as "this effect is small, probably a false positive and should not be considered" (Lambdin, 2012; Nuzzo, 2014).

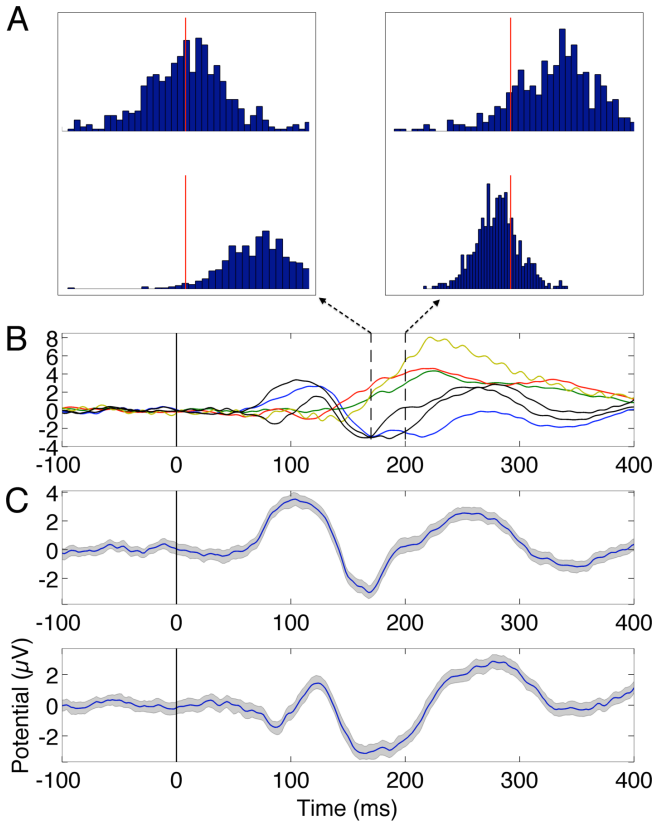

Figure 23 – Some reasons why parametric statistical tests might not be appropriate for cognitive electrophysiology. 544 trials from channel PO8 from 30 resampled subjects (see text) were used to generate (A) histograms of trials from 2 subjects at 170 and 200 ms. Red line indicates 0 (zero). (B) Sample ERPs from 5 resampled subjects, different colored ERPs represent different subsampled subjects while black lined ERPs represent the subjects whose data are plotted in A and C. (C) ERPs for 2 selected subsampled subjects used to compute A, with confidence intervals (grey boundaries)

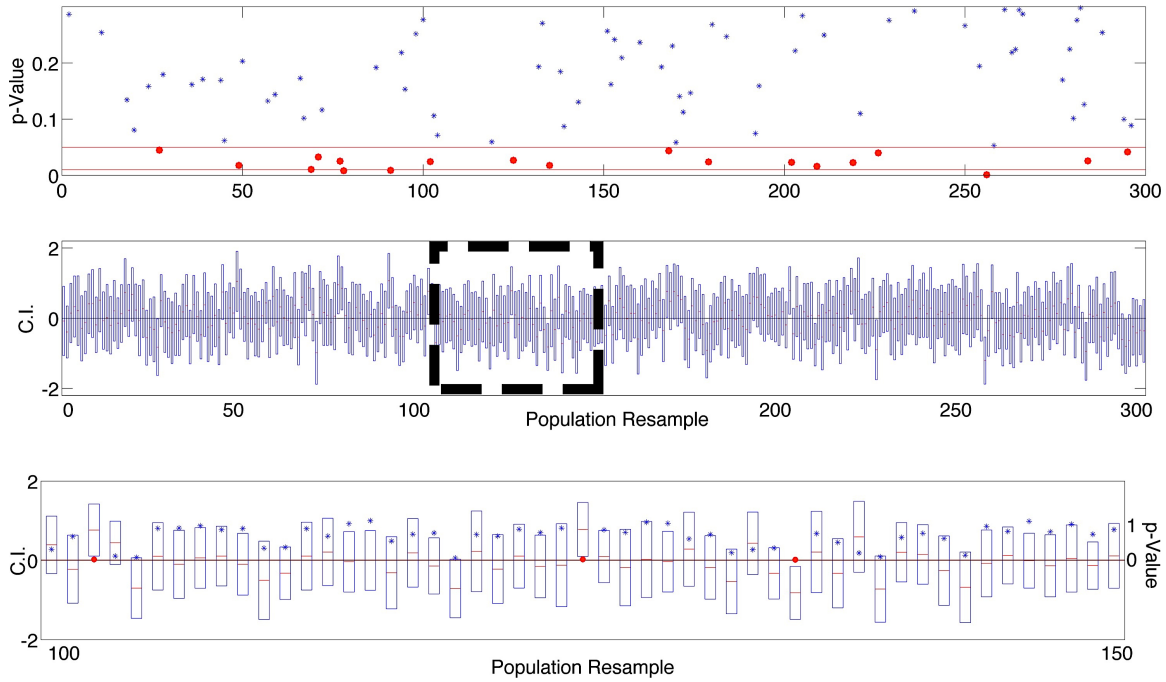

Figure 24 – Results from 300 resampled experiments testing differences between N170 ERP component quantified from 30 resampled subjects in 2 resampled conditions. Top panel displays p-values associated with each resampled experiment. Significance thresholds at 0.05 and 0.01 are signaled by horizontal red lines. P-values associated with a significant effect (<0.05) are plotted as red dots. Middle panel displays confidence intervals associated with each resampled experiment. Rectangle indicates the range of data with p-values and confidence intervals plotted in the bottom panel

In contrast, Figure 25 was made using data from the same 300 resampled experiments displayed in Figure 24. This time, however, instead of comparing N170s from both resampled conditions I compared the N170 from resampled condition 1 to baseline (-50 ms) in resampled condition 2. Thus ensuring a significant difference. Results are shown in the same fashion as Figure 24. This time ~10% of the resampled experiments p-values missed the effect; we know these are false negatives. Whereas confidence intervals indicate that although the effect might be small for certain resampled experiments the effect is robust.

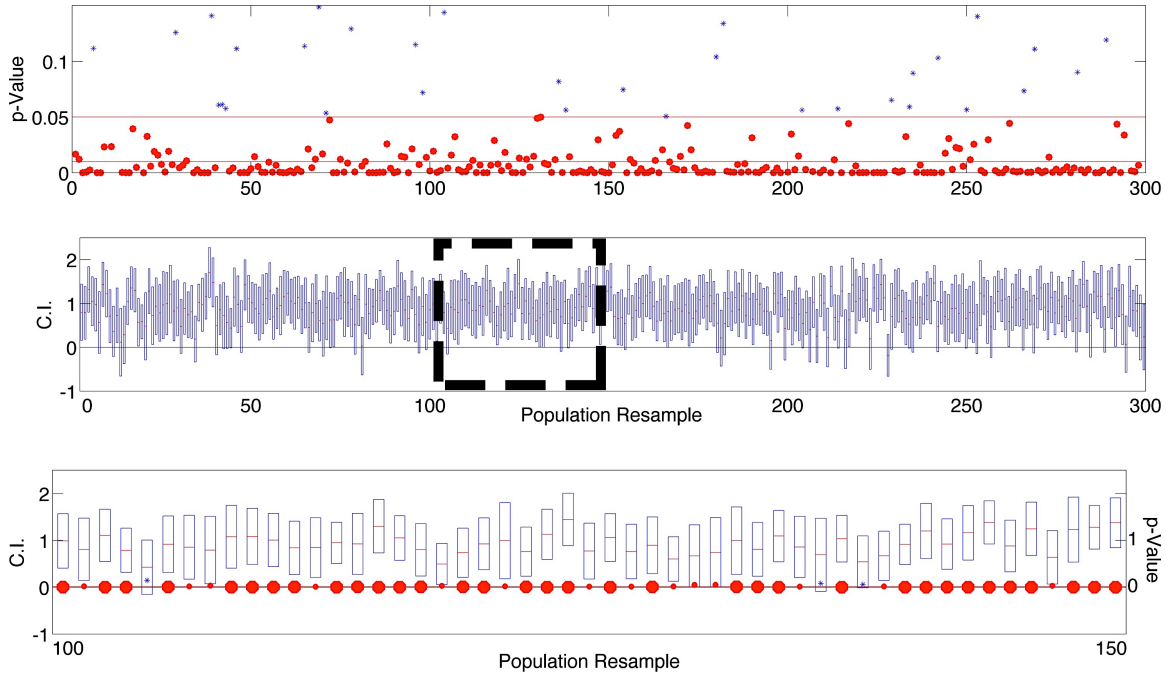

Figure 25 – Same exercise as in Figure 24. However, this time the N170 was compared against baseline to ensure a significant effect. Top panel displays p-values associated with each resampled experiment. Significance thresholds at 0.05 and 0.01 are signaled by horizontal red lines. P-values associated with a significant effect (<0.05) are plotted as red dots. Middle panel displays confidence intervals associated with each resampled experiment. Rectangle indicates the range of data with p-values and confidence intervals plotted in the bottom panel

In summary, in this simple exercise I applied the regular procedures of ERP research simulating 300 experiments investigating the effects of a categorical manipulation over the popular N170 ERP component. We can furthermore see the benefit of moving away from interpreting our results based only on p-values. Although no "real effect" existed between our resample conditions, significant results were found in about 10% of our resampled experiment (Type I error, Figure 24). Similarly, when a "real effect" was forced to exist, we failed to detect such differences in about 10% of our resampled experiments (Type II error, Figure 25). Showing the importance of considering robust methods based on bootstrapping or permutation when testing for significant effects

(Wilcox, 2005a). Importantly, in this exercise nothing was done in order to deal with the concerns raised in Figure 23. In this dissertation, in order to test for significant effects and to take care of outliers, skewness, and intra- and inter-subject variance I used 2-level robust non-parametric permutation testing for both linear and non-linear EEG measures (see 3.6 Statistical Testing).

The Non-Parametric Permutation Testing Framework

The framework provided by permutation testing allows psychologists, and cognitive electrophysiologists to assess the statistical significance of given time or time-frequency point(s). Due to the non-Gaussian nature of data distribution and the multidimensionality of results, non-parametric permutation testing framework has been suggested as absolutely necessary for time-frequency analysis (Maris & Oostenveld, 2007). The power of permutation testing comes from its assumption-free nature. Unlike the popular *F*-ANOVA, as implemented in SPSS and other commercial statistical software, no assumptions have to be made about the distribution of data (Maris & Oostenveld, 2007; Theiler, Eubank, Longtin, Galdrikian, & Doyne Farmer, 1992; Wilcox, 2005a).

In parametrical tests, it is assumed that data points are drawn for Gaussian distributions. However, the exercise in Figure 23 shows that this assumption is violated in EEG data. In order to reject the null-hypothesis, parametric tests compare the statistic of interest (e.g. *F* or *t* value) against an idealized distribution of that given statistic expected under the null hypothesis (Wilcox, 2005a). Using these theoretical distributions a *p*-value is computed in order to assess the probability of observing the empirical results by

chance. The size of the obtained *p*-value should indicate the likelihood of the null-hypothesis of being true (Wilcox, 2005a).

In radical contrast, non-parametric permutation testing assumes nothing. Data points can be thus drawn from any kind of distribution, presenting no problem for statistical power. Furthermore no theoretical assumptions are made about the distribution of test statistics under the null-hypothesis (Wilcox, 2005a). Instead of assuming the existence of an idealized test statistic distribution, a data-driven distribution is generated under the null-hypothesis.

Another exercise was made using the categorical comparison of N170 ERP component shown in Figure 23, Figure 24, and Figure 25. This time, instead of running 300 different resampled experiments with 30 different resampled subjects each time, I performed a group-level analysis on 30 resampled subjects using 1000 permutations. Thus, condition labels between resampled condition 1 and resampled condition 2 were swapped 1000 times. In permutation testing the mapping between the dependent and independent variables is shuffled; but data are not altered in any way (Wilcox, 2005a). Top left panel in Figure 26 show data-driven distributions of test statistic values observed under the null-hypothesis was created for both comparisons (i.e. resampled condition 1 N170 vs. resampled condition 2 N170 and resampled condition 1 N170 vs. baseline). In permutation testing, comparing the "real" observed value against the null-hypothesis distribution assesses statistical significance (Wilcox, 2005a).

Top left panel in Figure 26 depicts the data-driven *t* statistic distribution for one set of 30 resampled subjects testing differences in the N170 ERP component between resampled condition 1 and resampled condition 2. Since I build the subjects randomly, no

significant differences were expected. The non-parametric permutation testing framework allowed the confirmation of the story told by confidence intervals (Figure 24, bottom panel); no significant effect exists between the N170 component elicited by resampled condition 1 when compared against resampled condition 2. The observed value was indistinguishable from values observed under the null-hypothesis. Furthermore, when the N170 was compared against baseline, the significant effect was not missed (Figure 26, top right panel). Fundamentally, the distribution of parameters describing the data, the presence of outliers, and data points with non-representative values had no impact in the obtained results (Wilcox, 2005a). Real data looks very different from the idealized theoretical distribution that is commonly used in cognitive electrophysiology (Figure 26, bottom panel); non-parametric permutation testing is indeed a superior framework for cognitive electrophysiologists (Maris & Oostenveld, 2007).

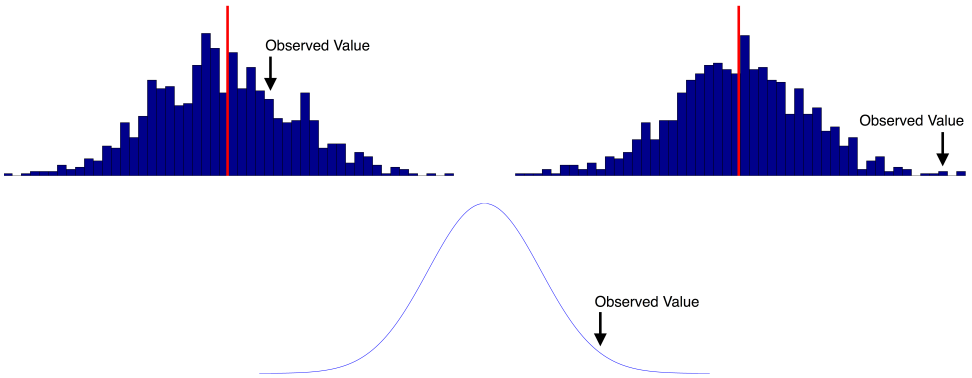

Figure 26 – Data-driven and theoretical test statistic distributions. Non-parametric permutation testing allows the creation of data-driven test statistics distribution under the null-hypothesis (top panels). Red vertical line indicates zero. In contrast, parametric tests assume the underlying distribution is Gaussian (bottom panel).

The main disadvantage of non-parametric permutation testing is that comparing the observed value to 1 null-hypothesis test statistic is useless. Therefore, as shown in Figure 26, the permutation procedure has to be done hundreds or thousands of times. This

procedure can become computationally expensive. There is no optimal or magic number of permutations to be implemented. However, for most procedures, 1000 permutations have been recommended (Wilcox, 2005a). If we consider that 1000 permutations will have to be performed for each trial, channel, time point, and frequency computation time can easily span several weeks. I take as a rule of thumb that the noisier the data, the fewer the trials, the fewer the subjects, and the larger the disparity between trials present in each condition, the larger the number of permutations needed. In this context, more iterations of the process are always better. Yet, this disadvantage should be completely ignored nowadays because most laboratories possess adequate computational power.

Correction for Multiple Comparisons

Due to the simplicity of the exercise presented in figures 21 – 23, no correction for multiple comparisons had to be implemented. However, this is not the usual situation cognitive electrophysiologists face in their research. Thus, multiple comparison correction (MCC) is a common procedure applied in cognitive neuroscience. It is hard to imagine a published article that applies no correction for multiple comparisons. A particularly useful feature of the non-parametric permutation testing framework is that correction for multiple comparisons can be naturally implemented in any analysis pipeline. The most common and popular method for multiple comparison correction is the Bonferroni correction. Most commercial statistical software packages implement Bonferroni correction by default, perpetuating its usage in thousands of cognitive electrophysiology studies. However, the Bonferroni method has been criticized over the years in multiple disciplines. Authors have pointed at its flaws that range from

mathematical to logical to practical (Maris & Oostenveld, 2007; Moran, 2003; Narum, 2006). Bonferroni correction consists in dividing the desired *p*-value threshold (e.g. 0.05) by the number of tests performed. In the simplest ERP study, at least 2 electrodes will be tested, usually left and right hemisphere electrodes. Thus, the new Bonferroni-corrected *p*-value of 0.05 for such a study is 0.025. In this situation, the method is appropriate. However, this scenario can be rarely encountered when doing research with real cognitive neuroscience datasets.

Most cognitive neuroscience studies are somewhat exploratory. They mix hypothesis-driven approaches with exploratory ones. Cognitive electrophysiology is no different. Tests are performed at multiple electrodes, at different time points or temporal components, at different frequencies, etc. In these situations the Bonferroni method is usually not appropriate. The first obvious problem is that in order to ask interesting questions to a data set, more complicated analyses need to be performed[26]. Testing 1 time point at 2 different channels would probably answer a very specific and simple question. However, even when specific questions are asked, Bonferroni might not be the most appropriate method.

What if a scientist would like to know if increasing image contrast modulates posterior gamma power (30 and 70 Hz) between 100 and 300 ms? (Schadow et al., 2007). In this case, we would have ~100 time points, ~13 channels, and ~21 frequency bands leading to 27,300 between-condition tests. If we consider this very realistic situation, our Bonferroni-corrected *p*-value of 0.05 would be 0.0000018; so small that not even real

[26] More complicated than 1 time point at 1 electrode between 2 conditions

effects would be detected. Moreover, so many tests are performed that the number of false positives would also increase dramatically.

Furthermore, Bonferroni correction is blind to the nature of the data a scientist is working with. Imagine a researcher that knows the N170 ERP component is sensitive to facial expressions in humans (Blau et al., 2007). This researcher wants to know when does the amplitude of N170 measured at channel PO8 starts distinguishing "positive" facial expressions from "negative" facial expressions. Our scientist will therefore test for differences in amplitude within a time window comprising 50 to 250 ms. Just like hundreds of ERP studies data will be sampled at 250 Hz. In this case, 51 tests will be performed. Bonferroni-corrected *p*-value of 0.05 would be 0.00098. What if data was sampled at 500 Hz? Now our scientist has 101 tests to be performed. Bonferroni-corrected *p*-value of 0.05 would be 0.00049. Finally, if data were sampled at 1000 Hz, the new p-value would be 0.00024. Bonferroni correction went from an excessive 0.00098 to an unrealistic 0.00024 as a threshold for significance. In this case, the number of data points inside the window to be tested should not be considered as independent. In our realistic example, no additional information is obtained when testing 51 or 201 time points within 50 and 250 ms. Bonferroni fails at acknowledging this relationship and the statistical significance threshold is negatively affected. The same argument can be applied to the frequency, sensor, and time-frequency domains.

Finally, imagine that the same scientist wants to know what the effects of perception of emotional faces are not only on the N170 but also on the P250 ERP component. Thus, bilateral test statistics for peak analysis would be performed at 2 different, yet continuous time-points. Yet Bonferroni correction would assume that each

test was independent. Thus, the corrected *p*-value of 0.05 for the N170 component is 0.025. Likewise, the corrected *p*-value of 0.05 for the P250 component is 0.025. These 2 corrected *p*-values are very reasonable and significant effects might be expected. However, the independence of these 2 ERP components is not a straightforward and easy to argue assumption. A more appropriate method should take into account the high autocorrelation between time points in the ERP time series. Therefore, our scientist should have used a Bonferroni-corrected *p*-value of 0.0125 instead of 0.025. Once again, Bonferroni failed at acknowledging the nature of the data.

In summary, the main problem with the standard method of multiple comparison correction is that it can be described as a "cookie-cutter" strategy. Lack of flexibility in research has always been and will always be a problem. The Bonferroni correction blindly applies a pre-defined criterion based on the number tests performed regardless of the nature of the data or the scientific question.

In contrast, the non-parametric permutation testing framework offers the opportunity to implement tailor-made methods for correction of multiple comparisons depending on the nature of the data and the scientific question at hand. Flexile strategies such as false-discovery rate (Benjamini & Hochberg, 1995; Genovese, Lazar, & Nichols, 2002) and Gaussian random-field theory (Kilner, Kiebel, & Friston, 2005; Pantazis, Nichols, Baillet, & Leahy, 2005) have been suggested in the literature. Surveying strategies to correct for multiple comparisons is beyond the scope of this dissertation, therefore I will focus on the one I have implemented in this dissertation, which is the temporo-spatial clustering technique (Maris & Oostenveld, 2007).

Clusters of significant data points can be flexibly defined in the time, time-sensor, time-frequency, frequency-sensor, frequency-frequency, time-frequency-frequency, and time-frequency-sensor space as needed. The logic behind generating clusters of significant points is that given the large amount of autocorrelation in data, it is expected that statistically significant effects extend across the different data dimensions regardless of it being time, frequency, and/or space. Thus, a single isolated time-frequency point that is significant is most probably a false alarm. In summary, this multidimensional strategy of correcting for multiple comparisons takes into account the nature of EEG data and is most suitable for cognitive electrophysiology (Maris & Oostenveld, 2007).

3. Methods

3.1 Participants

Participants where recruited from the Indiana University Bloomington community. Thus, 12 participants (3 males) between the ages of 20 – 40 participated in this study after providing written consent. All participants were free of neurological conditions according to their self-report. All participants reported normal or corrected-to-normal vision. All procedures conformed the requirements of the local Institutional Review Boards (IRB). Due to the large amount of number of conditions I have, each participant run 2 sessions of the experiment in order to increase the signal-to-noise ratio.

3.2 Stimuli, Task, and Procedure

The stimuli consisted on composite Car/Face images. A grayscale frontal view of a human face with neutral expression generated from a database of facial features was

used. This face was chosen because it is carefully controlled across several statistical dimensions and has been used in a previous study by our research group (Schneider, DeLong, & Busey, 2007). Also, a grayscale side view of a car was used. Image statistics, including amplitude spectrum and overall energy were equated for both pictures; these low-level characteristics thus become non-diagnostic features for the tasks. This means that participants will not be able to use low-level visual features, such as contrast or energy of one image alone, in order to perform the tasks. In order to minimize confounding factors, contrast was also varied within 2 levels on each presentation of the test image. This, along with the 7 mixing levels between car and face also prevented participants from using spurious features, such as small changes in contrast, to accomplish the tasks.

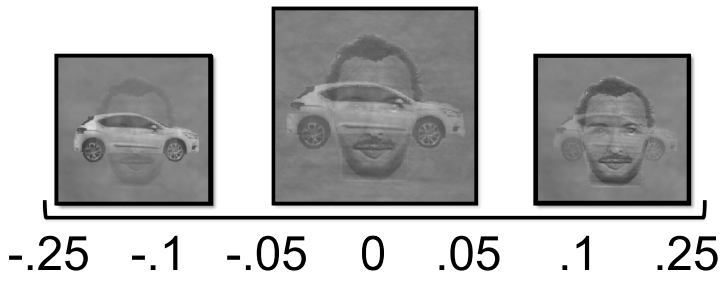

Figure 27 – Idealized stimuli sample. A composite image of a human face and a car was generated automatically using MATLAB in each trial. The proportion of face within each composite image was parametrically manipulated. The mixing level parameter that controlled the face proportion is shown along with an idealized version of the composite

The face subtended a visual angle of 3.6º width and 4.8° height while the car subtended a visual angle of 4.8º width and 3° height. At each trial a new Car/Face composite image was generated at random. In the first interval, the proportion of face visible was randomly selected from a "standard face proportion" parameter:

Parameter 1 – Standard Face Proportion

Standard Face Proportion = [0.3 0.4 0.5 0.6 0.7]

This composite image was presented as a single Car/Face mixture for 100 ms. The first presentation of a composite image will be referred to simply as the 'standard'. In the second interval, a new composite image was generated with a potentially different mixture level. The "test face difference" parameter was:

Parameter 2 – Test Face Difference

Test Face Difference (υ) = [-0.25 -0.1 -0.05 0 0.05 0.1 0.05]

This composite image was also presented as a single Car/Face mixture for 100 ms. I will refer to the second presentation of a composite image as the 'test image'. Figure 27 shows an idealized representation of the stimuli. The central value of the "test face difference parameter" (zero, 0) generated a composite image that contained equal amounts of face and car as the standard. In contrast, the extreme values (-0.25, 0.25) generated a composite image that contained 75% less face and 75% more face from the standard.

Stimuli were shown in a 21-inch (53.34 cm) cathode ray tube [CRT] monitor at 120 Hz. In each new trial a Car/Face composite image was shown twice. The top part of Figure 28 depicts a graphic representation of a trial. The structure of this idealized trial will remain the same throughout the whole experiment and both sessions. After presenting the standard, a blank screen appeared for 500 ms followed by a new composite

image presented for 100 ms. Each test was generated using a value from the mixing level parameter. Each test image mixture level represents a condition. There are 7 conditions in total. Each composite image was randomly generated on a trial-by-trial basis.

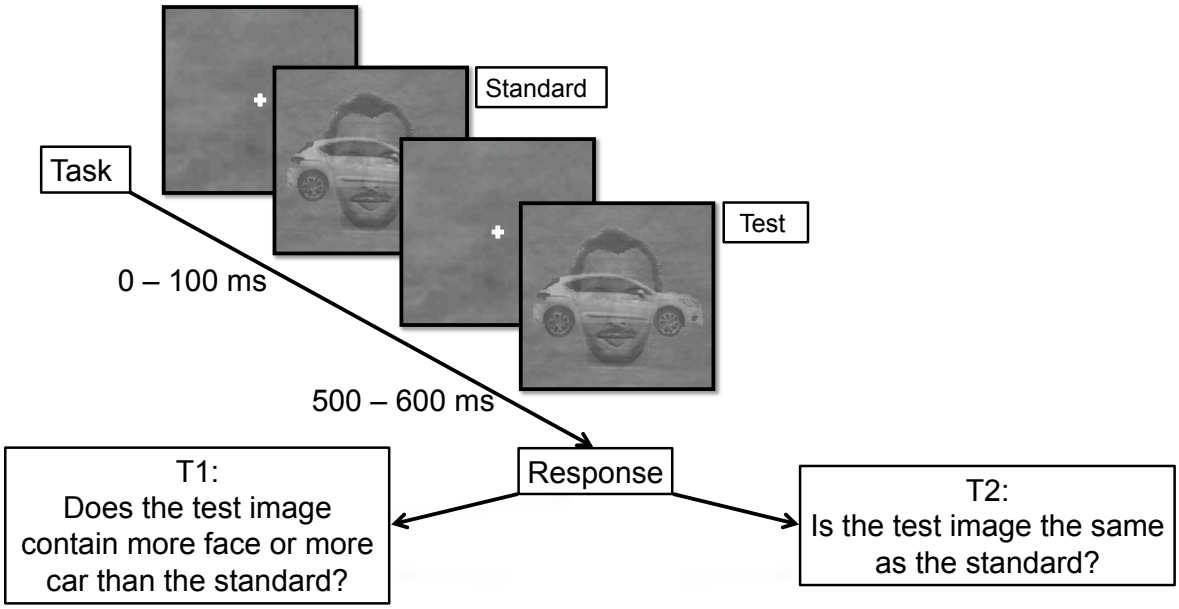

Figure 28 – Schematic representation of an idealized trial. In each block, participants were told which task to perform (T1 = more car/more face judgment or T2 = same / different judgment). In each trial, a standard image was presented followed by a test image. Participants indicated their decision by pressing the button of a computer mouse

Participants performed 2 tasks. Each task had 7 conditions (from the mixing level parameter). Each task was randomly assigned at the beginning of each block, forcing participants to accommodate to a new task in each block of trials. The first task consisted in detecting the amount of face/car proportion present in the test image using the standard as comparison. Thus, participants had to judge whether the test image contained more face or more car in comparison to the previously shown standard image. The second judgment was based on a matching task where participants had to decide if the test image

was the same as the previously shown standard image. Participants were instructed to inform their judgments using one of the two buttons of a computer mouse. Participants were also instructed to limit both their body and eye movements while a stimulus was on the screen. The whole procedure is representation in an idealized form in Figure 28.

In some trials, the mixture difference will be large enough so participants will have enough information to perform a decision (easy trials, e.g. mixture level = -0.25, 0.25). In some other trials the mixture difference will be small increments thus the difficulty of the decision is much higher (hard trials, e.g. mixture level = -0.1, 0.1). Block design was used in order to increase the signal-to-noise ratio for the task manipulation.

3.3 EEG data acquisition

Electrophysiological signals were collected using a 32-channel Sensorium EEG amplifier (Figure 29). Data was sampled at 1000 Hz amplified by a factor of 20,000. EEG signals were acquired with a nose reference. Impedance was kept below 5 kΩ for all electrodes. EEG data were recorded for a total of 1800 ms. Recording started 500 ms before the presentation of the standard image. Recording concluded 1300 ms after the presentation of the standard image.

To ensure as-clean-as-possible EEG signals, all recordings were made inside a Faraday cage. Moreover, eye blink and eye movement calibration trials were performed at the beginning of each recording session in order to improve the efficacy of later artifact-removal procedures (see 3.4 EEG data pre-processing). In order to ensure an appropriate number of trials on each condition, participants ran in the experiment twice

on separate days. Data from each session was combined into a single data matrix for further analysis.

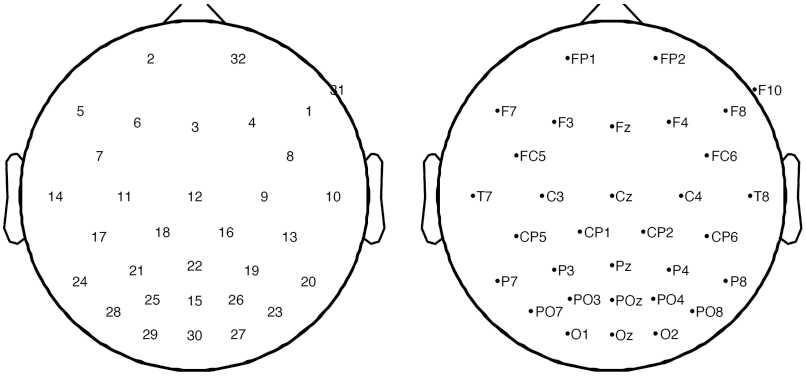

Figure 29 – Topographical representation of electrode locations. Default numbering scheme for our 32-channel system (left) and its correspondent standard 10-20 international naming scheme (right)

3.4 EEG data pre-processing

Pre-processing procedures were performed using functions from the EEGLAB toolbox (Delorme & Makeig, 2004) as well as custom in-house MATLAB routines. Epoched data from both sessions were merged into a single data matrix per subject. A broad band filter (0.1 – 100 Hz) was applied to each electrode's raw EEG signal using a finite impulse response filter[27] with frequency-dependent order that balances temporal and frequency resolution; a common procedure implemented in analysis packages such as EEGLAB (Delorme & Makeig, 2004) and FieldTrip (Oostenveld et al., 2011).

The length of each data trial was 1800 ms where 500 ms corresponded to pre-stimulus onset baseline and the following 1300 ms corresponded to post-stimulus onset

[27] firfilt 1.5.1 by Andreas Widmann, EEGLAB toolbox

period. Long segments of EEG data were used in order to provide sufficient padding for band-pass filters used in the time-frequency analysis, thus avoiding the necessity to zero-pad the data (Christoph S Herrmann et al., 2005). Given that the lowest frequency for analysis is ~4 Hz, on each side of each trial 250 ms will be considered as distorted and will not be used for analyses purposes. Thus, the period used for statistical testing was from -200 ms before standard onset and 1000 ms after the standard onset.

Visual data inspection was performed in order to discriminate the trials that contained excessive muscle movements, amplifier drifts, and other obvious sources of noise. Trials containing such artifacts were excluded from analysis. No subject had more than 20% of all trials rejected. Furthermore, no channel interpolation was necessary as all electrodes were kept with good impedance (<5 kΩ).

After visual inspection of the data, an additional artifact rejection procedure based on independent component analysis (ICA) was performed as implemented in the *runica.m* function of the EEGLAB toolbox (Delorme & Makeig, 2004). ICA is a linear decomposition technique, often classified under machine learning, used by certain groups of cognitive electrophysiologists in order to estimate underlying statistical sources of linearly mixed M/EEG signals (Delorme & Makeig, 2004; Makeig et al., 2004).

ICA is considered to be a powerful un-mixing tool. It has therefore gained a particularly privileged status among certain groups of cognitive electrophysiologists. ICA has been shown to successfully un-mix common artifacts such as line-noise and eye-blinks from neurophysiological signals (Jung et al., 1998; Xue, Li, Li, & Wan, 2006). Impressively, ICA has been demonstrated to be capable of un-mixing the electrical signal of an unborn baby's heartbeat from the mother's heartbeat, measured from a multi-

channel recording from a pregnant woman's abdomen (Viola, Debener, Thorne, & Schneider, 2010). Furthermore, ICA has been recently used to un-mix electrical brain signals from muscle movements under extreme conditions, such as walking and running (Gwin, Gramann, Makeig, & Ferris, 2010). Thus, when using optimal parameters, ICA is a powerful technique for electrophysiological data processing, artifact removal, and mining (Makeig et al., 2004).

In this dissertation I used the basic ICA model implemented in EEGLAB (Delorme & Makeig, 2004) as an artifact removal technique. Artifacts were mostly of physiological origin (e.g. eye blinks, carotid pulse) as our Faraday cage prevented line noise from being a problem in our recordings.

The obtained two-dimensional 32-channel EEG data matrix time-series was decomposed into a weighted linear mixture of independent signals (Delorme & Makeig, 2004). The output of ICA is stored in a squared matrix (W, channels x components). Equation 1 was used in order to obtain independent components (IC), multiplying the EEG data matrix by the ICA weights (W).

Equation 1

$$IC = EEGdatamatrix * W$$

An important assumption of ICA is that the number of sources is not larger than the number of sensors (Onton, Westerfield, Townsend, & Makeig, 2006). Cognitive electrophysiologists often run ICA without taking into account this important assumption,

leading to unsuccessful results. Thus, in order to estimate the number of ICA components to be used, the total number of data points was calculated per subject (Parameter 3).

Parameter 3 – Total Data Points

Total Data Points = Number of Time Frames * Number of Trials

Considering the number of total data points per subject, a data threshold for ICA has to be calculated (Parameter 4). If the value of Parameter 3 is smaller than the value of Parameter 4 there are not enough data points in the dataset in order to perform full-rank ICA[28]. The number 20 has been recommended as an appropriate "rule of thumb" in order to improve ICA reliability (Delorme & Makeig, 2014; Onton et al., 2006; Viola et al., 2010). According to this rule, in my data, at least 20,480 Total Data Points were needed in order to perform full-rank ICA. In this dissertation the *Rule* value used was 40 instead of the recommended 20. Thus, the threshold for full-rank ICA was computed:

Parameter 4 – Data threshold for ICA

Rule = 40

Threshold = Rule * Number of Channels^2

According to the computed threshold (Parameter 4), a total of 40,960 data points were needed in order to perform full-rank ICA. All subjects passed this threshold. Thus, enough data was provided to the ICA algorithm so full-rank ICA decompositions were performed for each participant. A total of 32 ICA components were generated for each

[28] "Full-rank" ICA means that the output of the ICA decomposition will be a squared weighting matrix (W) that will contain as many components as sensors

subject. Artifactual components were selected by visual inspection of their scalp topographies, overall activity spectra, and time courses. Selected artifactual components were removed from further analysis by zeroing-out from space (W^{-1}) and time (IC) as needed. Finally, the ICA-pruned EEG data matrix was reconstructed using Equation 2.

Equation 2

$$EEGdatamatrix = W^{-1} * IC$$

A final trial-by-trial visual inspection of the ICA-pruned reconstructed EEG data matrix was performed so as to detect any possible additional residual artifacts. This second visual inspection led to no trials being rejected for any subject. Finally, all artifact-free EEG data were digitally re-referenced to an average reference for further analysis.

3.5 EEG data analysis

Linear and non-linear measures were computed from artifact-free EEG signals. In order to compute power- and phase-based measures, the analytic signal of recorded EEG was extracted using complex Morlet wavelets (CMW). CMW have a real and imaginary part; occupying a 3-dimensional space composed of time (Equation 3, *t*), imaginary (Equation 3, *i*), and real domains. A CMW is displayed in Figure 30.

Multiplying a Gaussian (Equation 3, first exponential) by a complex sine wave (Equation 3, second exponential) creates CMWs. The Gaussian is composed the factor *A*, which is a frequency band-specific scaling factor. The standard deviation of the Gaussian (Equation 3, *s*) is obtained by dividing the number of wavelet cycles (Equation 3, *n*) by the

product of 2π and parameter f (peak frequency in Hz). The complex sine wave is created using Euler's formula (Equation 3, $e^{i\phi}$). M represents magnitude (length of the vector between the center of the plane and the dot product, Figure 31 A). ϕ is the angle formed by the vector formed with respect to the real axis (Figure 31 B).

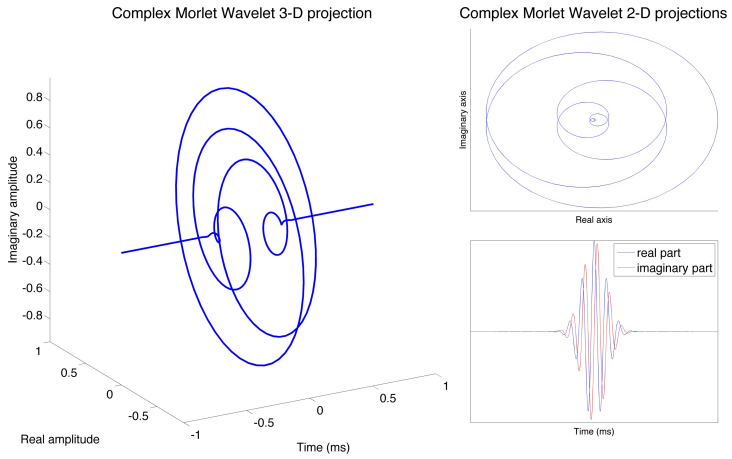

Figure 30 – A complex Morlet wavelet represented in different dimensions. Left panel represents the projection of a complex Morlet wavelet in 3-dimensional space. Right panels depict the projection of a complex Morlet wavelet into 2-dimensional space

CMWs were used in order to extract the analytic signal of EEG at each electrode and trial. Since CMWs have to be "slid" through time in order to compute a time-series of complex EEG signals, temporal precision gets decreased for all time-frequency-based analyses. The complex output of each step of the convolution between a raw EEG signal and a wavelet can be conceptualized as one point in a complex polar plane (i.e. dot product, represented as a red dot in Figure 31). Concatenation in time of consecutive dot products generates a time-series of complex numbers (Figure 31, D) that can be used in order to extract time-frequency EEG power (Figure 31, A) and phase (Figure 31, B).

Equation 3

$$CMW = Ae^{-t^2/(2s^2)}e^{i2\pi ft}$$

$$A = \frac{1}{(s\sqrt{\pi})^{1/2}}$$

$$s = \frac{n}{2\pi f}$$

$$e^{i\phi} = M\left[\cos(\phi) + i\sin(\phi)\right]$$

$$M = \sqrt{\left(real^2 + imag^2\right)}$$

$$\phi = \arctan\left(\frac{imag}{real}\right)$$

Time-frequency EEG power was calculated independently at each electrode (*ch*) and trial (*r*). The length of the vector (*v*) from the origin of the complex polar plane to the dot product of each wavelet convolution step was squared in order to estimate a time-frequency point of EEG power (Figure 31 A, Equation 4).

Equation 4

$$EEGpower_{(ch,r)} = \left|length(v)\right|^2$$

Equation 5

$$EEGphase_{(ch,r)} = angle(v)$$

Time-frequency EEG phase was calculated independently at each electrode (*ch*) and trial (*r*). The angle produced by the vector (*v*) from the origin of the complex polar plane to the dot product with respect to the real axis was considered the phase angle of the given time-frequency point (Figure 31 B, Equation 5).

Thus, I calculated time-frequency-based linear and non-linear EEG measures. Since EEG epochs were 1.5 s long, the lowest value for parameter *f* (Equation 3) was 4 Hz; ensuring good signal to noise ratio for the low-frequency spectrum. Since sampling rate was 500 Hz I had no restrictions for the highest value for parameter *f* (Equation 3). 70 Hz was arbitrarily chosen, since a range of 4 – 70 Hz is likely to capture the main spectral dynamics elicited by the present experimental paradigm. Furthermore, 34 linearly spaced frequency centroids were generated as values for parameter *f* (Equation 3). In order to avoid wavelet edge artifacts, the parameter *t* (Equation 3) was set to 2 s. Thus, wavelets were defined using a time-range of -2 to +2 s and centered in the window at 0. Furthermore, in order to optimize the trade-off between temporal and frequency precision, I used a variable number of cycles for the Gaussian taper (parameter *n*, Equation 3). Thus 3 to 7 cycles were linearly increased in the same number of steps as the *f* parameter (Equation 3). Wavelet-transformed EEG data was arbitrarily downsampled to 55.5 Hz in order to make further time-frequency analyses more computationally affordable. Such heavy decimation can be done due to the large autocorrelation of the wavelet-transformed EEG signal. Each time-frequency point is the result of the weighted combination of the surrounding points; adjacent time-frequency points do not carry new information. Thus, all analyzed time-frequency measures were sampled at 55.5 Hz.

In general, linear measures of brain activity are widely used in cognitive neuroscience. As discussed earlier, ERP is the most widely used technique (see section 2.1.1 Event-Related Potentials (ERP)). Furthermore, ERSP is gaining a lot of interest in the community and is by far the most used time-frequency measure (see section 2.2.1 Event-Related Spectral Power (ERSP)). The combination of ERP and ERSP is an

approach that has being neglected in cognitive electrophysiology. I hope it will be embraced in the future as the standard, leading to a fruitful framework of linear measures of brain activity (A. Rossi, Parada, Kolchinsky, & Puce, 2014).

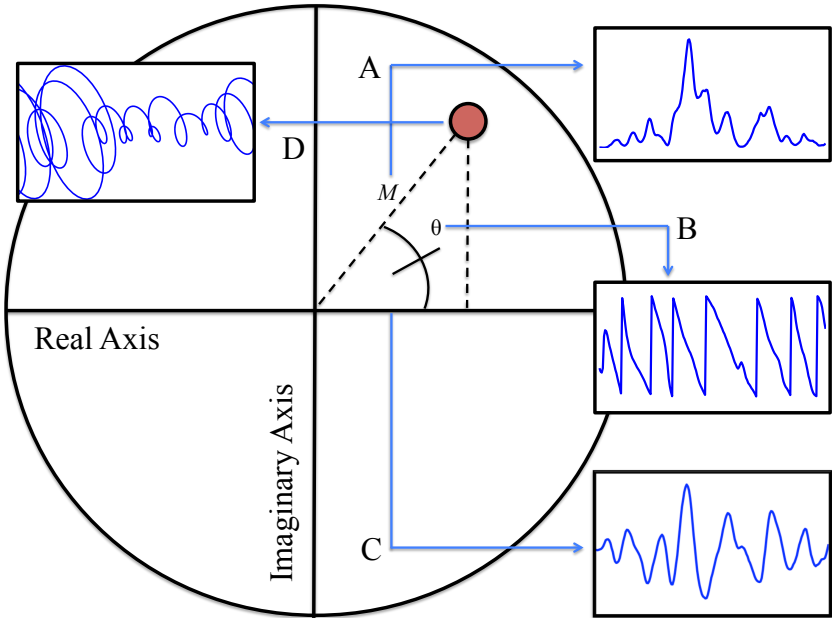

Figure 31 – Ideal representation of the dot product output (red dot) of 1 step of wavelet-convolved EEG signals on a complex polar plane. Time-frequency spectral power is obtained by squaring the length of the vector from the origin to the dot product (A, Equation 4). Time-frequency phase is obtained from the angle of the vector from the origin to the dot product with respect to the real axis (B, Equation 5). The projection of the dot product into the real axis produces a band-passed signal (C). Shown power (A), phase (B), band-passed (C), and complex signal time series (D) are obtained by concatenating consecutive dot products in time

Non-linear measures (i.e. ITPC and ISPC) cannot be analyzed using the linear model implemented in this dissertation. Thus, non-linear measures of brain activity were analyzed using robust subject- and group-level statistics using the non-parametric permutation testing framework.

Cross-frequency coupling, a non-linear measure of brain activity, has gained a lot of theoretical relevance in the field (Canolty & Knight, 2010). However, very little evidence exists for functional cross-frequency interactions in the cognitive electrophysiology literature making its functional interpretation not straightforward. I have learned that relying on robust measures and appropriate experimental designs is a must when analyzing neural time series[29]. Although ERPAC is a non-linear measure of brain activity, ERPAC can benefit from the linear model implemented in this dissertation in order to better link phase-amplitude coupling dynamics to behavior.

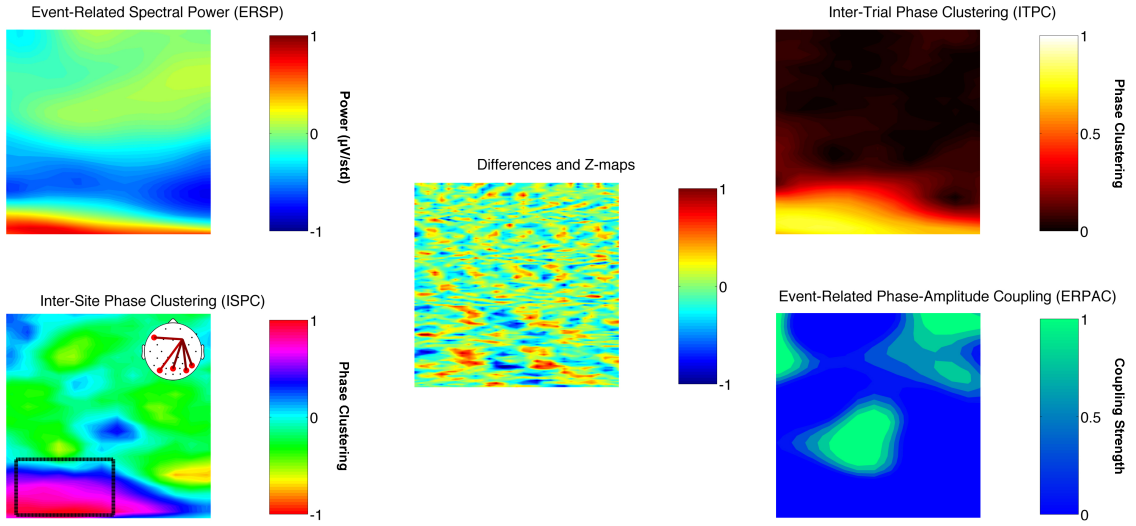

Figure 32 – Example of Color-coding scheme for visualization of results. For each measure a particular colormap was chosen that helps distinguishing from similar measures. ERSP will use *jet* (top left corner), ITPC will use *hot* (top left corner), ISPC will use *hsv* (bottom left corner), and ERPAC will use *jet* (bottom right corner). Maximization of color difference between measures that will be likely displayed together was preferred. Another factor chosen was the range of values each measure could reach

[29] I recently got an article rejected from NeuroImage where the main concern was produced by the lack of clear interpretations of effects from the data due to a rudimentary experimental design

Visualization of all time-frequency domain measures is color-coded throughout this dissertation. Figure 32 displays the color scheme for each neural measure. ERSP is represented using the bipolar *jet* MATLAB colormap (Figure 32, top left panel). ERSP is not bounded so it can reach any positive and negative value.

In contrast to ERSP, ITPC is bounded from 0 to 1. The MATLAB colormap used to represent this measure is the unipolar scale *hot* since it clearly distinguishes low (dark) form higher (bright) values (Figure 32, top right panel). Although ISPC is also measure of phase clustering, it is not bounded from 0 to 1, because it is computed with phase angle differences between 2 electrodes (see

2.3.1 Inter-Site Phase Clustering (ISPC)). *Hsv* was the colormap used because positive and negative extremes of the color spectrum are interpreted similarly; increased phase clustering across trials between sensors from baseline (Figure 32, bottom left panel). ISPC plots will be accompanied by rectangles signaling time-frequency points used to generate the associated topographic maps indicating the spatial location of electrodes used for estimation of ISPC (Figure 32, bottom left panel insets). Finally, since the ERPAC measure is bounded from 0 to 1 it is *(in)*appropriately plotted using the *winter* colormap (Figure 32, bottom right panel).

Between-subject statistical analysis results are presented in 2 ways. The observed differences per comparison are shown side-by-side with cluster-corrected z-maps (created with 10,000 permutations and multiple comparison corrections). Both are displayed using the bipolar colormap *jet* because these both observed differences and z-maps maps are not bounded. This color scheme is consistently used throughout the dissertation. Figure 32 can be used as a guide or color-lookup table to navigate results if necessary.

3.5.1 Analysis of linear measures

Artifact-free data were analyzed using a multilinear model using functions from the Linear Modeling EEG toolbox (Pernet et al., 2011). This analysis was performed in a single-subject fashion[30]. This technique was preferred because allows using single-trial information in order to generate weighted factors associated to the particular regressor (Equation 6 and Equation 7, see 2.4 Linear Modeling of EEG Measures). Thus, multiple

[30] These type of analyses are known as "within-subject analysis" or "level 1 analysis" (Wilcox, 2005)

regression was used in order to generate regression coefficients (beta weights, β_w) mapping each one of the regressors to the data.

Each trial (r) for the measure of interest (M) was independently expressed at each time point (t) and electrode (ch) using the following linear model (Equation 6, (S. J. Kiebel & Friston, 2004a, 2004b)).

Equation 6

$$M_{(r)_{(t,ch)}} = \beta_{w0} + \beta_{w1}T1 + \beta_{w2}T2 + \beta_{w3}\upsilon + \beta_{w4}RT + \varepsilon$$

Trials were modeled as the sum of a constant term β_0, tasks (Task 1, $T1$ and Task 2, $T2$), the mixing level (υ, Parameter 2 – Test Face Difference), the reaction times (RT), and an error term (ε). The regressors for task demands ($T1$ and $T2$) were categorical factors. Stimulus information is the stimulus mixing level manipulation and was a continuous factor (υ, Parameter 2 – Test Face Difference). Finally, behavioral outcome is reaction time (RT). All predictors were used in order to generate a design matrix of size trials x predictors (D_{mat}, Figure 33). The model estimated beta parameters relying on standard ordinary least squares (OLS) (S. J. Kiebel & Friston, 2004a, 2004b; Litvak et al., 2011; Pernet et al., 2011). Although (Pernet et al., 2011) argued that the most appropriate solution in order to make regressions more robust is estimating beta parameters using weighted least squares (WLS), a robust implementation does not exist yet. Thus, OLS has been recommended as the safest solution, until a robust implementation of WLS is published (Pernet et al., 2011).

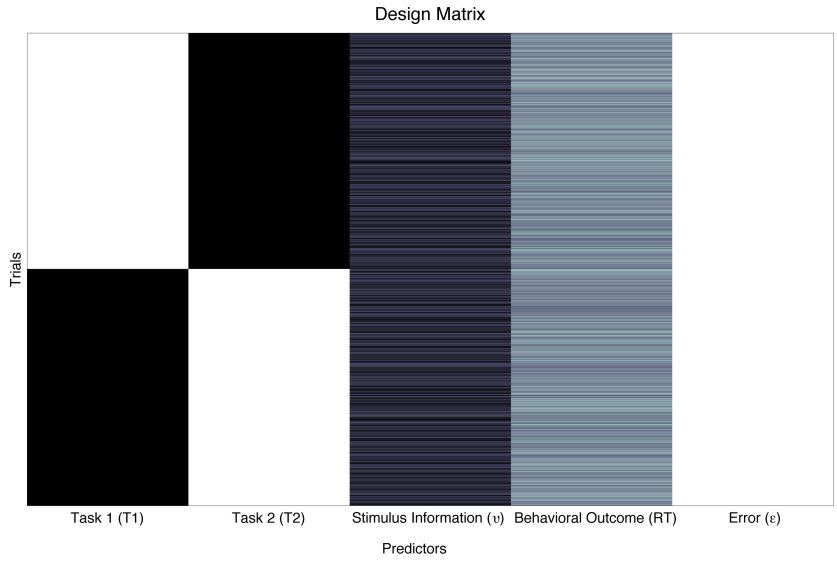

Figure 33 – Example of the design matrix used for the linear model. For each subject a design matrix (D_{mat}) was constructed. Each matrix was of size trials x predictors. Predictors for task demands (T1, T2) were categorical, they indicate trial belonging to Task 1 or Task 2. Predictors for stimulus information (υ) and behavioral outcome (RT) were continuous. Each continuous predictor was z-scored independently per subject before its incorporation in the design matrix. The final column represents a constant error term (ε)

The solution to ordinary least squares (Equation 6) was obtained using Equation 7, where β_w is estimated using the design matrix (D_{mat}) and the data matrix (Y). Superscript T indicates the transpose of a given matrix (S. J. Kiebel & Friston, 2004a, 2004b; Litvak et al., 2011; Pernet et al., 2011).

Equation 7

$$\beta_w = \left(D_{mat} D_{mat}^{-T} \right)^{-1} D_{mat} Y^T$$

Using Equation 6 and Equation 7 I obtained 5 different regression coefficients, 4 of them associated to each one of the dimensions of the present paradigm, represented in the

design matrix (Figure 33). The 5th regression coefficient was associated to the error term and will not be used further.

Equation 8

$$\beta w_{SIT1} = \beta_{w1} T1 + B_{w3} \upsilon$$
$$\beta w_{SIT2} = \beta_{w2} T2 + B_{w3} \upsilon$$

From the 4 paradigm-related coefficients, one of them was merged in order to obtain a descriptor of the effects of stimulus properties on task demands. In other words, in order to generate beta weights quantifying the influence of stimulus information on task demands (βw_{SIT}), the beta weight associated with stimulus information ($\beta_3 \upsilon$) was combined with beta weights associated with each task ($\beta_1 T1$, $\beta_2 T2$) using Equation 8.

The new beta weights associated with the effect of stimulus information on task demands (βw_{SIT}) were used for group-level analyses[31] in order to test the influence of stimulus properties on task demands. Furthermore, the beta weights independently associated with task 1 ($\beta_1 T1$) and task 2 ($\beta_2 T2$) were also used for group-level statistical analysis. Moreover, beta coefficients associated to stimulus properties ($B_{w3} \upsilon$) and to behavioral outcome ($\beta_{w4} RT$) were individually tested at the group-level analyses. Thus, between-subject analyses for linear measures were made in order to answer 4 specific questions derived from the present experimental design (2.4 Linear Modeling of EEG Measures).

[31] These analyses are also known as "between-subjects" or "level 2 analysis" (Wilcox, 2005)

The main advantage of this approach is that each one of these analyses answered a specific question regarding one of the dimensions of the present design (see 5. Discussion).

Event Related Potentials (ERP)

Event-related potentials (ERP) were computed per subject independently at each electrode (*ch*) by adding raw voltage at each time-point for all trials (*r*) and diving the resulting value by the number of trials (*n*).

Single-trial baseline normalization was used for ERP as implemented by the *rmbase.m* function of the EEGLAB toolbox (Delorme & Makeig, 2004). Baseline period was arbitrarily defined from -100 to 0 ms. This period was chosen because it is a common period used in other ERP studies providing a good reference of pre-stimulus onset EEG activity.

Equation 9

$$ERP_{(ch,t)} = 1/n \sum_{i=1}^{n} r_i$$

Since averaging can be conceptualized as a low-pass filter, unlike many ERP studies that apply further 30 or 40 Hz low-pass filtering, no additional filtering was applied to ERPs in this dissertation. Thus, the range of frequencies included in the ERP measure was 0.1 – 100 Hz.

Single-trial ERPs were linearly modeled at the single-subject level using Equation 6 and Equation 7. ERP beta weights for stimulus information over task demands (stimulus

difficulty, ERP βw_{SIT}) were obtained using Equation 8. ERPs are reported in units of μV/std.

Event-Related Spectral Power (ERSP)

Event-related spectral power (ERSP) was computed per subject independently at each frequency, electrode, and trial. The first step to compute ERSP was to choose appropriate parameters to generate complex Morlet wavelets. Wavelet parameters were kept constant for ITPC, ISPC, and CFC analyses (see 3.5 EEG data analysis). A total of 34 linearly spaced frequency centroids were obtained from 4 to 70 Hz. A total of 200 time-frequency points were obtained from the wavelet-convolved EEG data using Equation 3. Raw EEG power was estimated using Equation 4 on the complex time-series output from Equation 3.

Single-trial baseline normalization was applied to the total raw EEG power according to the guidelines suggested by Grandchamp and Delorme (2011). Baseline period was arbitrarily defined from -200 to -50 ms. This period was chosen because it provides a good reference of pre-stimulus onset EEG power activity, without going into the distorted edge of the trial (-500 to -250 ms). Frequency-specific baseline power was computed within the specified window and then removed from the rest of the epoch in a trial-by-trial fashion. This procedure allowed the estimation of total ERSP (see Figure 12). I will refer to "total ERSP" simply as "ERSP".

Single-trial ERSPs were linearly modeled at the single-subject level using Equation 6 and Equation 7. ERP beta weights associated with the influence of stimulus information over task demands (stimulus difficulty, ERSP βw_{SIT}) were obtained using

Equation 8. No further transformations were applied. ERSPs are reported in units of μV/std.

Event Related Phase-amplitude Coupling (ERPAC) analysis

Event-related phase-amplitude coupling (ERPAC) was computed per subject independently at each frequency pair, electrode (*ch*) and trial (*r*) according to the method described by Voytek et al. (2013). In order to keep consistency with the other time-frequency measures, ERPAC was computed using the analytic signal obtained using the parameters implemented for ERSP, ITPC, and ISPC (3.5 EEG data analysis). Thus, a total of 34 frequency centroids were linearly obtained from 4 to 70 Hz.

Voytek's cross-frequency approach (2013) was chosen because it allows the computation of phase-amplitude coupling (PAC) across trials in time. In contrast, regular PAC methods only allow the computation of phase-amplitude coupling on a pre-defined time window, requiring several samples for increased signal-to-noise ratio (Canolty et al., 2006; M. X. Cohen, 2008; Penny et al., 2008; Tort et al., 2010).

In traditional PAC estimation, the time-varying time-series of high-frequency power is used in order to assign a "weight" to a given phase angle (Canolty et al., 2006; M. X. Cohen, 2008; Penny et al., 2008; Tort et al., 2010). The phase angle vector of a low frequency (ϕ) and the vector length of a high-frequency power (a) at a given time-point (t) represented in polar space will create a "phase/amplitude angle". A pre-defined time-window can be used to generate as many "phase/amplitude angles" as time points (n). The length of the average vector of "phase/amplitude angles" is the measure of phase-amplitude coupling at that particular time-frequency time window (Equation 10, i =

imaginary operator from Euler's formula) and is usually interpreted as in arbitrary units of coupling strength.

Equation 10

$$PAC_{ch} = \left| n^{-1} \sum_{t=1}^{n} a_t e^{i\phi t} \right|$$

In contrast, ERPAC was computed based on circular-linear correlation using the circular statistics MATLAB toolbox (Berens, 2009). Each low frequency phase (ϕ) was linearized using *circ_corrcl.m.* Thus, a single correlation coefficient ($\rho_{\phi a}$ Equation 11) based on Pearson product-moment correlation coefficient (c) can be computed between the linearized low frequency phase and a high-frequency amplitude (a, linear by default).

This method allows computing the correlation between a high-frequency amplitude and a low-frequency phase at each time point (t), without the necessity to integrate "phase/amplitude angles" across a pre-defined temporal window as in Equation 10. Thus transient event-related phase-amplitude coupling (ERPAC) can be quantified in a point-by-point fashion (Voytek et al., 2013).

Equation 11

$$\rho_{\phi_t a_t} = \sqrt{\frac{(Pc_{ca}^2 + Pc_{sa}^2 - 2Pc_{ca}Pc_{sa}Pc_{sc})}{(1 - Pc_{sc}^2)}}$$

$$Pc_{ca} = c(\cos\phi, a)$$
$$Pc_{sa} = c(\sin\phi, a)$$
$$Pc_{sc} = c(\sin\phi, \cos\phi)$$

In order to compute phase-amplitude cross-frequency coupling, a "source" low frequency phase has to be chosen. Due to the lack of a better method at the time (see 7. Future Directions) the center frequency of the theta (4 – 8 Hz) and alpha (8 – 12 Hz) frequency bands was arbitrarily chosen. Thus, the selected low frequency phase for theta-based phase amplitude coupling was 6 Hz whereas the selected low frequency phase for theta-based phase amplitude coupling was 10 Hz.

Although a non-linear measure, ERPAC was used as a linear measure in order to take advantage of the linear model implemented in this dissertation, better explaining data variance at the single-trial, single-subject, and group levels (see 3.5.1 Analysis of linear measures). Single-trial baseline normalization (Grandchamp & Delorme, 2011) was applied to ERPAC. Baseline period was arbitrarily defined from -200 to -50 ms. This period was chosen because it provides a good reference of pre-stimulus onset coupling strength, without including data points that might be potentially distorted with edge artifacts (-500 to -250 ms). Frequency-specific baseline phase-amplitude coupling strength was computed within the specified window and then removed from the whole epoch in a trial-by-trial fashion.

Single-trial ERPAC was linearly modeled at the single-subject level using Equation 6 and Equation 7. ERP beta weights associated with the influence of stimulus information over task demands (stimulus difficulty, ERSP βw_{STT}) were obtained using Equation 8. No further transformations were applied. ERPAC are reported in arbitrary units of coupling strength bounded from -1 to 1.

3.5.2 Analysis of Non-Linear Measures

In addition to linear measures, I implemented non-linear measures of EEG. Non-linear dynamics have been less explored in cognitive electrophysiology and little is known about their temporospatial dynamics. Ideally, assigning weights to single-trial phase angles according to parameterized predictors would have been an appropriate approach to analyze phase-based EEG dynamics. However, non-linear measures cannot be linearly modeled. Thus, the exploration of phase-based measures of brain activity will not be able to benefit from the linear model implemented in this dissertation (3.5.1 Analysis of linear measures).

By the time of the analyses were made[32] I did not know a method to assign weights to single-trial phase angles. However, I have recently found out a method solve this problem (M. X. Cohen & Cavanagh, 2011). Unfortunately, there was no time to update the analyses. However, I have added a section regarding this issue (see 5. Discussion).

[32] January/February 2014

Inter-Trial Phase Clustering (ITPC) analysis

Inter-trial phase clustering (ITPC) was computed per subject at the estimated R^2-optimized sensor (R^2_ϕ) for trials belonging to task 1 and task 2. The first step to compute ITPC was to choose appropriate parameters to generate complex Morlet wavelets (3.5 EEG data analysis). A total of 34 frequency centroids were linearly obtained from 4 to 70 Hz. These parameters are the same for ERSP, ISPC, and CFC analyses (see 3.5 EEG data analysis).

Equation 12 denotes the computation of ITPC. Where n is the number of trials. $e^{ik_{tfr}}$ is derived from Euler's formula which represents the phase angle (k) from trial (r) at time-frequency (tf) in the complex polar plane (e.g. Figure 31). In ITPC the magnitude of the vector is not taken into account. Thus, the length of the vectors at each time-frequency point and trial is set to 1 (J. P. Lachaux, E. Rodriguez, J. Martinerie, & F. J. Varela, 1999).

Equation 12

$$ITPC_{R^2_{\phi tf}} = \left| n^{-1} \sum_{r=1}^{n} e^{ik_{tfr}} \right|$$

No baseline normalization procedures are necessary for the computation of ITPC (J. P. Lachaux et al., 1999). ITPC is presented in bounded arbitrary units of phase clustering (0 – 1).

Inter-Site Phase Clustering (ISPC) analysis

Inter-site phase clustering (ISPC) was computed per subject independently, per frequency (*f*) at each pair of electrodes in regard to a "source" electrode defined by the estimated R^2-optimized sensor (R^2_ϕ) for trials belonging to task 1 and task 2. The first step to compute ISPC was to choose appropriate parameters to generate complex Morlet wavelets (3.5 EEG data analysis). A total of 34 frequency centroids were linearly obtained from 4 to 70 Hz. These parameters are the same for ERSP, ITPC, and CFC analyses (see 3.5 EEG data analysis).

Equation 13 was used to estimate ISPC at each frequency (*f*) between the R^2_ϕ-optimized sensor and all other electrodes (*y*), where *n* is the number of trials. The difference between phase angles recorded at the R^2_ϕ-optimized sensor ($\phi_{R^2_\phi}$) and the phase angles of another electrode (ϕ_y) was averaged across trials (*r*).

Equation 13

$$ISPC_f = \left| n^{-1} \sum_{r=1}^{n} e^{i\left(\phi_{R^2_\phi r} - \phi_{yr}\right)} \right|$$

Equation 13 is very similar to Equation 12. However ISPC instead of taking the average of phase angles, takes the average of phase angle differences between 2 signals from different electrodes (Lachaux et al., 2000; Mormann, Lehnertz, David, & E Elger, 2000).

As explained before (

2.3.1 Inter-Site Phase Clustering (ISPC)), baseline normalization is required in order to assess event-related inter-site phase clustering. Baseline period was arbitrarily defined from -200 to -50 ms. This period was chosen because it provides a good reference of pre-stimulus onset ISPC activity, without including data points that might be potentially distorted with edge artifacts (-500 to -250 ms). Frequency-specific baseline mean phase angle differences value was obtained and subtracted from the remaining part of the epoch. ISPC is reported in unbounded arbitrary units of phase clustering.

3.6 Statistical Testing

Within-subject analyses (level 1) and group-level analyses were performed for all measures implemented in this dissertation. Linear and non-linear dynamics were analyzed using separate pipelines but the same technique.

All analyses in this dissertation were performed on the complete time-series[33]. Within-subject ERP analysis was conducted at all electrodes. Between-subject analyses were performed at the R^2_{ERP}–optimized electrode per regressor (β_w), across all 601 time points comprising the time frames between -200 to 1000 ms. Thus, a total of 1803 tests were run for the ERP measure.

Within-subject ERSP and ERPAC analysis were conducted at all electrodes. Between-subject analyses were run at the R^2_{ERSP}– and R^2_{ERPAC}–optimized electrode per regressor (β_w) for ERSP and ERPAC respectively. All 34 linearly-spaced frequency bands were tested at 159 time points comprising the time frames between -200 to 1000

[33] Ignoring the 300 ms of padding at each side of the epoch

ms. A total of 16,218 tests were run for the ERSP measure. While a total of 69,165 tests were run for ERPAC.

Statistical tests for ITPC and ISPC were run at an estimated electrode based on the mean of all available R^2. All 34 linearly spaced frequency bands were tested at 159 time points comprising the time frames between -200 to 1000 ms. A total of 5,406 tests were run in ITPC, while a total of 167,586 tests were run for ISPC.

R^2–optimized electrodes for linear measures and the estimated R^2 electrode for non-linear measures were used as a dimensionality reduction technique, decreasing the amount of statistical tests in ~90%[34]. The *n*-dimensional clustering technique was used in order to correct for the increased number of statistical tests performed along the time-series (Litvak et al., 2011; Maris & Oostenveld, 2007; Pernet et al., 2011). Statistical threshold for all analyses was 0.01.

Within-Subject (Level 1) analysis

Within-subject analysis can be used for establishing statistical significance within each subject. Importantly, it can also help decreasing small sample bias. Furthermore, it can be used in order to generate robust estimates of effect sizes and studying individual differences (Wilcox, 2005a). Hence, level 1 analysis is a powerful approach that has encountered little use in cognitive electrophysiology (Rousselet & Pernet, 2011).

In this dissertation, instead of using within-subject analysis to establish statistical significance *per se* I implemented it in order to generate robust measures of temporal

[34] In comparison to a complete exploratory approach in time and space

dynamics taking into account single-trial, single-subject variance. Thus providing more appropriate measures for group-level analyses.

For level 1 analysis, linear measures benefited from multilinear regression, generating a linear mapping between EEG time and time-frequency features to regressors derived from the present parametric design and participants' behavior (2.4 Linear Modeling of EEG Measures and 3.5.1 Analysis of linear measures). Thus, for linear measures, beta weights were estimated per subject using Equation 6 and Equation 7. This procedure led to 4 different regression coefficients. Each coefficient was associated with a different dimension of the present paradigm (see 2.4 Linear Modeling of EEG Measures). Individual beta weights were used in subsequent group-level statistical analysis.

Since non-linear measures could not benefit from the multilinear regression implemented in this dissertation, non-parametric permutation was used to perform within-subject analysis. The analytic signal of EEG was divided into trials belonging to task 1 and trials belonging to task 2. Level 1 analysis for both phase-based measures (ϕ_m) was implemented independently. I computed Equation 12 and Equation 13 500 times. Each time, trials were randomly shuffled from task 1 and task 2 per subject. Creating thus 500 null-model ($\phi_{m_{null}}$) ITPC and ISPC. The final step used Equation 14 in order to create robust phase-based measures (ϕ_{m_z}) per subject, which were used for group level statistical analysis.

Importantly, unlike group-level analysis, within-subject analysis was performed at all time-points and at all electrodes.

Equation 14

$$\phi_{m_z} = \left(\phi_m - 1/n \sum_{i=1}^{n} \phi_{m_{null_i}} \right) \Big/ std\left(\phi_{m_{null}} \right)$$

Between-Subjects (Level 2, group) analysis

Group-level statistics were performed on beta coefficients for linear measures (Equation 6, Equation 7). In contrast, in order to explore non-linear brain dynamics, normalized phase-based measures were used (Equation 14). Although level 1 analysis for linear and non-linear measures differed in strategy it was implemented for all measures and all participants. Furthermore, group-level analyses were implemented using non-parametric permutation testing for all measures in order to assess statistical significance.

In general, level 2 analyses use gran average means per subject in order to assess statistical significance at the group level. I implemented this part of the analysis using the non-parametric permutation testing framework to generate null-model distributions (Wilcox, 2005a). Thus, group-level analyses were performed on linear measures to answer 4 specific questions (3.5.1 Analysis of linear measures):

1. The goal of the first analysis is to explore the possible impact of stimulus features (Parameter 2 – Test Face Difference) on linear measures of brain dynamics. Thus, beta coefficients associated with mixing level of the composite image ($\beta_{w3}\upsilon$) were tested against a null-model generated with 10,000 permutations. The null hypothesis was that a particular time or

time-frequency feature described by $\beta_{w3}\upsilon$ is not reliable or consistent across subjects. Hence, in each one of the iterations participants were resampled with replacement and their time-frequency time series were shifted by a random amount. Thus generating a null-model where time-frequency points had no temporal correlation to the stimulus onset across subjects. The original $\beta_{w3}\upsilon$ was thresholded using the null-model in order to establish statistical significance. Correction for multiple comparisons using *n*-dimensional clustering technique was applied to the whole time series and time-frequency maps

2. The second analysis focused on differences quantified by all measures produced by task demands. For linear measures, beta coefficients associated with task 1 ($\beta_{w1}T1$) were tested against beta coefficients associated with task 2 ($\beta_{w2}T2$). For non-linear measures, the robust measures of ITPC and ISPC associated with task 1 (ϕ_{m_z}, Equation 14) were tested against robust measures of ITPC and ISPC associated with task 2 (ϕ_{m_z}, Equation 14). The null-hypothesis for this analysis assumed no differences between task 1 and task 2 across subjects. I used a bootstrap-*t* technique with 10,000 resamples. At each one of the iterations data from each subject from both conditions were resampled with replacement in order to generate 10,000 new subject groups under the null-model (Z-map). The original observed difference between task 1 and task 2 was

compared against the null-model at each time and time-frequency point in order to establish significant differences. Correction for multiple comparisons using *n*-dimensional clustering technique was applied to the whole time series and time-frequency maps

3. The goal of the third analysis was to uncover linear EEG features associated with the trial-by-trial variation of response times (RT). Thus, beta coefficients associated with participants' reaction time ($\beta_{w4}RT$) were tested against a null-model generated with 10,000 permutations. Just like the null-model for the first analysis, this null hypothesis assumed no real correlation between time-frequency points described by $\beta_{w4}RT$ and response time. Hence, in each one of the iterations participants were resampled with replacement and their time-frequency time series were shifted by a random amount. Thus generating a null-model where time-frequency points had no temporal correlation to participants' response time. The original $\beta_{w4}RT$ was thresholded using the null-model in order to establish statistical significance. Correction for multiple comparisons using *n*-dimensional clustering technique was applied to the whole time series and time-frequency maps

4. The fourth analysis focused on the effects of stimulus difficulty defined by stimulus properties over task demands. Beta coefficients

associated with task 1 ($\beta_{w1}T1$) were combined with beta coefficients associated with stimulus properties ($\beta_{w3}\upsilon$) using Equation 8. Likewise, beta coefficients associated with task 2 ($\beta_{w1}T2$) were combined with beta coefficients associated with stimulus properties ($\beta_{w3}\upsilon$) using Equation 8 giving way to combined beta weights ($\beta_{w_{SIT}}$). The combined beta weights ($\beta_{w_{SIT1}}, \beta_{w_{SIT2}}$) were tested for significant differences. The null-hypothesis for this analysis assumed no differences between $\beta_{w_{SIT1}}$ and $\beta_{w_{SIT2}}$ across subjects. I used a bootstrap-*t* technique with 10,000 resamples. At each one of the iterations data from each subject from both combined beta weights were resampled with replacement in order to generate 10,000 new subject groups under the null-model (Z-map). The original observed difference between $\beta_{w_{SIT1}}$ and $\beta_{w_{SIT2}}$ was compared against the null-model at each time and time-frequency point in order to establish significant differences. Correction for multiple comparisons using *n*-dimensional clustering technique was applied to the whole time series and time-frequency maps

Although statistical tests could have been performed at all electrode sites, I used the mean coefficient of determination (R^2, see 2.4 Linear Modeling of EEG Measures) as a dimensionality reduction technique (Foxe & Simpson, 2002; Liu, Harris, & Kanwisher, 2002; Rousselet, Husk, et al., 2008; Rousselet, Pernet, et al., 2008). This procedure allowed me to considerably reduce the number of statistical tests performed while

avoiding circular inferences. Thus, group-level statistical tests in linear measures were performed at the correspondent R^2–optimized electrode per regressor.

No R^2–optimized electrode was obtained for non-linear measures, therefore I estimated one (R^2_ϕ). The estimated R^2_ϕ allowed me to considerably reduce the number of statistical tests performed in non-linear measures. Considering the ISPC measure where an exploratory approach would lead to 1,383,936 tests. R^2_ϕ reduced this number to 167,586. Thus, group-level statistical tests in non-linear measures were performed at the estimated R^2_ϕ–optimized electrode.

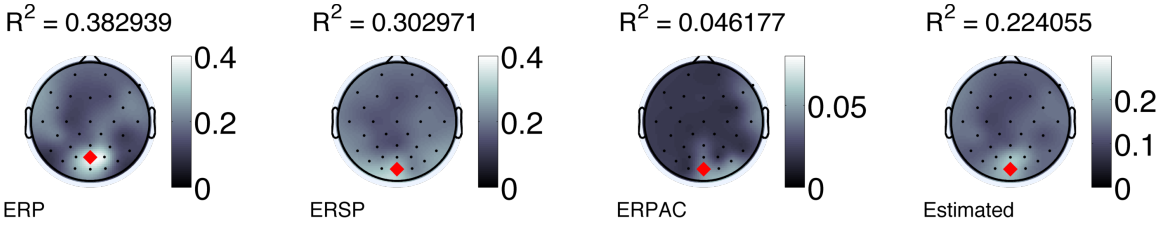

Figure 34 – Topographical representation of maximum mean R^2 per measure and the estimated R^2 defined as the mean of all quantified R^2 that were used to select the electrode for group-level analyses in each linearly-modeled measure

Results for between-subject analysis will be presented in "z-maps" in order to compare results across measures and analyses. Z-maps were computed after 10,000 permutations derived from observed differences (O_{diff}) and permuted values (P_{diff}) expected under the null hypothesis using Equation 15.

Equation 15

$$Z - map = \left(O_{diff} - 1/n \sum_{i=1}^{n} P_{diff_i} \right) \Big/ std(P_{diff})$$

Correction for Multiple Comparisons

Control for multiple comparisons was implemented using non-parametric permutation and *n*-dimensional clustering technique (Litvak et al., 2011; Maris & Oostenveld, 2007; Pernet et al., 2011).

ERP analyses were performed in the time domain. ERSP, ITPC, and ERPAC analyses were performed in the time-frequency domain. ISPC analysis was performed in the time-frequency-space domain. For all between-subject analyses, building clusters of statistically significant time, time-frequency, and time-frequency-space points implemented correction for multiple comparisons.

Maris and Oostenveld (2007) suggest that the most appropriate technique for establishing corrected-significance in electrophysiological recordings is to build clusters by applying an "uncorrected pre-cluster threshold" of 0.01 to the whole time, time-frequency, or time-frequency-sensor map for each one of the iterations in the permutation. Since clusters were generated under the null-hypothesis, all surviving clusters to this "pre-cluster threshold" have to be considered a false alarm and further proof of their statistical significance is needed. This technique is sensitive to small clusters with highly significant test statistic values, and to large clusters with mildly significant test static values.

Thus, at each one of the iterations, the sum of the maximum test statistic for each one of the supra-threshold clusters generated under the null hypothesis was obtained and stored. This process was repeated 10,000 times per measure, per analysis. In order to threshold the observed data[35] or the Z-maps[36], the distribution of the largest supra-threshold clusters expected by chance was used to identify the observed data clusters that were lower than 99% of the null-hypothesis (Maris & Oostenveld, 2007). These clusters were removed generating cluster-corrected time, time-frequency, and time-frequency-space maps from observed differences or Z-maps.

4. Results

In the following sections I will describe the results obtained in the group-level analysis. Although between-subject analyses were run on specific R^2-optimized electrodes, when appropriate I will display the data with as much context as possible.

I will describe results organized by measure. Thus, I will start off with Event-related potentials (ERP) followed by event-related spectral power (ERSP) and inter-trial phase clustering (ITPC). Finally, I will describe inter-site phase clustering (ISPC) and event-related phase-amplitude coupling (ERPAC) results.

Furthermore, when describing results I will subdivide them according to the group-level analyses. This is 1) Sensitivity to Stimulus Properties, 2) Sensitivity to Task Demands, 3) Sensitivity to Behavioral Outcome, and 4) Sensitivity to Stimulus Properties over Task Demands.

[35] i.e. non-permuted, from real subjects
[36] i.e. generated under the null-hypothesis from 10,000 permutations

4.1 ERP results

Event-related potentials were robustly elicited by all conditions. Grand average ERP across all trials and participants at the R^2-optimized electrode shows clear ERP components (Figure 35).

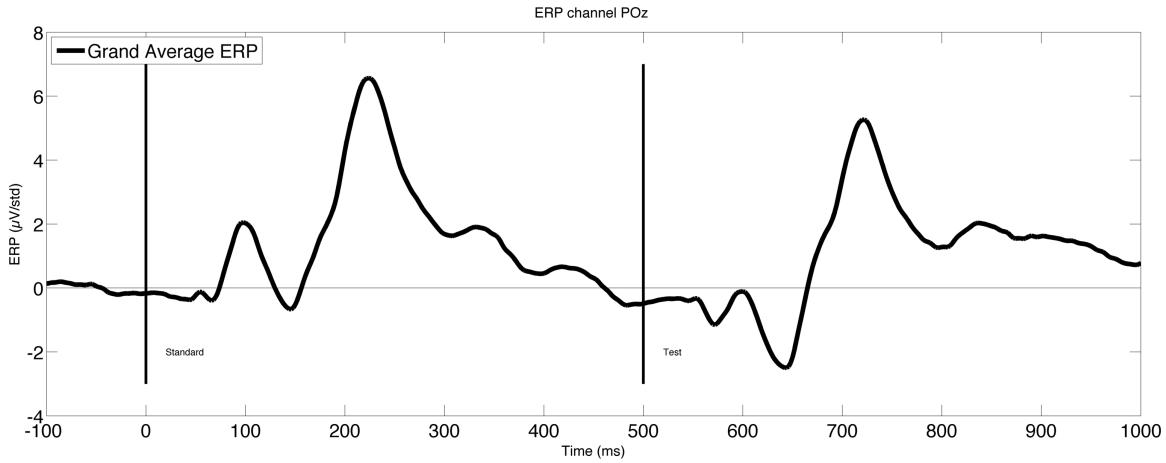

Figure 35 – Grand average ERP across all trials and participants. Clear responses for the standard stimulus (C1, P1, N1, P2), while the standard elicited C1, P1, N1, and P2 ERP components

Clear P1, N1 and P2 components were elicited by presentation of the standard composite image. Furthermore, clear C1, P1, N1, and P2 were elicited by the presentation of the test image (Figure 35, left).

No statistically significant results were found for ERP in any of the 4 group-level analyses (Figure 36).

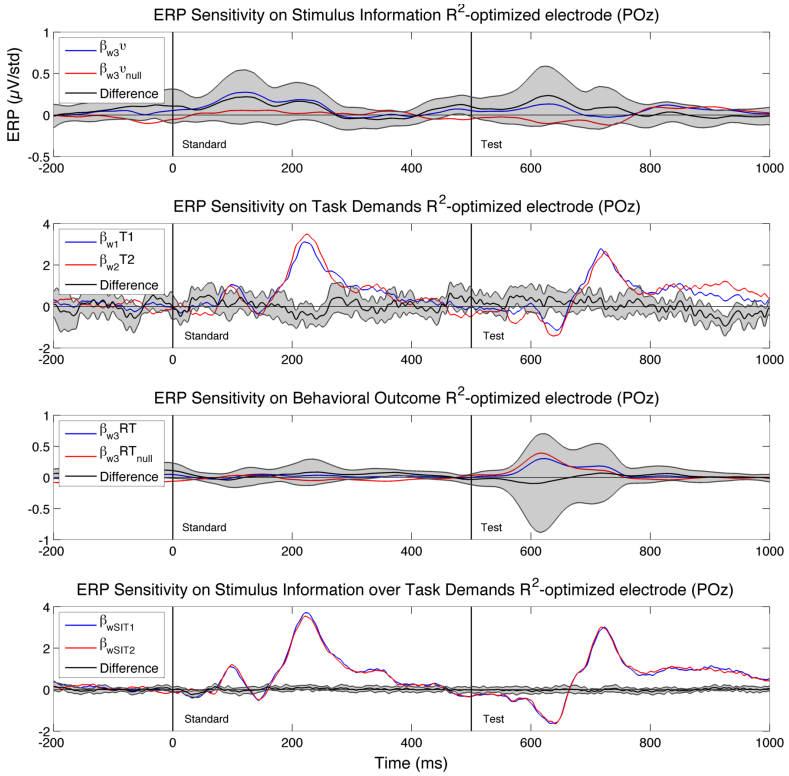

Figure 36 – ERP results for the 4 group-level analyses at the R^2–optimized electrode. No statistically significant results were found. Shaded areas indicate 99% confidence intervals

4.2 ERSP results

Time-frequency specific changes in spectral power were quantified by event-related spectral power (ERSP) in all conditions. Grand average ERSP across all trials and participants at the R^2-optimized electrode shows clear changes in mean spectral power from baseline. Figure 37 shows that both standard and test composite images elicited similar spectral components.

Most notably broadband power increments extending from ~100 to ~250 ms, peaking around 200 ms in the 4 to 12 Hz range after both standard and test onset. Furthermore, a broadband power decrement is seen starting ~300 ms after both standard

and test onset and extending for about 250 ms. Specific spectral features were seen in the gamma range (30 to 70 Hz). First, an "early" gamma burst (~100 ms after standard and test onset) between 30 and 40 Hz followed by a higher-frequency component between 45 and 70 Hz extending from ~100 to 200 ms. Finally, a "late" gamma burst (~300 ms after standard and test onset) between 35 and 60 Hz.

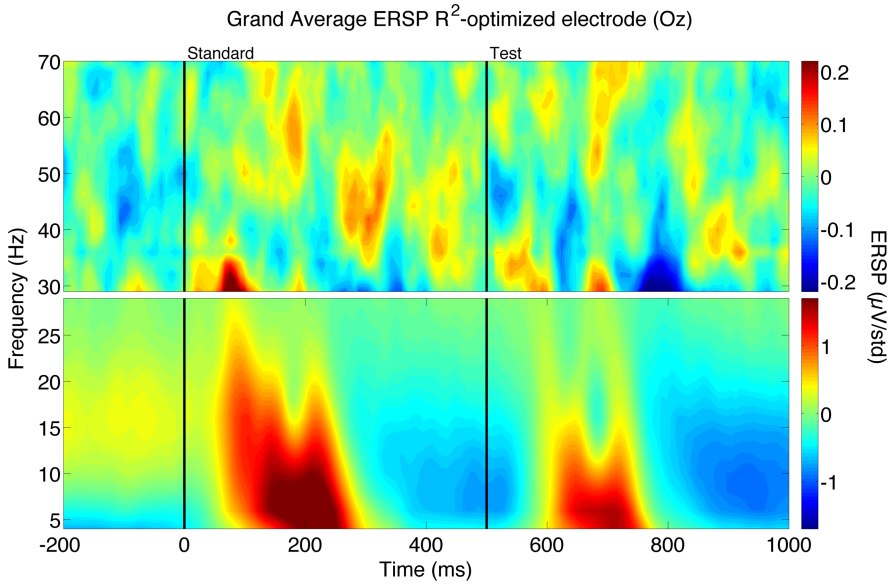

Figure 37 – Grand average ERSP for all trials and participants at the R^2–optimized electrode Oz. Clear time-frequency features elicited by stimuli presentation are quantified by ERSP

4.2.1 Sensitivity to Stimulus Properties

Results for this analysis are presented in Figure 38. Small power changes can be seen in the observed beta weight associated with stimulus properties ($\beta_{w_3} \upsilon$). The largest increments in power were seen in the 4 to ~15 Hz range occurring 100 ms before the standard onset. Furthermore a high-frequency gamma burst (~50 to ~60 Hz) at ~200 ms

post-stimuli onset can be seen after the presentation of both standard and test onset (Figure 38 left panel).

Right panel of Figure 38 displays the z-map obtained with 10,000 permutations. No supra-threshold clusters are seen.

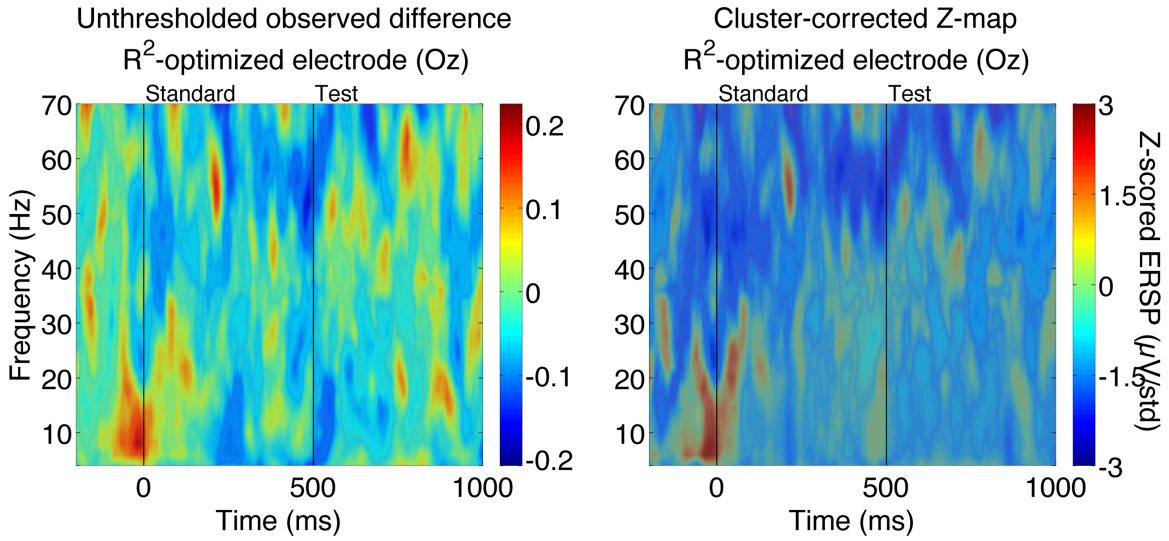

Figure 38 – ERSP sensitivity to stimulus properties. LEFT panel displays a time-frequency representation of the observed beta weight for stimulus properties ($\beta_{w_3 v}$). RIGHT panel displays cluster-corrected Z-map for stimulus properties after 10,000 permutations. No supra-threshold clusters are found

4.2.2 Sensitivity to Task Demands

Results for this analysis are presented in Figure 39. Top panels of Figure 39 show time-frequency representations of beta weights associated with each task. Mean spectral power differences from baseline display very similar responses in the lower range of the frequency spectrum (4 – 30 Hz). Both stimuli elicited strong broadband power increase (4 – ~25 Hz) extending from ~60 to ~250 ms post-stimuli onset followed by power decrements in a similar broadband range for both tasks (Figure 39, top panels).

Bottom left panel of Figure 39 shows the observed difference between regressors associated with task demands ($\beta_{w_1}T1$ and $\beta_{w_2}T2$). High-frequency power (>30 Hz) was mostly augmented for Task 1 throughout the epoch, whereas low-frequency power (<30 Hz) was overall larger for Task 2.

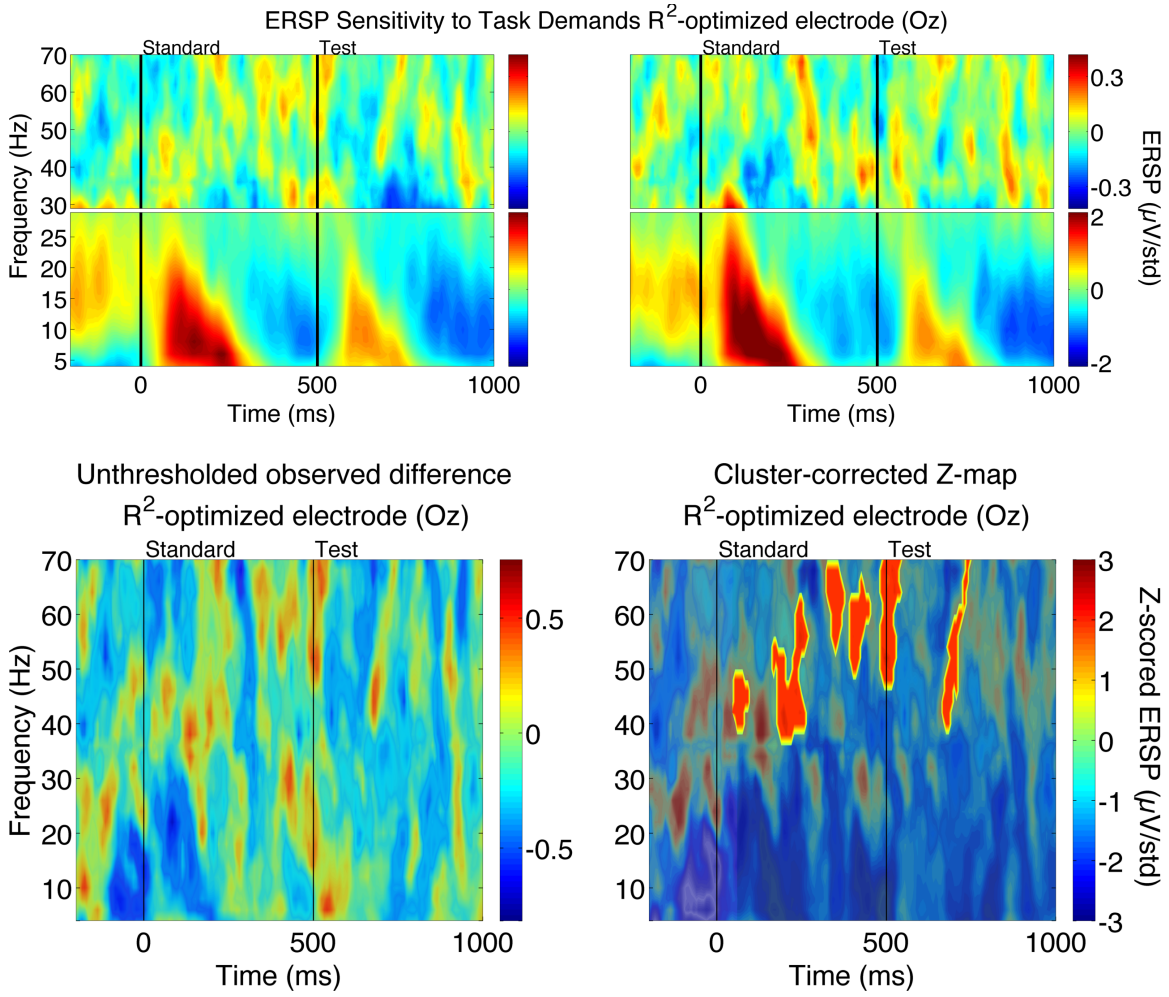

Figure 39 – ERSP sensitivity to task demands. TOP panels display time-frequency representations of observed data for beta weights associated with Task 1 (left, $\beta_{w_1}T1$) and Task 2 (right, $\beta_{w_2}T2$). BOTTOM LEFT. Observed difference between beta weight for Task 1 minus beta weight for Task 2. BOTTOM RIGHT. Cluster-corrected time-frequency representation of the z-map obtained after 10,000 permutations. Highlighted areas indicate statistically significant clusters

Figure 39, bottom right panel displays the z-map obtained after 10,000 permutations. Presentation of both test and standard images elicits larger spectral power in the high frequency range (> 25 Hz). In contrast, presentation of both test and standard images in task 2 elicits stronger power in lower frequencies (<25 Hz).

Group-level analysis reveals no statistically significant time-frequency clusters below ~35 Hz (Figure 39, bottom right panel). In contrast, statistically significant clusters were found in the gamma range above ~35 Hz. Six[37] different significant time-frequency supra-threshold clusters are observed. The first one occurs at ~60 ms after standard onset. Two of them occur at ~200 ms after stimuli onset for both standard and test (Figure 39, bottom right panel). These clusters have a similar time and frequency range extending for about 100 ms from ~40 to ~70 Hz. The next three clusters occur consecutively in time (~310 to ~550 ms post-standard onset) consistently from ~50 to 70 Hz (Figure 39, bottom right panel). Thus, statistically significant increments in gamma power are seen for the more car/more face discrimination judgment (Task 1) in contrast to the similarity judgment (Task 2).

4.2.3 Sensitivity to Behavioral Outcome

Results for this analysis are presented in Figure 40. Right panel shows the observed ERSP for the beta weight associated with behavioral outcome ($\beta_{w_4} RT$). Mean spectral power differences from baseline display small power changes throughout the epoch. The largest increments in power are seen in the 4 to ~10 Hz range occurring ~100 ms before the standard onset. Later in the epoch a high-frequency gamma increment (55

[37] Possibly 7

– 60 Hz) and decrement (~40 – 55 Hz) at ~200 ms post-test onset are seen. Although these specific time-frequency features were robust enough across subjects, they did not survive the group-level analysis. Thus, no statistically significant differences were found when the Z-map created with 10,000 permutations was cluster-corrected for multiple comparisons using 2-dimensional clusters in the time and frequency domains.

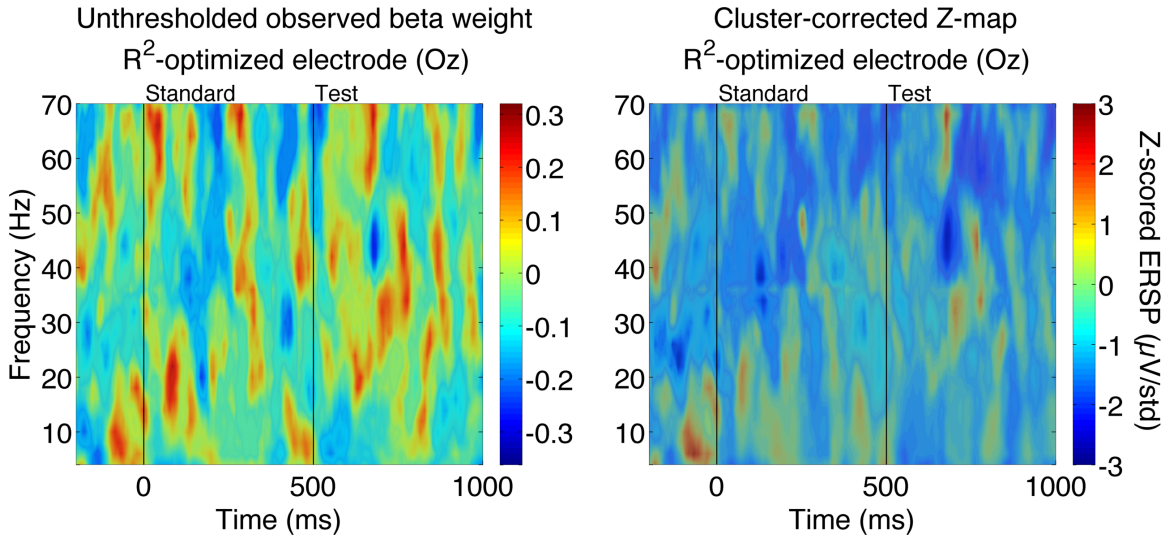

Figure 40 – ERSP sensitivity to behavioral outcome. LEFT panel displays time-frequency representations of beta weights for behavioral outcome ($\beta_{w4}RT$). RIGHT panel displays the cluster-corrected Z-map after 10,000 permutations. No statistically significant results are observed

4.2.4 Sensitivity to Stimulus Difficulty

Results for this analysis are presented in Figure 41. Top panels display the observed activity associated with the combined beta weights for task demands ($\beta_{w_1}T1$ and $\beta_{w_2}T2$) and stimulus properties ($\beta_{w_3}\upsilon$). Mean spectral power differences from baseline display clear and strong responses within a broadband frequency range

extending from 4 to ~ 40 Hz. Power increments are followed by power decrements after both standard and test onsets in both tasks (Figure 41, top panels). Most notably, both stimuli elicited strong broadband power increase (4 – ~40 Hz) at ~100 ms extending from ~60 to ~250 ms post-stimuli onset followed by power decrements in very similar broadband ranges (Figure 41, top panels). These similarities also extend in the time domain. The high-end of gamma band (40 – 70 Hz) shows discrete power increments. Although power notably increments at ~300 ms extending from ~40 to ~60 Hz (Figure 41, top panels) for both conditions, it is seen larger for task 2.

The observed difference between both combined betas displays diverse increments in power for both task 1 and task 2. However, task 1 elicits greater power when compared to task 2 in both high and low frequency ranges (Figure 41, bottom left panel). Most notably, gamma power is stronger for task 1 within the ~40 to ~50 Hz range at ~100 ms after presentation of both standard and test stimuli. Furthermore, stronger high gamma power (>50 Hz) is seen starting at ~300 ms up and ending right at the presentation of the test image (Figure 41, bottom left panel).

Between-subject analysis reveals no statistically significant increments in gamma power for the more car/more face discrimination judgment (Task 1) in contrast to the similarity judgment (Task 2) (Figure 41, bottom right panel). However, some robust features can be seen in the z-map generated after 10,000 permutations. Gamma power increases at ~100 ms within ~40 to ~45 Hz post-standard and post-test onset (Figure 41, bottom right panel). Both spectral features are congruent in time and frequency.

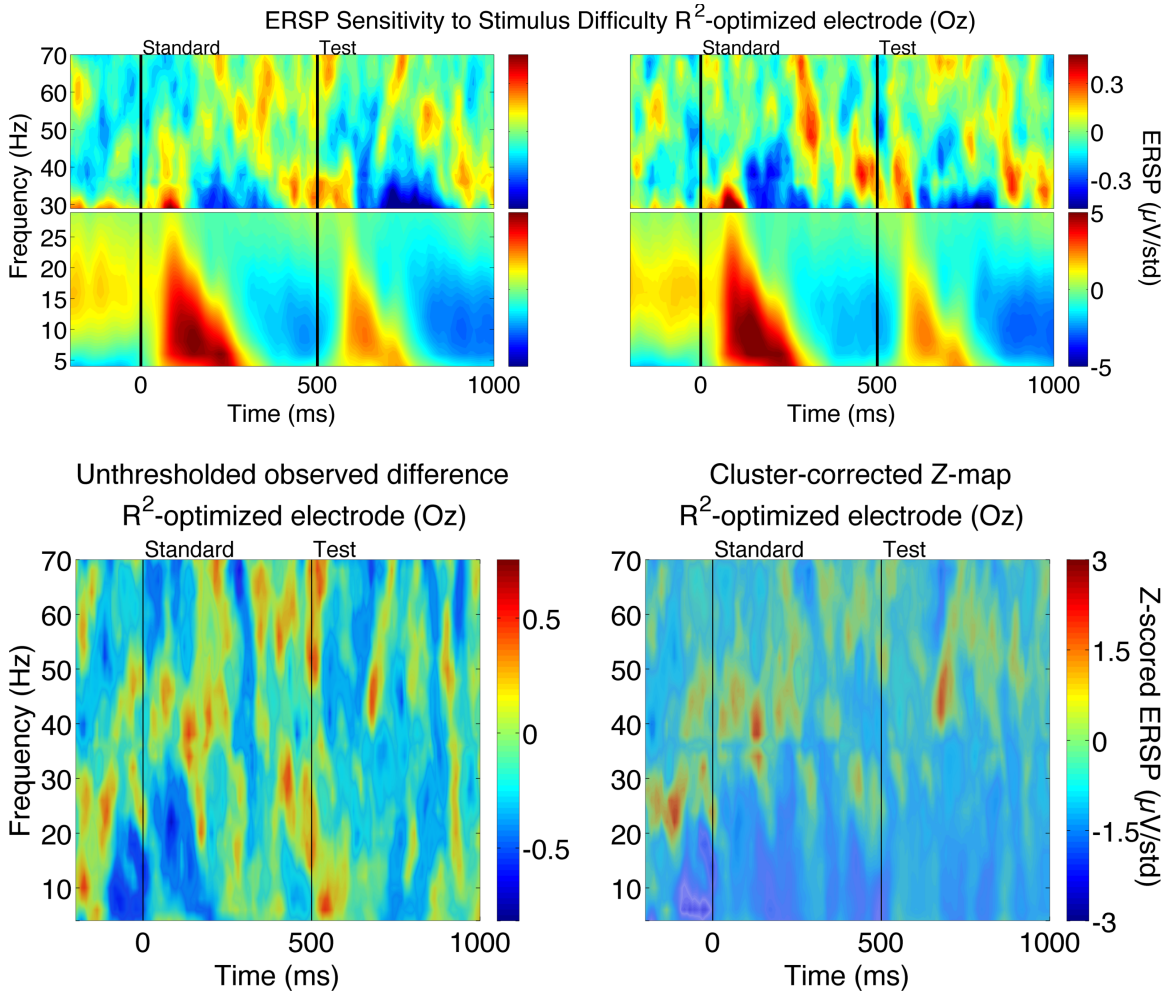

Figure 41 – ERSP sensitivity to stimulus difficulty. TOP panels display time-frequency representations of observed data for combined beta weights associated with effect of stimulus properties over task 1 (top left, $\beta_{w_{SIT1}}$) and task 2 (top right, $\beta_{w_{SIT2}}$). BOTTOM LEFT. Observed difference between beta weight for Task 1 minus beta weight for Task 2. BOTTOM RIGHT. Cluster-corrected time-frequency representation of z-map obtained after 10,000 permutations. No supra-threshold clusters are found

4.3 ITPC results

My results display clear and strong phase clustering in time and frequency. Figure 42 shows a grand average of all trials and all participants at the estimated R^2_ϕ electrode. Presentation of both standard and test composite images was followed by broadband

phase clustering within the ~10 to ~20 Hz range at ~150 ms post-stimuli onsets and extending to lower frequencies (4 Hz) around ~200 ms. Mean ITPC in the high frequency range (30 – 70 Hz) displayed increased consistency in 2 bouts. First period of high frequency phase consistency is seen at ~100 ms post-stimuli onset for both test and standard. Second period of phase consistency is seen at ~200 ms post-stimuli onset for both test and standard images (Figure 42).

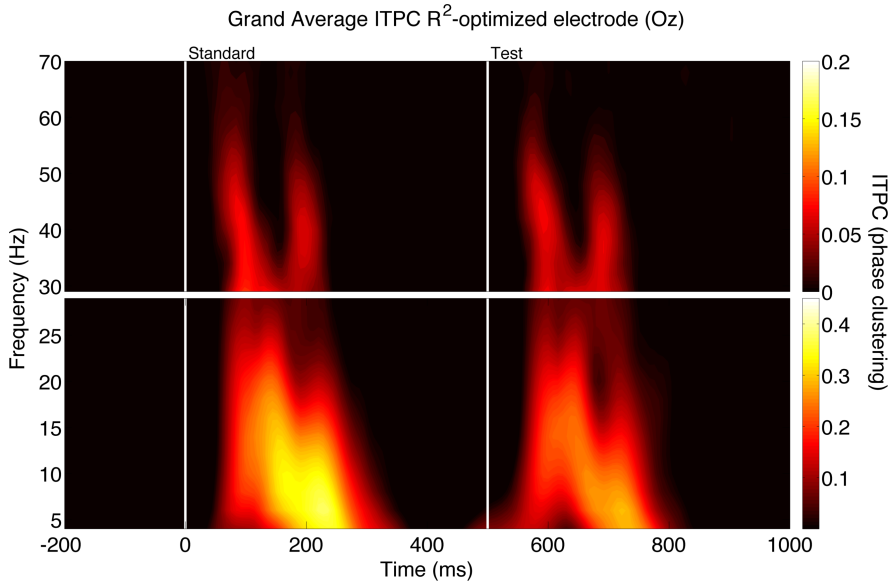

Figure 42 – Grand Average ITPC for all trials and participants at the estimated R_{ϕ}^{2} – optimized electrode Oz. Periods of phase consistency are seen after presentation of both standard and test stimuli

4.3.1 Sensitivity to Task Demands

Results for this analysis are presented in Figure 43. Top panels display the observed activity for ITPC for task 1 (left) and task 2 (right). Phase clustering for both tasks display very similar responses in the lower range of the frequency spectrum (4 – 30

Hz). Presentation of stimuli is followed by strong phase consistency peaking between 4 and ~15 Hz and extending from ~50 to ~350 ms post-stimuli onset (Figure 43, top panel).

The unthresholded observed difference time-frequency representation is shown in the bottom left panel of Figure 43. Small differences can be seen between task 1 and task 2.

Bottom right panel of Figure 43 displays results from the group-level ITPC analysis. No statistically significant time-frequency points are found.

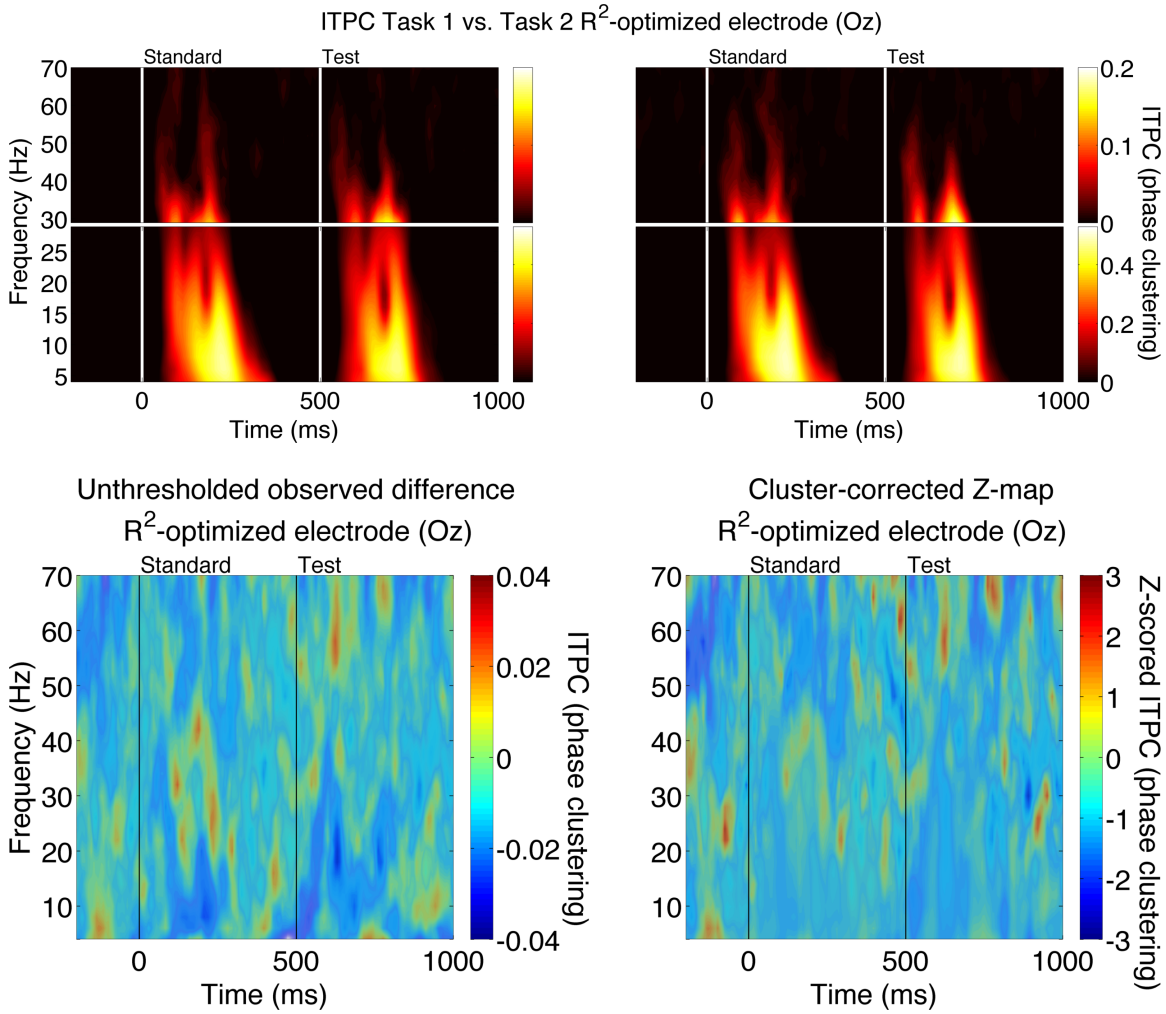

Figure 43 – ITPC results for comparison between Task 1 and Task 2. TOP panels display time-frequency representations of observed data for Task 1 (top left) and task 2 (top right). BOTTOM LEFT. Observed difference between Task 1 and Task 2. BOTTOM RIGHT.

Cluster-corrected time-frequency representation of z-map obtained after 10,000 permutations. No supra-threshold clusters are found

4.4 ISPC results

Clear phase clustering in time and frequency are quantified by ISPC. Figure 44 displays a grand average of all trials and all participants of ISPC between the estimated R_{ϕ}^{2} electrode (Oz) and all other electrodes. Presentation of both standard and test composite images was followed by broadband phase clustering starting at ~150 ms post-stimuli onset extending between 4 and ~25 Hz. In the high-frequency spectrum (>30 Hz) a more diverse behavior is seen. Presentation of the standard image is preceded by increments in phase consistency with diverse time and frequency distribution. In contrast, presentation of the test image is preceded by 3 bouts of gamma phase consistency seen at ~100, ~200, and ~300 ms between 50 and 70 Hz (Figure 44).

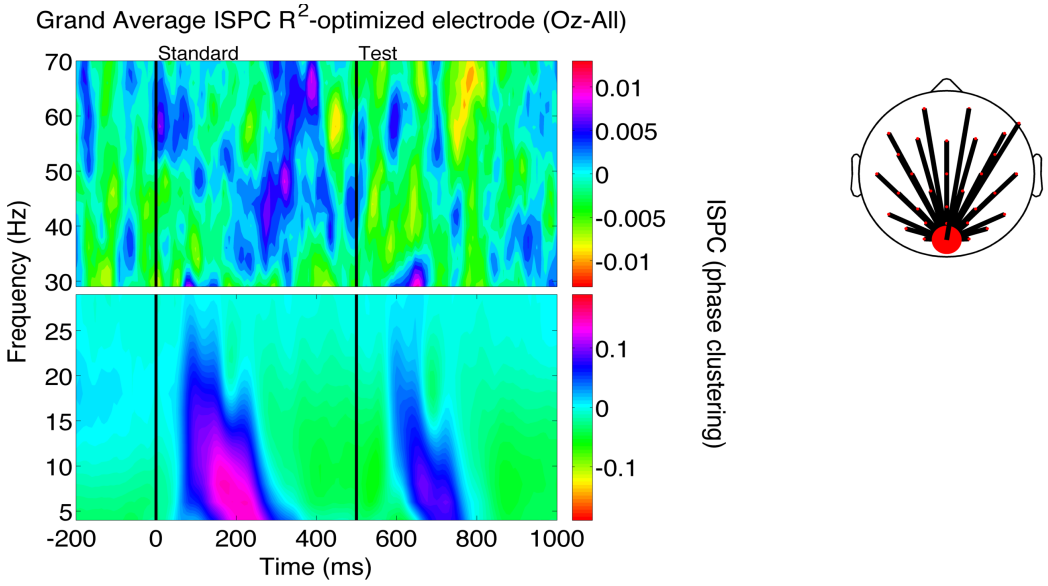

Figure 44 – Grand average ISPC for all trials and participants between the estimated R_{ϕ}^{2} – optimized electrode Oz and all other sensors. Periods of phase consistency are seen after presentation of both standard and test stimuli

4.4.1 Sensitivity to Task Demands

Between-subject analysis suggests that 7 out of 31 electrodes present supra-threshold inter-site phase clustering with the R^2-optimized electrode Oz. Supra-threshold electrodes are FP1, F7, F3, and FC5 in the left anterior scalp around 270 ms at ~45 Hz post-standard onset (yellow window in Figure 45). Green window in Figure 45 and Figure 46 display temporal and spatial distribution of supra-threshold inter-areal gamma phase synchrony (~30 - ~60 Hz) at ~250 ms post-test onset over left frontocentral (FP1, F7, F3, and FC5) and posterior sensors (O1, O2, and PO8). Near the end of the epoch supra-threshold inter-areal gamma phase synchrony (~25 - ~65 Hz) clusters at ~900 ms are found for electrodes are FP1, F7, F3, FC5, Fz, and FP2 in the frontal scalp (magenta window in Figure 45).

Results for anterior supra-threshold electrodes are shown in Figure 45. Results for posterior supra-threshold electrodes are shown in Figure 46.

Top panels in Figure 45 display phase clustering between the estimated R_{ϕ}^{2} electrode (Oz) and all supra-threshold electrodes located in the left frontal scalp (FP1, F7, F3, FC5, Fz, and FP2). In order to avoid displaying data from 4 different electrodes for the first ~850 ms and data from 6 electrodes for the rest of the epoch, the individual beta weights displayed are averages of individual beta weights quantified by all anterior supra-threshold electrodes (i.e. FP1, F7, F3, FC5, Fz, and FP2).

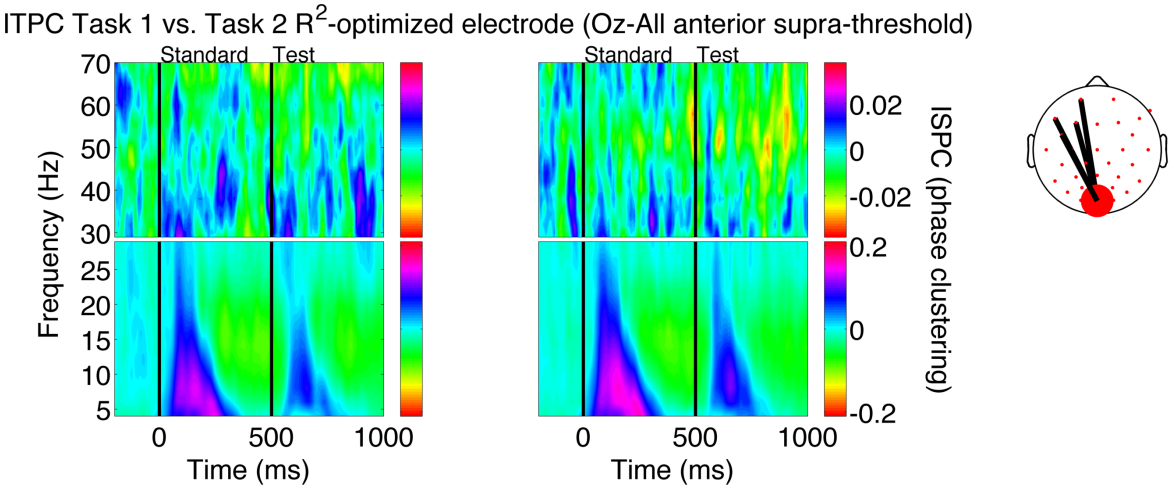

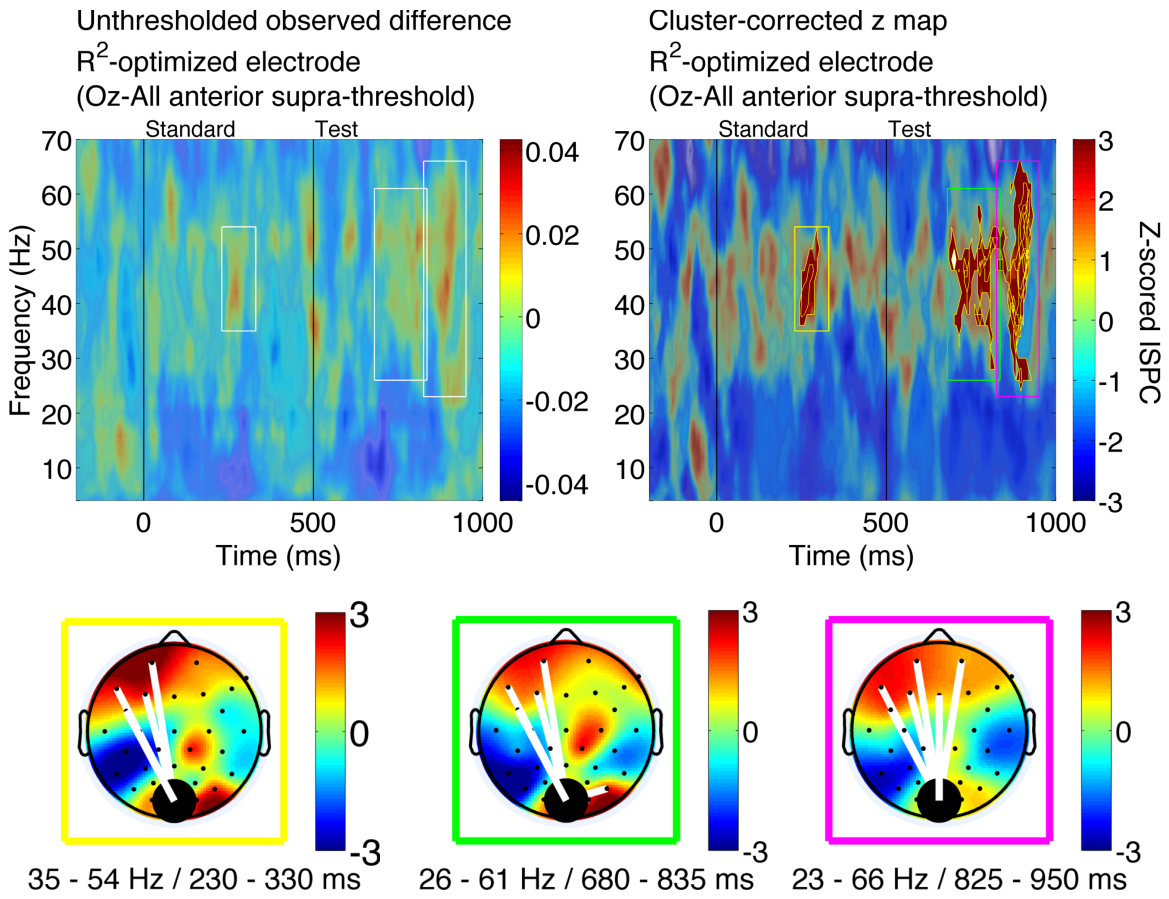

Figure 45 – TOP panels. Grand average ISPC between Oz and all supra-threshold anterior electrodes (FP1, F7, F3, FC5). Periods of phase consistency are seen after presentation of both standard and test stimuli. Topographic representation shows electrodes locations included in the average with respect to Oz. MIDDLE panels. Observed difference (left) and cluster-corrected z-map obtained after 10,000 permutations (right). Highlighted areas show statistically significant time-frequency points. Overlaid rectangles indicate time-frequency windows of supra-threshold clusters. BOTTOM panels. Topographical representations of supra-threshold cluster time-frequency windows, colored rectangles represent temporal windows in middle right panels

Inter-electrode clustering of low frequency phases across trials follows a very similar pattern for both tasks after the presentation of both images. In contrast, high-frequency phase clustering follows more diverse distributions in time and frequency. Specific time-frequency points are found to be above threshold for statistical significance after 10,000 permutations and correction for multiple comparisons. Middle left panel in

Figure 45 displays the observed difference between ISPC between Oz and all supra-threshold anterior electrodes (FP1, F7, F3, FC5, Fz, and FP2) for task 1 and task 2. In order to avoid displaying data from 4 different electrodes for the first ~850 ms and data from 6 electrodes for the rest of the epoch, the observed difference displayed is an average of the observed differences of all anterior supra-threshold electrodes (i.e. FP1, F7, F3, FC5, Fz, and FP2).

Middle right panel in Figure 45 displays the cluster-corrected z-map obtained after 10,000 permutations. Likewise, in order to avoid displaying data from 4 different electrodes for the first ~850 ms and data from 6 electrodes for the rest of the epoch, the z-map displayed is an average of z-maps generated for electrodes FP1, F7, F3, FC5, Fz, and FP2. Colored windows indicate time-frequency windows where supra-threshold clusters were found and the time-frequency ranges that were integrated in order to generate the displayed topographical representations in bottom panel of Figure 45. Highlighted areas in the middle right panel in Figure 45 represent the actual supra-threshold time-frequency clusters found at individual electrodes. In order to generate the middle right panel in Figure 45, supra-threshold clusters belonging to electrodes FP1, F7, F3, FC5, Fz, and FP2 were overlaid on top of each other.

Supra-threshold clusters are found at ~270 ms (yellow window), ~850 ms (green window), and ~900 ms (magenta window) after standard onset. Topographical representations of these windows are shown in the bottom panel of Figure 45. White lines overlaid in topographical maps indicate statistically significant phase synchrony between electrodes. For visualization purposes, all supra-threshold phase synchrony occurring during the green time-frequency window is shown.

Top panels in Figure 46 display phase clustering between the estimated R^2_ϕ electrode (Oz) and all supra-threshold electrodes located in the occipital scalp (i.e. O1, O2, and PO8). In order to avoid displaying data from 3 different electrodes, the individual beta weights displayed are averages of individual beta weights quantified by all posterior supra-threshold electrodes (i.e. O1, O2, and PO8). Inter-electrode clustering of low frequency phases across trials is strong and follows a very similar pattern for both tasks after the presentation of standard and test images. In contrast, high-frequency phase clustering follows more diverse distributions in time and frequency.

Middle left panel in Figure 46 displays the observed difference between ISPC between Oz and all supra-threshold posterior electrodes for task 1 and task 2. In order to avoid displaying data from 3 different electrodes, the observed difference displayed is the average observed difference of all supra-threshold posterior electrodes (i.e. O1, O2, and PO8). Middle right panel in Figure 46 displays the cluster-corrected z-map obtained after 10,000 permutations. In order to avoid displaying data from 3 different electrodes, the z-map displayed is an average of z-maps for electrodes O1, O2, and PO8. The colored window indicates time-frequency windows where supra-threshold clusters were found for these electrodes.

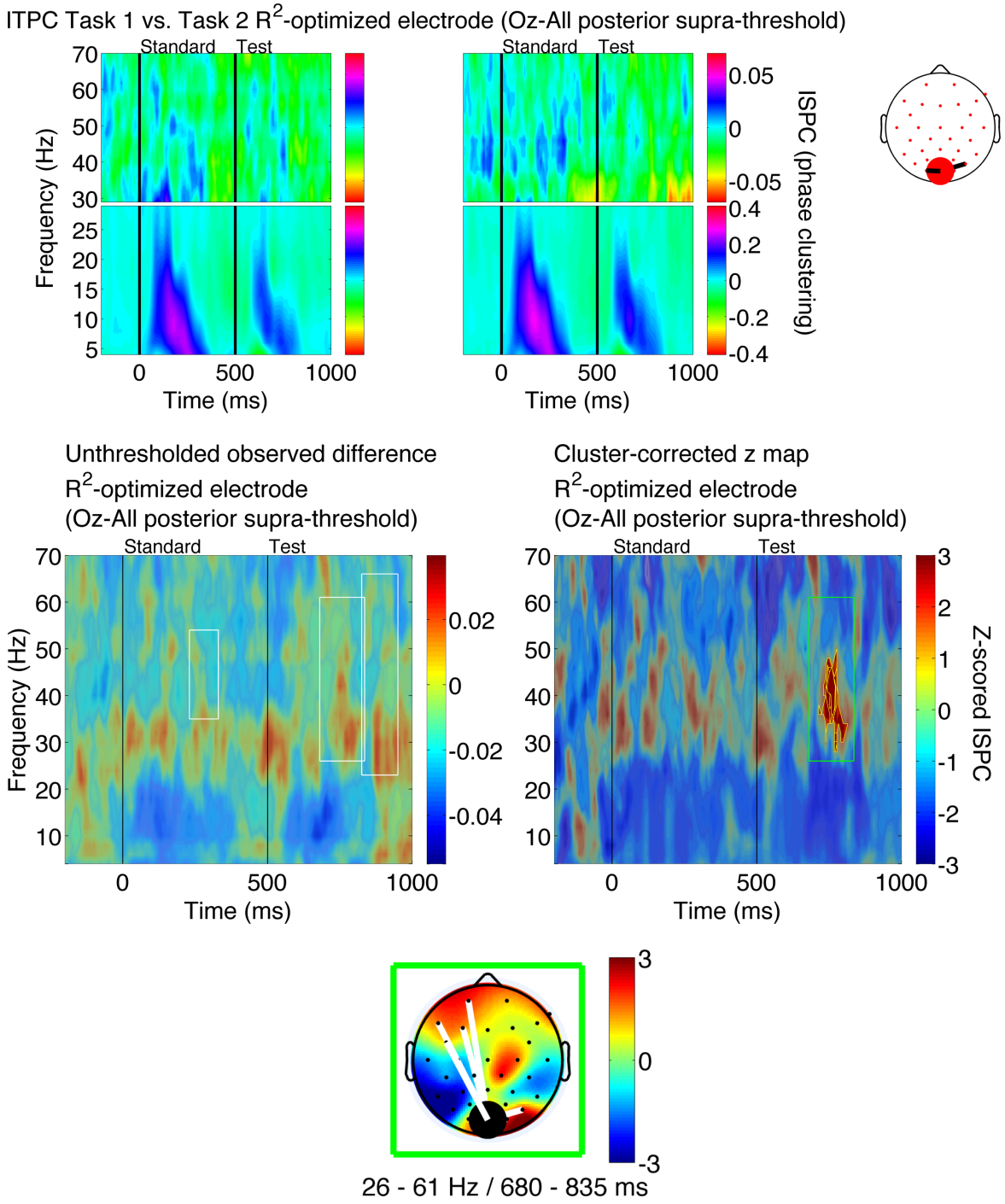

Figure 46 – TOP panels. Grand average ISPC between Oz and all supra-threshold posterior electrodes (O1, O2, PO8). Topographic representation signals the location of electrodes included in the average with respect to Oz. MIDDLE panels. Observed difference (left) and cluster-corrected z-map obtained after 10,000 permutations (right). Overlaid rectangles indicate time-frequency windows of supra-threshold clusters. BOTTOM panels. Topographical representations of supra-threshold cluster time-frequency windows, colored rectangles represents temporal windows in middle right panels

Highlighted areas in the middle right panel in Figure 46 represent the actual supra-threshold time-frequency clusters found at individual electrodes. In order to generate the middle right panel in Figure 46, supra-threshold clusters belonging to electrodes O1, O2, and PO8 were overlaid on top of each other.

A supra-threshold cluster is found at ~250 ms after test onset (green window). A topographical representation of this window is shown in the bottom panel of Figure 46. White lines overlaid in topographical maps indicate statistically significant phase synchrony between electrodes. For visualization purposes, all supra-threshold phase synchrony occurring during this time-frequency window is shown.

4.5 ERPAC results

Few time-frequency specific changes in coupling strength were quantified by event-related phase-amplitude coupling (ERPAC) in all my analyses. Grand average ERPAC across all trials and participants shows small changes in coupling strength between the selected low frequency phases in the theta and alpha range and high-frequency power (Figure 47).

A summary of between-subject analyses results for both theta- and alpha-based phase-amplitude coupling analysis is presented in Figure 48. After 10,000 permutations, no supra-threshold clusters are found.

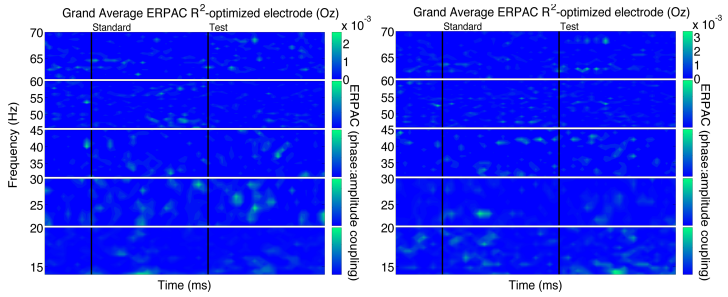

Figure 47 – LEFT panel. Grand Average theta-based ERPAC for all trials and participants at the R^2–optimized electrode Oz. RIGHT panel. Grand Average alpha-based ERPAC for all trials and participants at the R^2–optimized electrode Oz

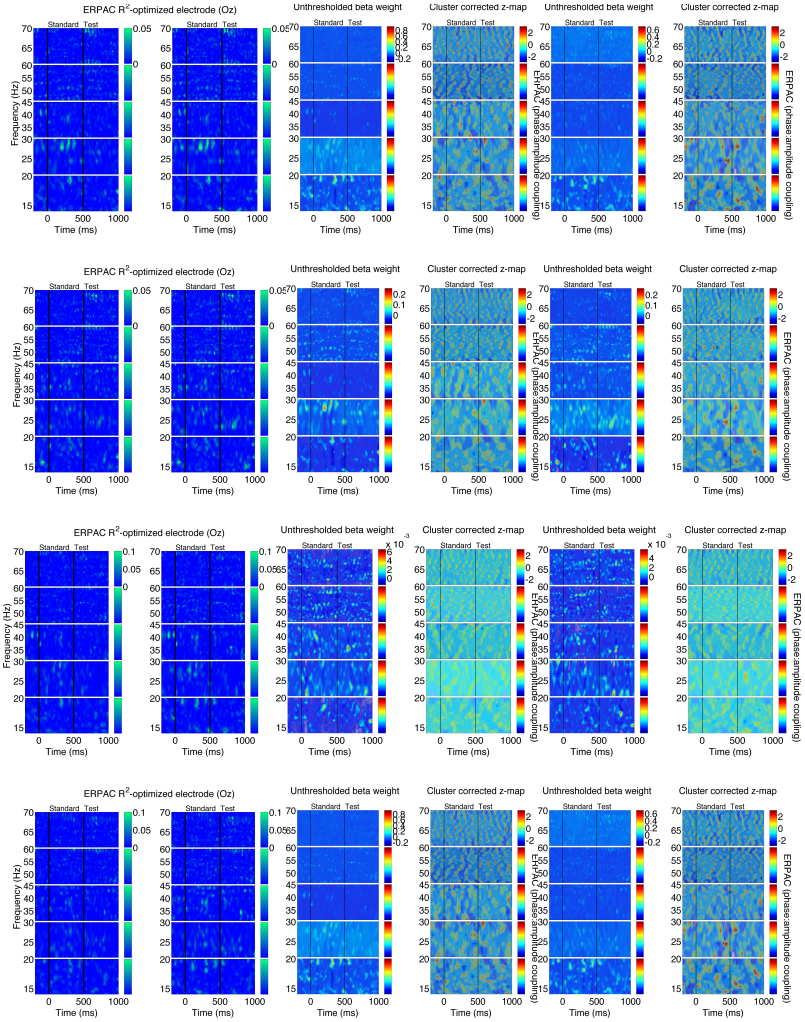

Figure 48 – Theta- and alpha-based summary of results. No supra-threshold clusters are found

5. Discussion

The general goal of this dissertation is to provide an in-depth analysis of scalp-recorded neurophysiological signals associated with the time-course of perceptual decisions. Thus I used a semi-exploratory approach in order to explore the temporal dynamics of perceptual decisions. Healthy human volunteers performed 2 tasks based on different perceptual judgments using the same physical stimuli (Figure 28). I controlled available perceptual evidence in each trial (Figure 27). Thus, I implemented a blocked dual-task two-interval parametric design using composite images.

Different neural time series analyses were implemented on the acquired data. Each one of the quantified measures models particular dimensions of the electrophysiological signal (Figure 3, see 2. Exploring Cognitive Dynamics Using Scalp-Recorded Neural Signals). From the implementation of linear and non-linear measures of brain activity emerges a problem related to the analysis search space. An increased number of points in the time, frequency, and space dimensions require mining and further statistical testing. The present parametric design allowed me to implement a linear model in order to mine linear measures at the single-subject and single-trial level (Figure 33) (S. J. Kiebel & Friston, 2004a, 2004b; Litvak et al., 2011; Pernet et al., 2011). Moreover, the coefficient of determination (R^2) quantifying goodness of fit of the model per measure is used as a dimensionality reduction technique. Thus, an R^2-optimized electrode was identified using the maximum R^2 value per measure (Figure 22, Figure 34). Furthermore, the non-parametric permutation testing framework was used in order to implement robust

statistics (Wilcox, 2005a) and appropriate multiple comparison correction procedures (Maris & Oostenveld, 2007; Pernet et al., 2011).

In the following sections I will discuss the grand average of the data and the results obtained by between-subject analyses.

5.1 Grand Average Measures

5.1.1 Event-Related Potentials (ERP)

Event-related potential (ERP) analysis revealed strong amplitude changes from baseline following the presentation of standard and test stimuli (Figure 35). A very small C1 at 60 ms, a P1 at 100 ms, a N1 at 155 ms, a large P2 at 220 ms, and two late positive components peaking at 320 and 420 ms (LPC3, LPC4) follow the presentation of the standard composite images. Likewise, a large C1 at 60 ms, a small P1 at 100 ms, N1 at 150 ms, a large P2 at 210 ms, and a late positive component at 320 ms follow the presentation of the test composite images (Figure 35).

Importantly, no late positive potential at 420 ms is seen after the presentation of the test image. This suggests that LP4 might be a *specific*[38] response elicited by the standard image, possibly related to memory processes. In memory tasks, it has been observed that recognized items elicited larger ERP amplitude in contrast to unrecognized items. Amplitude increments are seen during the encoding phase only for the recognized items extending between 400 to 1000 ms over frontal left scalp sensors (Friedman & Trott, 2000). Such associations between late ERP components and memory have also a functional magnetic resonance imaging (fMRI) counterpart (Thompson-Schill,

[38] The words "specific", "selective", and "preferential" will be *italicized* and will follow the logic presented by (Fodor, 2001)

D'Esposito, Aguirre, & Farah, 1997). Likewise, late positive potentials (LPC) over parietal scalp within the 400 to 800 ms range have been reported (Addante, Ranganath, & Yonelinas, 2012; Finnigan, Humphreys, Dennis, & Geffen, 2002; Friedman & Johnson, 2000; Johnson, Pfefferbaum, & Kopell, 1985; Neville, Kutas, Chesney, & Schmidt, 1986). The amplitude of these LPCs is increased to new words in contrast to old words. Thus, these late positive modulations of ERP amplitude in memory contexts have been associated with some kind of elaborative processing leading towards recognition of items with associated contextual details (Addante et al., 2012; Friedman & Johnson, 2000; Yu & Rugg, 2010).

Therefore, the average ERP waveform suggests that a neural process, possibly linked to memory, occurs around 400 ms *specific* for the standard image. This prediction is congruent with oscillatory power results discussed later (5.7 Decision-relevant cognitive and neural events depend on the alpha cycle). Furthermore, a follow-up analysis is suggested to address this issue (see 7. Future Directions).

Finally, the excellent temporal resolution of the unfiltered ERP gives insight into a time-course of neural events linked to perceptual decision-making. Thus, 60 ± 25 ms, 100 ± 30 ms, 150 ± 50 ms, 220 ± 45 ms, 320 ± 20 ms, and 420 ± 20 ms post-stimulus onset[39] will be used as reference for the less temporally precise time-frequency analyses.

5.1.2 Event-Related Spectral Power (ERSP)

The event-related spectral power (ERSP) analysis revealed strong mean spectral power deviations from baseline following the presentation of standard and test stimuli

[39] Timing measured across subjects and trials composing the grand average ERP shown in Figure 35

(Figure 37). Standard composite images are followed by strong broadband power increment starting at ~60 ms extending from ~6 to ~35 Hz. At ~100 ms a smaller broadband power increment starts, extending for ~100 ms within 4 and ~20 Hz with maximum power at ~150 ms. A final broadband power increment within 4 and ~20 Hz starts at ~200 ms, extends for about 100 ms, and peaks at ~220 ms.

These increments in spectral power are followed by broadband power decrease in the theta and alpha bands (4 - ~14 Hz) starting at ~300 ms and extending for ~250 ms. The peak of this power decrease occurs around 8 Hz and coincides with the presentation of the test images at 500 ms after test image onset. This event is followed by a 2 consecutive broadband power increments in the theta and alpha bands (4 - ~14 Hz) occurring at ~150 and ~220 ms after test onset. At ~300 ms, strong broadband power decrease within ~10 and ~45 Hz extends up until the end of the epoch. Interestingly, the peak of this power decrement occurs in similar time-frequency space than the previous power decrement (Figure 37).

Thus, temporal dynamics of EEG spectral power within 4 and ~35 Hz suggest the occurrence of specific neural events, possibly neural synchrony, unfolding in time and frequency. These events are congruent for both standard and test images. However, standard images are followed by 3 discrete broadband power increments (~60, ~150, and ~220 ms) whereas test images lack the earlier broadband spectral component at ~60 ms (Figure 37). Interestingly, the discreteness of the spectral power components occurring at ~150 and ~220 ms is suggested by a brief return to baseline at ~180 ms seen in the alpha and beta bands (~10 - ~25 Hz).

Spectral events in the gamma band (>30 Hz) have an interesting relationship with the timing suggested by the lower-frequency spectrum (<30 Hz). Power increments around 60 ms post stimuli onset are seen extending from ~30 to ~35 Hz. For the standard image, this early spectral component might be a residual from lower-frequency broadband power at ~60 ms. However, this conclusion is not so straightforward for the test image-related gamma band counterpart at ~60 ms. Thus it might be the case that these gamma band components are a stand-alone neural event and do not form part of the lower-frequency broadband component. Early gamma-band synchronization before 100 ms after stimulus onset has been suggested as an early correlate of attention as quantified by intracranial recordings in macaque (Fries, Reynolds, Rorie, & Desimone, 2001).

In humans, early gamma band responses around ~100 ms are associated with the encoding of stimulus features. Busch, Debener, Kranczioch, Engel, and Herrmann (2004) parametrically manipulated size, duration, and eccentricity. Their results show a monotonic relationship between gamma-band power and such stimulus properties extending from ~40 to ~120 ms post stimulus onset mostly around 40 Hz (although effects are seen within 30 and 100 Hz depending on manipulation and subjects). Furthermore, early gamma band has been also shown to be sensitive to memory (C. S. Herrmann, Lenz, et al., 2004), being larger for know objects in comparison to unknown objects. Thus, previous literature suggests that these early gamma-band responses are indeed separate neural events probably linked to the encoding of visual stimulus properties and not residuals from the broadband synchronization occurring at lower frequencies.

At ~150 ms, gamma band power slightly decreases between ~30 and ~45 Hz after standard onset. In contrast, a larger power decrement is seen post-test onset. At 200 ms a high-frequency gamma component between ~50 and ~70 Hz peaks after onset of both images. This gamma component temporally coincides with the return to baseline in the lower-frequencies and with an increment in power at ~30 Hz. Interestingly, gamma band returns to baseline at ~220 ms and is followed by power decrement part of a broadband event. Gamma-band synchronization strongly increases at 300 ms and >400 ms post-standard onset. The first increment also occurs after test onset but is smaller whereas the later increment is not present for the test image (Figure 37).

5.1.3 Inter-Trial Phase Clustering (ITPC)

Inter-trial phase clustering (ITPC) analysis revealed strong phase consistency following the presentation of standard and test stimuli (Figure 42). Standard and test composite images are followed by strong phase consistency starting at ~60 ms extending until ~300 ms within ~4 to ~60 Hz. It is not clear if these are broadband responses or individual bouts of phase clustering. Given the timing of events provided by ERP (Figure 35) it is likely that ITPC quantifies at least 3 processes occurring below ~30 Hz. The first increment in phase consistency starts smaller around 100 ms and extends from ~5 to ~25 Hz. A large increment in phase consistency with the same frequency distribution occurs around 150 ms. Finally, a large increment in theta/alpha (4 - ~15 Hz) phase clustering occurs at ~220 ms.

In contrast, gamma phase dynamics display only 2 clear increments in phase consistency. The first event at ~100 ms corresponds to the “early” evoked gamma

component and it has been indirectly studied using evoked power (Busch et al., 2004). The second event at ~200 ms corresponds to the "late" gamma, often accompanied with evoked and induced gamma power (Gruber, Muller, & Keil, 2002). "Late" gamma phase synchrony has been suggested to be a signature of cortical object representation (Gruber et al., 2002).

5.1.4 Inter-Site Phase Clustering (ISPC)

Inter-site phase clustering (ISPC) analysis shows long-range phase consistency patterns congruent with what is seen in local measures such as ERP, ERSP, and ITPC. Figure 44 displays that the inter-site phase clustering in the frequency spectrum below ~30 Hz is congruent with results found in ERSP and ITPC. Thus, increments in phase consistency starting at ~60 ms extending until ~300 ms within ~4 to ~25 Hz are seen following the presentation of standard and test stimuli. Given the timing of events provided by ERP (Figure 35) it is likely that just like local phase clustering, ISPC quantifies at least 3 processes occurring below ~25 Hz. The first increment in phase consistency is seen at ~100 ms and extends from ~5 to ~25 Hz. The second increment in phase consistency shares the same frequency distribution and occurs around 150 ms. A final clustering is seen in theta/alpha (4 - ~15 Hz) at ~220 ms. Although both patterns are shared by activity following standard and test images, the test image presents lower inter-site phase clustering than the standard (Figure 44).

In contrast, gamma phase dynamics display very diverse behavior. Furthermore the strength of these inter-site phase dynamics in the gamma band is very weak. This is due to the extra constraint imposed by ISPC itself. Phase at a given time-frequency point

has to be consistent across trials and for 2 different electrodes. Moreover this grand average combines values from Oz and all other electrodes. Given these 2 reasons, high frequency phase is spuriously reduced in this graph.

5.1.5 Event-Related Phase-amplitude Coupling (ERPAC)

Grand averages for theta- and alpha-based event-related phase-amplitude coupling are shown in Figure 47. Coupling strength is very weak, in the order of 0.003, rendering these results unintelligible. This failed result is product of a blind and an arbitrary decision I made.

First, for the sake of consistency, the same wavelet parameters were blindly used for all time-frequency analyses. These parameters were originally optimized for ERSP, ITPC, and ISPC analyses not for cross-frequency coupling. Keeping parameters equal is recommended good practice for ERSP, ITPC, and ISPC because they can be understood as "extensions" of one another (M. X. Cohen & Gulbinaite, 2014; Christoph S Herrmann et al., 2005). However, cross-frequency coupling analysis implies a whole different set of assumptions, processes, and computations (see 2.3.2 Cross-Frequency Coupling (CFC) and the methods section on Event Related Phase-amplitude Coupling (ERPAC) analysis). Second, I arbitrarily chose the "source" low-frequency phase as the centroid of the theta and alpha band so as to reduce the search space.

The impact of these decisions is clearly seen in the poor performance of the linear model for the ERPAC measure (Figure 34). R^2 for ERP reached a very good value of 0.38 while ERSP is expected to be lower due to the integration across several frequencies; it still reaches a very good value of 0.3. R^2 for ERPAC was very small (~0.05). Thus, it is

not surprising that grand average ERPAC denotes the "unhealthiness" of the computed ERPAC (Figure 47). Furthermore this is evidenced in the full set of null results displayed in Figure 48. I return to this failed outcome and propose a solution in 7. Future Directions.

In the next sections, I will discuss the obtained results using ERP, ERSP, ITPC, and ISPC divided per analysis.

5.2 No impacts of systematic low-level differences in stimuli are seen in my results

Between-subject analyses suggest that no supra-threshold temporal clusters are seen for ERP (Figure 36) or for ERSP (Figure 38). Although no significant results were obtained for the analysis of beta weight dynamics for stimulus sensitivity ($\beta_{w_3}\upsilon$) the obtained null results are informative nonetheless.

A small ERP preferential response to stimulus mixing level (Parameter 2, Figure 27) is seen between ~60 and ~220 ms following the presentation of both images (top panel Figure 36). These increments in ERP amplitude are not statistically significant. I interpret these null results as indicative of the success of the present experimental design. This is, although composite image mixing was manipulated (Parameter 2, Figure 27), the image statistics across images were kept as equal as possible. Thus, any systematic physical stimulus differences as evidenced by ERPs were eliminated. The impact of low-level stimulus features is a well-documented topic in ERP research (Celesia & Peachey, 1993) and has been pointed out as the main cause of false-alarm ERP modulation (Rousselet & Pernet, 2011; Vanrullen, 2011).

Despite not having supra-threshold clusters, ERSP provides additional information about the impact of stimulus properties on temporal brain dynamics ($\beta_{w_3} \upsilon$, Figure 38). Cluster-corrected z-map in Figure 38 displays 2 under-threshold clusters in the gamma band (~50 to ~65 Hz). Although they are not statistically significant, these high-frequency components at 200 ms are interesting because (i) given that high-frequency spectral components are highly affected by temporal jitter, gamma at 200 ms is seen even after 10,000 trial permutations with small temporal shifts and (ii) these components are present in the grand average ERSP (Figure 37). However, these preferential spectral components occur too late to be product of low-level systematic differences in stimuli (Pulvermüller, Keil, & Elbert, 1999).

Therefore, along with my null ERP results, the ERSP sensitivity to stimulus properties analysis confirms the success of the experimental manipulation.

5.3 Sensitivity to Behavioral Outcome

Between-subject analyses suggest that no supra-threshold clusters are seen for ERP (Figure 36) or for ERSP (Figure 38). Although no significant results were obtained for the analysis of beta weight dynamics for behavioral outcome ($\beta_{w_4} RT$) the obtained null results of ERP are nonetheless informative.

The beta weight associated with ERP sensitivity to behavioral outcome shows no increments in amplitude from baseline after the presentation of the standard image ($\beta_{w_4} RT$, middle bottom panel Figure 36). In contrast, a *specific* response following the presentation of the test image is seen between ~60 and ~250 ms. This response has no

consistent polarity between subjects and no statistically significant temporal clusters are found. However, the fact that this small potential deflection is specific for the test image presentation indicates that trial-by-trial variation of response times has a potential relation with the first ~250 ms after test image onset. In contrast, it is possible that a small to no relationship might exist between the trial-by-trial response time variation and other time periods during the epoch. Importantly, such relationships cannot be described by the current analysis.

The idea of a *specific* ERP response linked to reaction time variability is consistent with literature suggesting that neural events linked to information accumulation/processing start around ~80 ms after stimulus onset (Schyns et al., 2007; VanRullen & Thorpe, 2001). Furthermore, it has been suggested that decision-related neural events start around 150 ms after stimulus onset and extend for about 100 ms (Philiastides et al., 2006; VanRullen & Thorpe, 2001). Likewise, Smith and Ratcliff (2004) suggest that evidence accumulation towards a decision happens during the time period comprised between ~150 and ~350 ms post-stimulus onset.

Thus my semi-exploratory ERP analysis generates a specific hypothesis about the time-course of events that have an impact in response times and dictates a follow-up analysis testing the specific ERP response to behavioral outcome (see 7. Future Directions).

5.4 Task demands do not modulate ERP and ITPC

Beta weights associated with task 1 and task 2 ($\beta_{w_1}T1, \beta_{w_2}T2$) were compared against each other in order to assess ERP and ERSP sensitivity to task demands (Figure 36

and Figure 39). Furthermore non-linear measures were separated into trials belonging to task 1 and task 2 and compared.

Figure 36 shows strong ERP amplitude modulations following the presentation of both images resembling the grand average shape. A classic tri-phasic visual ERP shape follows presentation of the standard image presentation is followed by (P1 ~100 ms, N1 ~155 ms, P2 ~220 ms). In contrast, test image presentation elicits an early C1 (~60 ms) followed by the tri-phasic response. No supra-threshold temporal clusters were found in this analysis. The lack of statistically significant differences in this analysis reveals that ERPs are not sensitive to task demands which can be understood as a high-level cognitive process. Thus, although preferential ERP responses associated to task demands are seen these are not selective to the different judgments.

The presence of the C1 ERP component ~60 ms after test image onset is interesting (middle top panel Figure 36). C1 is thought to represent early responses in the visual cortex and the beginning of bottom-up feedforward processing (Martinez et al., 1999). Therefore, ERP amplitude increments starting ~60 ms after test image onset may reflect attentional processes linked to perception of task-relevant information (Kanwisher & Wojciulik, 2000). Importantly, the effects of attention at this early stage of visual processing would be present for the test image and not for the standard. Putatively, C1 might indicate differential task-related early processing of information. However, the present analysis cannot reveal such interaction. Therefore, my current semi-exploratory ERP analysis suggests a specific follow-up analysis where ERP waveforms elicited by the test image are compared against the ERP time series elicited by the standard image (see 7. Future Directions).

Results show that no statistically significant differences in phase clustering are found between tasks. These null results can be interpreted in two ways. First, oscillatory phase dynamics might not be affected by task demands. It is thought that the clustering of phases across trials represents two dimensions[40] of functional organization of neural networks triggered by perceptual or cognitive events (F. Varela et al., 2001). So it is plausible that although different judgments are required in the implemented tasks, these are not modeled by phase clustering. By definition, ITPC has an intrinsic technical flaw; it requires phase angles to be clustered across trials with regard to the stimulus onset. Thus, any phase dynamics that have a trial-by-trial variation but not locked to the stimulus onset, will be missed by ITPC. A solution for this issue was unknown to me at the time of these analyses (see 7. Future Directions).

The second interpretation relies on putative missed effects. In order to implement a consistent approach throughout the dissertation, the electrode with maximum mean R^2 across linearly modeled measures was used (Figure 34). Inter-site phase clustering analysis reveals that increased phase dynamics in the posterior electrodes is shifted towards the right hemisphere (topographical maps in Figure 45 and Figure 46). It could well be that Oz might not be the best electrode for ITPC analysis. Furthermore, non-linear measures did not benefit from the linear model. Ideally, single-trial analysis should be applied to non-linear measures in order to better link it to behavior (see 7. Future Directions). Thus, it is possible that phase consistency dynamics might be an appropriate measure of the neural basis of perceptual decision-making; I might have just missed the effect due to arbitrary decisions.

[40] Time as measured by phase and frequency

5.5 Decision-specific cognitive demands modulate early gamma power

Top panels of Figure 39 display time-frequency representations of individual beta weights associated with task 1 and task 2 ($\beta_{w_1}T1, \beta_{w_2}T2$). Supra-threshold clusters are found in the ERSP sensitivity to task demands analysis comparing beta weights for task 1 and task 2. This indicates that in contrast to ERP, high-level cognitive processes such as different judgments regarding the same physical stimuli are effectively modeled by oscillatory power.

Spectral behavior within 4 and ~30 Hz is very similar to the one observed in the grand average ERSP (Figure 37, 5.1.2 Event-Related Spectral Power (ERSP)) this is furthermore reflected by the lack of supra-threshold clusters under 35 Hz. In contrast, gamma-band power (>30 Hz) present two overall characteristics. First, stronger gamma power is elicited by task 1 in comparison to task 2 throughout the epoch. Second, some of these power increments are statistically significant (Figure 39).

Overall differences in gamma power between tasks are not surprising. It has been shown that in general, cognitive tasks consistently augment gamma power (Fitzgibbon, Pope, Mackenzie, Clark, & Willoughby, 2004). The nature of the judgments in the tasks is very different. Task 1 requires participants to use specific composite image features from the standard presentation in order to judge if the test image contains *more car* or *more face* in comparison to the standard. In contrast, task 2 requires participants to judge if the test image is the *same* as or *different* than the standard (Figure 28). It could be argued that the *more car*/*more face* judgment is more demanding than the *same*/*different* judgment. Gamma power increments have been reported for increased task difficulty in

auditory (Mulert et al., 2007), visual (Fitzgibbon et al., 2004), and working memory tasks (Meltzer et al., 2008). Thus, the increased overall gamma-band power for task 1 in contrast to task 2, might indicate that the *more car*/*more face* judgment is indeed more demanding.

The earliest supra-threshold cluster occurs between ~60 and ~106 ms around ~45 Hz after standard image onset consistent with the event timings provided by ERP (C1 and P1 components, Figure 35). This time-frequency component is weakly seen in the grand average ERSP (Figure 37) but strongly present in the actual beta weight for task 1 and in the observed difference (Figure 39). A parsimonious explanation for this gamma-band response would lie on systematic differences in low-level image features. This is an unlikely interpretation as stated by the ERP and ERSP sensitivity to stimulus properties analyses (see 5.2 No impacts of systematic low-level differences in stimuli, Figure 36 and Figure 38).

A more appropriate interpretation is suggested by the linear model and is based on task-dependent requirements. In the present paradigm, participants have to implement judgment-specific information acquisition strategies for the standard image. Task 1 demands the encoding of specific image features (i.e. amount of car/face mixture, Parameter 1) whereas task 2 can be solved only with the gist of the standard image. It has been suggested that perception of global scene or object features (i.e. the gist) relies on particular and specific neurobiological and cognitive dynamics (Bar, 2003, 2004; Oliva & Torralba, 2006; Oppermann, Hassler, Jescheniak, & Gruber, 2012). Thus, the neurobiological mechanisms involved in information acquisition from the standard image in feature-based discrimination tasks might be different from those recruited when

performing gist-based matching tasks. Importantly, the counterpart for this gamma band component after test onset does not differ between tasks[41]. This suggests that neural events associated with such early gamma power increment are selective for the standard image in task 1 (Figure 39).

These results indicate that neural operations correlated with early gamma power do not differ after test onset. This interpretation is congruent with the memory match and utilization model (MUM, C. S. Herrmann, Munk, et al., 2004). The "matching" process occurring at ~100 ms after test onset does not differ between tasks; it is relatively the same cognitive operation.

However, the interpretation provided by the MUM model is not appropriate for early gamma power after standard onset. A study by Oppermann et al. (2012) provides some insights. Early gamma-band responses were compared for the perception of conceptually related and unrelated objects (Oppermann et al., 2012). Their results show a modulation of early gamma-band response at ~70 ms in the 30 to 50 Hz range stronger for conceptually related objects. Indicating that after the perception of physically similar stimuli, early gamma power is modulated by previous knowledge about stimuli (Oppermann et al., 2012).

Results by Oppermann et al. (2012) are congruent with mine in the time and frequency domains. Specifically for my results I suggest that early gamma power after standard onset is modulated by different information-acquisition strategies demanded by each task. In other words, encoding of the standard image is different in each task,

[41] and actually going back to baseline, which indicates that there is no increment in oscillatory gamma power at this time period

whereas the encoding of the test image does not differ across tasks. This means that gamma power elicited by the standard image is functionally different from its test-related counterpart.

These results furthermore provide evidence of the early availability of task-specific knowledge in perceptual decision-making (Bar, 2004; Engel et al., 2001; Wolfe, Vo, Evans, & Greene, 2011). The architecture of the visual system suggests a hierarchic functional organization. However, the idea that concurrent bottom-up and top-down influence early stages in visual perception have been suggested (Bar, 2003, 2004; Engel et al., 2001; Grossberg, 1999; Ullman, 1995; Wolfe et al., 2011). Bar et al. (2006) showed that top down influences for object recognition over occipital cortex can occur as early as 50 ms. Furthermore, they suggest that top-down/bottom-up recurrent interactions are supported by orbito-frontal cortex (OFC) and the visual cortex, respectively (Bar, 2003, 2004; Bar et al., 2006).

In the context of this paradigm, such early top-down/bottom-up interactions would be of a slight different nature as the ones suggested by (Bar, 2003). I suggest that not only recognition-related facilitation might be at play at this time period but also task-dependent knowledge. This is, judgment-specific information acquisition strategies for the standard image.

5.6 Local and inter-areal gamma synchrony at ~200 ms reflects decision-dependent integration of distributed neural processing

The next statistically significant increment of gamma power occurs between ~170 and ~280 ms after standard and test onset (Figure 39). Additionally, inter-site phase

clustering (ISPC) results found phase synchrony between Oz and anterior (FP1, F7, F3, FC5) and posterior (O1, O2, PO8) electrodes within extending until near the end of the epoch (Figure 45 yellow, green and magenta windows, Figure 46 green window). Thus, supra-threshold power and phase clustering with ~30 to ~60 Hz is seen within between ~230 and ~330 ms after both standard and test images onset (Figure 45 and Figure 46).

The gamma supra-threshold cluster is "U shaped", leaving gamma-band power above 50 Hz at ~200 ms out of statistical significance (Figure 39). Interestingly, this period of gamma power returns to baseline (Figure 39). Importantly, a gamma-band component above 50 Hz at ~200 ms is associated with stimulus properties (Figure 38, 5.2 No impacts of systematic low-level differences in stimuli). It is possible that the "U shape" of the ~200 ms gamma supra-threshold cluster demonstrates that the linear model effectively separated activity related to stimulus properties from task demands.

Furthermore, these activations occur too late so as to be modulated by low-level systematic differences in stimuli (Pulvermüller et al., 1999). Therefore these effects cannot be explained by stimulus properties; the linear model suggests they are related to task demands.

Gruber et al. (2002) proposed different functional roles for induced gamma power and inter-site phase clustering[42] co-occurring in a window extending from 180 to 300 ms at 32 Hz in a visual perceptual learning task[43]. They indicate that induced gamma power

[42] Named "phase synchrony" in their analysis

[43] Their analysis tested the peak of gamma power and inter-site phase clustering within this window. No other time-frequency periods were subjected to power analysis. ISPC was tested in a previous and posterior window for comparison. In their results, gamma power is a clear broadband response extending from ~25 to ~80 Hz being maximal between 30 and 40 Hz. They do not display time-frequency representations of ISPC (Gruber et al., 2002)

and phase synchronization within this time range is a signature of the integration of different visual processes such as the processing of image features (Gruber et al., 2002).

Results are congruent with the interpretation provided by Gruber et al. (2002). It is plausible that after distributed task-mediated information-acquisition takes place around 100 ms post-standard onset (Bar, 2004; Wolfe et al., 2011), such processes are integrated at ~200 ms in a task-dependent manner. Different information-acquisition strategies would lead to different amounts and quality of information available (e.g. specific quantification of the amount of face within the standard composite image vs. global summary of the standard composite image). Such information-acquisition processes and the different visual features they acquire would require different integration strategies, putatively evidenced by ~200 ms supra-threshold gamma power and long-range phase clustering.

Additionally, the MUM model suggests that during this time period, attentional and memory processes are active in order to perform operations over the acquired perceptual information towards the coordination of task-related action (C. S. Herrmann, Munk, et al., 2004). Due to the cognitive demands of task 1 these processes are different to those elicited by task 2. Leading to stronger gamma oscillatory amplitude and phase synchrony during this time period (Figure 39, Figure 45, and Figure 46). It is possible that task 1 requires the allocation of a larger amount of information in working memory in comparison to task 2, leading to increased gamma oscillations (Meltzer et al., 2008; Tallon-Baudry, Bertrand, & Fischer, 2001; Tallon-Baudry, Bertrand, Peronnet, & Pernier, 1998; Tallon-Baudry, Mandon, Freiwald, & Kreiter, 2004).

The MUM model makes no prediction regarding phase dynamics. However, inter-site phase synchronization has been suggested as a neural mechanism facilitating information transmission and integration (Engel et al., 2001; Fries, 2005, 2009; Rodriguez et al., 1999; F. Varela et al., 2001). Thus, it is possible that long-range gamma phase synchrony is a signature of the enhancement of inter-areal information transmission. Performance of task 1 could require facilitated neural communication between distributed brain regions. Such facilitation can be implemented by increasing the precision of synaptic inputs in the millisecond range (Fries, 2005; F. Varela et al., 2001). Oscillatory gamma phase has been shown to provide such temporal precision (Engel et al., 2001; Fries, 2005, 2009; F. Varela et al., 2001).

I suggest that gamma phase synchrony elicited by the standard stimulus represents the facilitation of information propagation between low-level sensory processes and higher-level cognitive associative dynamics (Figure 45 and Figure 46, yellow and green windows). This interpretation is supported by results obtained by (Bar et al., 2006). Using MEG and fMRI they found that phase synchrony between orbitofrontal cortex (OFC) and the fusiform gyrus is increased during the period comprised between ~100 and ~200 ms. They interpret phase synchrony in this context as presumably supporting feedforward projections. OFC is located in the ventral regions of the frontal cortex. It is possible that EEG might not record its activation. However, dynamic causal modeling of EEG signals has shown that activations in OFC are indeed captured by EEG (Stefan J Kiebel, David, & Friston, 2006). Similar early long-range connections have been reported between frontal-eye fields and occipital regions (Gregoriou, Gotts, Zhou, & Desimone, 2009a,

2009b). Suggesting that attention-dependent early interactions between distant brain regions might be distributed networks more than specific regions (Olaf Sporns, 2011).

A final relevant point is that this supra-threshold cluster encompasses a time-period starting after N1 trough and extending after P2 peak (Figure 35). Suggesting that important cognitive neural events involving power and phase dynamics indeed occur beyond ERP peaks and troughs (M. X. Cohen, 2011; Rousselet & Pernet, 2011; Schyns et al., 2007).

5.7 Decision-relevant cognitive and neural events depend on the alpha cycle

A supra-threshold cluster extends from ~312 to ~380 ms between ~50 and 70 Hz in Figure 39, temporally correlating with the first late positive ERP component (Figure 35). The MUM model provides a specific interpretation for this spectral feature (C. S. Herrmann, Munk, et al., 2004). The model predicts the occurrence of a "late" gamma-band response at >200 ms after sensory information matching (<150 ms) and attentional/memory processes take place (>100 to <300 ms). This "late" gamma-band response is thought to be a signature of distributed information "utilization" processes geared towards the adaptive coordination of behavior (Engel et al., 2001; C. S. Herrmann, Munk, et al., 2004).

In the present paradigm, the functional "utilization" is twofold and I will refer to it as "the first" and "second utilization". For the standard image, the first utilization implies keeping acquired visual information in working memory. This process is different enough so as to generate statistically significant differences between task 1 and task 2, possibly associated with working memory load or task difficulty (Fitzgibbon et al., 2004;

Meltzer et al., 2008; Tallon-Baudry et al., 2001; Tallon-Baudry et al., 1998; Tallon-Baudry et al., 2004). In contrast, the processes involved in the second utilization are very different. The "utilization" process leads to a decision after the initial standard-to-test matching occurring at ~100 ms[44]. The "utilization" processes are geared towards a perceptual decision and the subsequent coordination of motor behavior.

The interpretation provided by the MUM framework nicely fits with the "late" gamma associated with the second utilization. No statistically significant differences are seen between task 1 and task 2 in the late gamma-band response (Figure 39). These null results suggest that the "utilization" processes underlying the generation of a perceptual decision and the subsequent implementation as motor behavior reflected by gamma oscillations do not differ at this stage.

In contrast, it is not clear that the interpretation provided by the MUM framework is equally appropriate for gamma power associated with the first utilization. I do think this component is associated with cognitive processes that are essential to accomplish the task at hand, however, not in the way the MUM model predicts. I therefore suggests that this ~300 ms component is related to the following two supra-threshold clusters. The fact that they share similar frequency distribution occurring at ~420 and ~500 ms after standard onset strongly supports this idea (Figure 39). My argument is furthermore advanced not only by frequency dynamics but also by the temporal dynamics of these three clusters.

The first supra-threshold cluster occurs between ~312 and ~380 ms, the second cluster occurs between ~388 and ~456 ms, and the third cluster occurs between ~478 and

[44] ~600 ms epoch time

~548 ms (Figure 39 and Figure 49). The individual extension of these clusters is 69, 69, and 71 ms respectively. Consequently, the total time period comprised by these 3 supra-threshold clusters is roughly 237 ms. Within this 237 ms window, 3 equally spaced sub-windows of 79 ms can be allocated. Considering these temporal dynamics it can be thus said that an ongoing process taking place every 74 ± 5 ms is reflected by each supra-threshold cluster. A graphic representation of these windows can be seen in Figure 49.

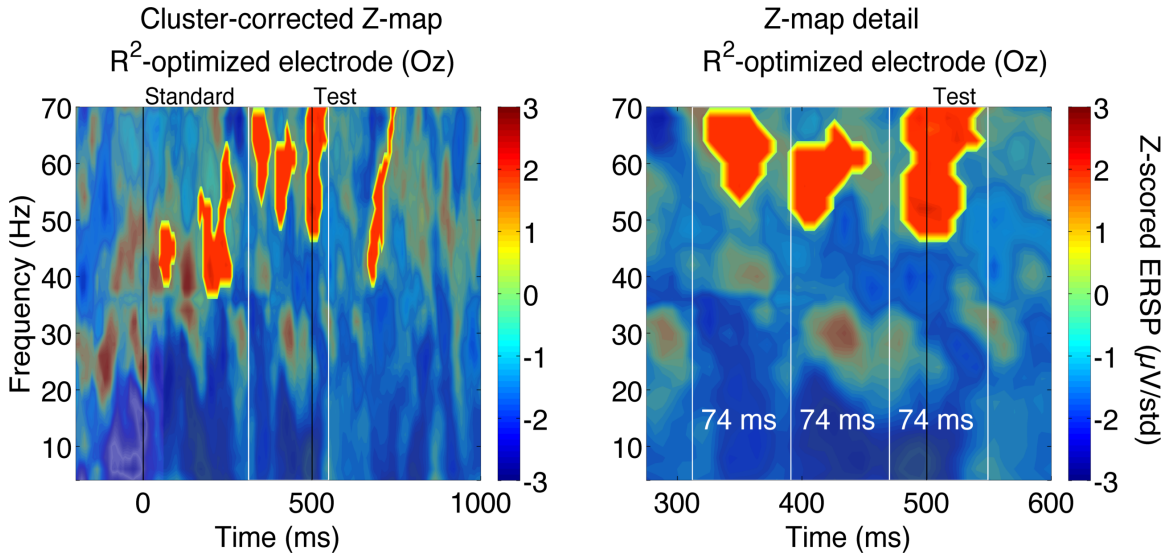

Figure 49 – LEFT. Cluster-corrected z-map for sensitivity to task demands analysis (same as left panel in Figure 39). White lines indicate period from ~312 to ~548 detailed in right panel

If my argument follows, given the 74 ± 5 ms process reflected by these 3 gamma-band responses, it is reasonable to think that a lower-frequency oscillation underlies these high-frequency power increments. Thus, these 3 consecutive supra-threshold clusters would be parts of the same functional cluster. I therefore suggest that these rhythmic synchrony increments are evidence for nested oscillations. I furthermore suggest that the

specific frequency ranges for such nesting are within the alpha (~12 and ~14 Hz) and gamma (~45 and ~70 Hz) bands.

Top panels in Figure 39 show clear decrements in alpha/low beta (~7 to ~16 Hz) synchrony in the range encompassing ~300 to ~550 ms. The functional role of alpha oscillations amplitude is a recurrent topic of discussion in electrophysiology (Klimesch, Sauseng, & Hanslmayr, 2007; S. Palva & Palva, 2007). The main interpretations suggest active inhibition of task-irrelevant cortical areas (Klimesch et al., 2007) or the active processing in task-relevant networks (S. Palva & Palva, 2007). The most widely accepted interpretation suggests that alpha negatively correlates with cortical activation (Handel, Haarmeier, & Jensen, 2011; Klimesch et al., 2007; Rihs, Michel, & Thut, 2007). Thus at the peak of each alpha cycle, inhibition would be strong and no neurons are able to fire. As the alpha cycle continues towards a trough, inhibition gets released and neurons can fire again. In Figure 49, each one of the gamma components would happen centered at the trough of each alpha cycle. Consequently, each alpha cycle would include between 3 to 5 gamma cycles.

Most cross-frequency coupling dynamics have been observed between theta phase and gamma amplitude. Several studies have linked theta:gamma phase-amplitude coupling to memory and navigation processes using hippocampal rat recordings (Bragin et al., 1995; Soltesz & Deschenes, 1993). Moreover, this observation has been also reported in the human cortex (Canolty et al., 2006).

In contrast to theta:gamma coupling, occipital alpha:gamma phase-amplitude coupling has been linked to visual perception (Osipova, Hermes, & Jensen, 2008; Voytek et al., 2010). (Osipova et al., 2008) showed that the strength of alpha-gamma PAC was

task-dependent. Additionally, (Voytek et al., 2010) extended Osipova and collaborators' (2008) results by showing that depending on the cognitive requirements, theta and alpha phase modulate gamma amplitude. This could be indicative of different functional roles for different configurations of phase-amplitude CFCs.

Thus, the scarce literature about the functional role of nested oscillations in humans, suggests that an alpha:gamma oscillatory coding mechanism for the maintenance of task-relevant visual information is plausible. Similar oscillatory coding mechanisms have been suggested between theta:gamma for memory (O. Jensen & J. E. Lisman, 1996; Ole Jensen & John E Lisman, 1996) and alpha:gamma for unattended stimuli (Jensen, Bonnefond, & VanRullen, 2012).

Furthermore, this interpretation of gamma power between ~300 and ~600 ms provides a clear and simple physiological mechanism for the maintenance of task-relevant information in visual short-term memory. Furthermore, this interpretation makes direct predictions about neural and cognitive dynamics of perceptual decision-making: (i) task-relevant visual information, neuronal firing, and oscillatory gamma amplitude depend on alpha oscillations and (ii) successful performance on this task can be impaired by disrupting the alpha cycle using transcranial magnetic stimulation (7. Future Directions).

5.8 The functional role of ongoing EEG phase in perception

Recent experimental findings by VanRullen et al. (2011) have recently shown that the phase of ongoing oscillations (particularly in the alpha range, between 7 and 12 Hz) are mechanistically linked to perception (Drewes & VanRullen, 2011; VanRullen et al.,

2011). These experimental findings demonstrate the discrete nature of perception (Busch et al., 2009; Busch & VanRullen, 2010; Chakravarthi & Vanrullen, 2012; Drewes & VanRullen, 2011; Dugue, Marque, & VanRullen, 2011; Jensen et al., 2012; VanRullen & Koch, 2003). Further suggesting that behavioral variations, such as choice uncertainty and reaction time variability can be understood as emergent properties of the discrete nature of active sensory sampling modalities (e.g. eye movements) (Bichot, Chenchal Rao, & Schall, 2001; J. Miller, 1988; VanRullen et al., 2011; VanRullen & Koch, 2003).

Furthermore, it has been recently shown that ongoing oscillations are linked to the processes of evidence accumulation (Wyart, de Gardelle, Scholl, & Summerfield, 2012). Wyart et al. (2012) displayed task-relevant visual evidence at a constant rate of 4 Hz while recording EEG. Delta-range (1-3 Hz) ongoing oscillations were linked to accumulation of the presented evidence. Moreover, higher-frequency beta oscillations (10-30 Hz) seemed to integrate the perceived evidence.

Thus, recent evidence suggests that evidence accumulation processes towards a decision might rely on ongoing rhythmic brain activity (for reviews see Uchida, Kepecs, & Mainen, 2006; VanRullen et al., 2011). Moreover, at present, it is not clear how discrete information sampling can lead to continuous integration of task-relevant (and important task-irrelevant) information. A possible answer may underlie on different frequencies of ongoing oscillatory brain activity (e.g. 1-3 Hz (Wyart et al., 2012), 5-7 Hz (Busch et al., 2009; Busch & VanRullen, 2010), 10-14 Hz (Drewes & VanRullen, 2011)) acting as flexible, context-dependent information gating mechanisms (Fries, 2005; Hoppensteadt & Izhikevich, 1998; Schroeder & Lakatos, 2009b; F. Varela et al., 2001).

For example, visual information for a simple perceptual judgment may come from direct sensory evidence or may come from memory. In this case, very different neural representations of information will be mapped onto the same motor response. I think that neural oscillations can support such flexible and selective neural communication. The results discussed in 5.7 Decision-relevant cognitive and neural events depend on the alpha cycle, provide indirect evidence for this idea.

6. Conclusion

I have implemented a consistent semi-exploratory framework to mine temporal and spatial dynamics of scalp-recorded neural signals of perceptual decision-making. The key aspects to this framework consist in (i) a parametric design implementing a specific experimental manipulation allowing me to separate stimulus properties from task demands (see 5.2 No impacts of systematic low-level differences in stimuli are seen in my results), (ii) exploring neurophysiological brain dynamics using a systematic analysis approach based on neural time-series analysis and the neuronal oscillations framework (see 2. Exploring Cognitive Dynamics Using Scalp-Recorded Neural Signals), and (iii) mining measures of brain activity using single-trial multiple regression in combination with modern statistical techniques (see 3.5.1 Analysis of linear measures).

Although my results used several independent measures of brain activity, they are consistent within each other. Moreover, my results are consistent with previous literature and furthermore provide novel insights about the functional role of oscillatory brain activity in perceptual decision-making.

More specifically, my results indicate (i) the success of the present experimental design (see 5.2 No impacts of systematic low-level differences in stimuli are seen in my results). (ii) Task-specific information might be readily available early in the sensory processing stream when acquiring information for perceptual decisions (see 5.5 Decision-specific cognitive demands modulate early gamma power). (iii) Gamma phase synchrony might be a neurobiological mechanism supporting propagation of information between bottom-up and top-down factors involved in perceptual decision-making (see 5.6 Local and inter-areal gamma synchrony at ~200 ms reflects decision-dependent integration of distributed neural processing). (iv) Nested alpha and gamma oscillations might play a central role in short-term visual memory for perceptual decisions (see 5.7 Decision-relevant cognitive and neural events depend on the alpha cycle and 5.8 The functional role of ongoing EEG phase in perception).

Furthermore, from my results a set of novel hypotheses emerges[45]: (i) A relationship exists between single-trial ERP amplitude and single-trial variability of response times between ~60 and ~250 ms after test onset. (ii) The C1 ERP component is a specific response elicited after the test image onset reflecting task-dependent changes in attentional demands. (iii) Task-specific visual information, neuronal firing rate, and oscillatory gamma amplitude depend on oscillatory activity in the alpha range.

Finally, the present results suggest a time-course including at least six neural events unfolding roughly at ~70, ~100, ~150, ~220, ~320, and ~420 ms. Results furthermore provide a small insight into the possible functional roles of the neural events occurring during the time-course of perceptual decision-making.

[45] Along with specific follow-up analyses (see 7. Future Directions)

7. Future Directions

7.1 Hypothesis-driven follow-up analyses

From the present results, interesting hypotheses were drawn. Consequently, from these hypotheses a set of specific follow-up analyses emerges: (i) ERP sensitivity to behavioral outcome beta weights have to be re-epoched in order to test ERPs elicited by the standard image against ERPs elicited by the test image. This analysis will reveal the *specificity* of ERP amplitude occurring within ~60 and ~250 ms uncovering a putative exclusive interaction between information (standard/test image) and process (information acquisition/information matching).

(ii) ERP sensitivity to task demands beta weights have to be re-epoched in order to test ERPs elicited by the standard image against ERPs elicited by the test image. This analysis will reveal the *selectivity* of the C1 ERP component amplitude uncovering a putative category (standard/test image) by task (information acquisition/information matching) interaction. This interaction will provide evidence for the attentional modulation of C1. Early effects of attention over striate cortex as measured by the BOLD signal are known (Kanwisher & Wojciulik, 2000; Martinez et al., 1999). However, attentional impacts in the temporal dynamics are still a heated topic of discussion in current attention research (Fu, Fedota, Greenwood, & Parasuraman, 2010; Rauss, Pourtois, Vuilleumier, & Schwartz, 2012; V. Rossi & Pourtois, 2012).

(iii) Hypothesis-driven phase-amplitude coupling analysis has to be computed for a time window comprised by ~300 and ~600 ms between gamma power in the ~45 to ~70

Hz range and alpha phase in the ~12 to ~14 Hz range. This analysis will provide evidence for a phase coding mechanism for short-term visual memory in perceptual decision-making. The causality and influence of this alpha-based coding mechanism over gamma oscillations and perceptual decision-making can be empirically tested using transcranial magnetic stimulation (TMS).

7.2 Robust implementation of neural measures as standard practice

As discussed earlier, the implementation of event-related phase-amplitude coupling analysis failed (see 5.1.5 Event-Related Phase-amplitude Coupling (ERPAC)). This inspired me to think about a way to generate a more robust implementation of this measure. I propose a trick that was used in this dissertation in order to test for statistical significance. I suggest that instead of ERPAC, a robust version of it can be calculated; $ERPAC_z$ can be computed at each electrode (*ch*) using non-parametric permutation testing.

I suggest quantifying ERPAC as recommended by (Voytek et al., 2013) using Equation 11. However, the ERPAC measure per subject can be recomputed under the null hypothesis that no temporal correlation existed between the chosen low-frequency phase and high-frequency amplitude ($ERPAC_{null}$). This null-model can be simply obtained by shifting the power time series by a frequency-specific random amount of time while keeping the phase time-series constant; thus destroying any temporal relation between phase and amplitude. This process can be repeated 500 times per subject, generating 500 different $ERPAC_{null}$. Null models should be stored after each one of the iterations.

Finally, the matrix containing $ERPAC_{null}$ can be used in Equation 16 to generate the *z*-scored version of event-related phase-amplitude coupling, $ERPAC_z$:

Equation 16

$$ERPAC_z = \left(ERPAC - 1/n \sum_{i=1}^{n} ERPAC_{null_i} \right) \Big/ std\left(ERPAC_{null} \right)$$

This simple procedure would allow having a robust measure per subject, with normalized scale in comparable units across subjects and recordings. Single-subject and group-level analyses could be normally implemented in $ERPAC_z$. Furthermore, a robust version of any time-frequency measure can be computed per subject, benefiting from the non-parametric permutation framework from the very beginning of the analysis pipeline.

7.3 Using weighted versions of non-linear measures to better link phase dynamics to behavior

Using continuous and discrete variables as regressors in a linear model brought fruitful results in this dissertation. Unfortunately, non-linear measures were not able to benefit from such technique. Due to the nature of computation of ITPC and ISPC (see 3.5.2 Analysis of Non-Linear Measures) I thought it was not possible to implement such analysis when using non-linear dynamics. Therefore, when these analyses were implemented no efforts were made in order to establish continuous relations with phase through reaction times or stimulus parameters. I recently found out that non-linear dynamics could indeed be successfully linked to trial-by-trial variables (Michael X Cohen & Voytek, 2013).

Thus, when using parametric designs such as the one implemented in this dissertation, an extension of ITPC should be used. Weighted inter-trial phase clustering (wITPC) is a way to establish a more direct link between phase angle dynamics and trial-varying variables such as reaction times or stimulus parameters (Michael X Cohen & Voytek, 2013). This measure of phase dynamics addresses one of the main concerns about ITPC; it is unable to uncover phase dynamics that are not necessarily linked to stimulus onset. Thus, wITPC is a superior metric to link non-linear dynamics to behavior or stimulus properties.

7.4 Zero phase-lag measures might be contaminated with volume-conducted signals

Electrical fields spread across the scalp, producing different EEG sensors to potentially measure the same electrical field as two separate sources. Thus, volume conduction sets strong confounds to zero-phase-lag measures such as ISPC. Inter-areal synchrony measured at the scalp can be potentially produced by the same sources and spuriously appear as true functional phase-based connectivity.

Consider two pairs of EEG electrodes. One pair is influenced by volume conduction; it measures spurious or conductance synchrony. The other pair records an actual neural coupling. If a phase consistency measure is applied, both pairs of electrodes will report phase synchrony with a value ranging from 0 (no synchrony) to 1 (complete synchronization), but only one of these is real.

Several methods have been suggested to deal with this situation. One of them implies calculating ITPC in the electrodes where ISPC has been already computed. After

calculating ITPC between these hypothetical signals, one matrix per electrode indicating synchronization strength is obtained. Using this information, one could calculate phase difference by subtracting the ITPC on one electrode from the other. This procedure should yield to different results in these two cases: due to its spurious nature, conductance synchrony should cancel out, whereas real synchrony would still report a number different than zero. Unfortunately, this might not always be the case. Since the two electrodes record the linear combination of the sources' amplitudes, the phase of these signals could be different unless the mixed sources share phase orientation. Hence, phase difference between conductance and real synchrony, might not be a good discrimination heuristic to apply (J. P. Lachaux et al., 1999).

An alternative option is given by diffusion synchrony. This is, if the two electrodes affected by conductance synchrony report high ITPC, large numbers of surrounding electrodes will also report high ITPC (Lachaux et al., 2000; J. P. Lachaux et al., 1999). In contrast, real synchrony has been shown to display small-world architecture (Stam & Reijneveld, 2007). High-density EEG and MEG recordings directly benefit from this principle, and nowadays more than 64 electrodes is the gold standard for phase synchrony analyses (Nunez & Srinivasan, 2006).

The application of second-order spatial filters such as Laplacians or linear data decomposition techniques such as principal and independent component analysis allow researchers to identify distinct sources of EEG signals (Makeig et al., 2004). Particularly, researchers have shown that ICA has a better overall performance than PCA and Laplacians in separating and clustering signals (Gleich & Zhukov, 2004). Therefore using

ICA-mined data for phase synchrony analysis has been a suggested approach (Makeig et al., 2004).

Finally, using phase-lag measures of phase dynamics has been suggested as the safest option to avoid conductance synchrony (Stam et al., 2007; Vinck, Battaglia, Womelsdorf, & Pennartz, 2012). These measures are based on the idea that spurious synchrony will have zero-phase-lag between the tested sensors. Thus, avoiding zero-phase-lag synchrony would prevent measuring conductance synchrony (Stam et al., 2007; Vinck et al., 2012). However, near-zero- and/or zero-phase-lag dynamics are a real phenomenon worth of study (Uhlhaas et al., 2009). Therefore, until a larger body of literature has been generated about the functional role of phase dynamics in cognition both zero-phase-lag (i.e. ISPC) and phase-lag-based measures of phase dynamics should be used. This approach was applied recently in order to examine the effects of context in perception; the article is currently in preparation (Parada et al., in preparation).

8. Concluding remarks

In this dissertation I have implemented an approach that benefits from the last 25 years of cognitive electrophysiology (see 2.2 Neural Dynamics in the Time-Frequency Domain), the last 15 years of advancements in statistics (see 2.5 Non-Parametric Permutation Testing) and the approximately 7 years I have been thinking about these topics.

I think the future of cognitive electrophysiology will rely on the proper understanding of analysis methods in order to generate new, more powerful approaches. Furthermore, the implementation of parametric experimental designs and systematic

analysis approaches in combination with modern robust statistics will allow a safer exploration of the rich multidimensional electrophysiological space. Additionally avoiding the danger of measuring minuscule hard-to-replicate effects or false-positives caused by violation of statistical test assumptions, "the dance" of p-values, or other artifacts.

I think working under the neural oscillations framework allows cognitive neuroscientists to avoid getting stuck on an "island of knowledge" where no information gets transferred from or to other fields. Furthermore, due to the intrinsic existence of periodic phenomena in nature[46], the neural oscillations framework provides a link to understand how evolution orchestrated environmental[47], physiological[48] and neurophysiological events[49] giving way to adaptive behavior that characterizes all living species.

I think the future of cognitive electrophysiology will rely on establishing a precise link between brain rhythms and embodied/situated cognition, perception, and behavior. The work presented in this dissertation is my microscopic contribution towards this goal.

[46] Periodic phenomena that defines *time* itself such as circadian rhythms
[47] Periodic phenomena in the world such as movement: if it is too fast or too slow it will not be seen
[48] Periodic phenomena that is foundational to behavior such as hormonal fluctuations
[49] Periodic phenomena such as neuronal firing rates

9. References

Addante, R. J., Ranganath, C., & Yonelinas, A. P. (2012). Examining ERP correlates of recognition memory: evidence of accurate source recognition without recollection. *Neuroimage, 62*(1), 439-450. doi: 10.1016/j.neuroimage.2012.04.031

Akam, T., & Kullmann, D. M. (2010). Oscillations and filtering networks support flexible routing of information. *Neuron, 67*(2), 308-320. doi: 10.1016/j.neuron.2010.06.019

Allen, C., & Bekoff, M. (1997). *Species of mind : the philosophy and biology of cognitive ethology*. Cambridge, Mass.: MIT Press.

Baars, B. J., & Franklin, S. (2007). An architectural model of conscious and unconscious brain functions: Global Workspace Theory and IDA. *Neural Netw, 20*(9), 955-961. doi: 10.1016/j.neunet.2007.09.013

Bar, M. (2003). A cortical mechanism for triggering top-down facilitation in visual object recognition. *J Cogn Neurosci, 15*(4), 600-609. doi: 10.1162/089892903321662976

Bar, M. (2004). Visual objects in context. *Nat Rev Neurosci, 5*(8), 617-629. doi: 10.1038/nrn1476

Bar, M. (2007). The proactive brain: using analogies and associations to generate predictions. *Trends Cogn Sci, 11*(7), 280-289. doi: 10.1016/j.tics.2007.05.005

Bar, M. (2009). The proactive brain: memory for predictions. *Philos Trans R Soc Lond B Biol Sci, 364*(1521), 1235-1243. doi: 10.1098/rstb.2008.0310

Bar, M., Kassam, K. S., Ghuman, A. S., Boshyan, J., Schmid, A. M., Dale, A. M., . . . Halgren, E. (2006). Top-down facilitation of visual recognition. *Proceedings of the National Academy of Sciences of the United States of America, 103*(2), 449-454. doi: 10.1073/pnas.0507062103

Benjamini, Y., & Hochberg, Y. (1995). Controlling the false discovery rate: a practical and powerful approach to multiple testing. *Journal of the Royal Statistical Society. Series B (Methodological)*, 289-300.

Berens, P. (2009). CircStat: a MATLAB toolbox for circular statistics. *Journal of Statistical Software, 31*(10), 1-21.

Bertalanffy, L. v. (1968). *General system theory: Foundations, development, applications*: Braziller. New York.

Bichot, N. P., Chenchal Rao, S., & Schall, J. D. (2001). Continuous processing in macaque frontal cortex during visual search. *Neuropsychologia, 39*(9), 972-982.

Blau, V. C., Maurer, U., Tottenham, N., & McCandliss, B. D. (2007). The face-specific N170 component is modulated by emotional facial expression. *Behav Brain Funct, 3*, 7. doi: 10.1186/1744-9081-3-7

Bragin, A., Jando, G., Nadasdy, Z., Hetke, J., Wise, K., & Buzsaki, G. (1995). Gamma (40-100 Hz) oscillation in the hippocampus of the behaving rat. *The Journal of neuroscience : the official journal of the Society for Neuroscience, 15*(1 Pt 1), 47-60.

Brandt, M. E., Jansen, B. H., & Carbonari, J. P. (1991). Pre-stimulus spectral EEG patterns and the visual evoked response. *Electroencephalogr Clin Neurophysiol, 80*(1), 16-20.

Bruns, A. (2004). Fourier-, Hilbert- and wavelet-based signal analysis: are they really different approaches? *J Neurosci Methods, 137*(2), 321-332. doi: 10.1016/j.jneumeth.2004.03.002

Burgess, A. P. (2012). Towards a unified understanding of event-related changes in the EEG: the firefly model of synchronization through cross-frequency phase modulation. *PloS one, 7*(9), e45630. doi: 10.1371/journal.pone.0045630

Busch, N. A., Debener, S., Kranczioch, C., Engel, A. K., & Herrmann, C. S. (2004). Size matters: effects of stimulus size, duration and eccentricity on the visual gamma-band response. *Clin Neurophysiol, 115*(8), 1810-1820. doi: 10.1016/j.clinph.2004.03.015

Busch, N. A., Dubois, J., & VanRullen, R. (2009). The phase of ongoing EEG oscillations predicts visual perception. *The Journal of neuroscience : the official journal of the Society for Neuroscience, 29*(24), 7869-7876. doi: 10.1523/JNEUROSCI.0113-09.2009

Busch, N. A., Herrmann, C. S., Muller, M. M., Lenz, D., & Gruber, T. (2006). A cross-laboratory study of event-related gamma activity in a standard object recognition paradigm. *Neuroimage, 33*(4), 1169-1177. doi: 10.1016/j.neuroimage.2006.07.034

Busch, N. A., Schadow, J., Frund, I., & Herrmann, C. S. (2006). Time-frequency analysis of target detection reveals an early interface between bottom-up and top-down processes in the gamma-band. *Neuroimage, 29*(4), 1106-1116. doi: 10.1016/j.neuroimage.2005.09.009

Busch, N. A., & VanRullen, R. (2010). Spontaneous EEG oscillations reveal periodic sampling of visual attention. *Proc Natl Acad Sci U S A, 107*(37), 16048-16053. doi: 10.1073/pnas.1004801107

Buzsaki, G. (1984). Feed-forward inhibition in the hippocampal formation. *Prog Neurobiol, 22*(2), 131-153.

Buzsáki, G. (2006). *Rhythms of the brain*. Oxford ; New York: Oxford University Press.

Buzsaki, G., & Draguhn, A. (2004). Neuronal oscillations in cortical networks. *Science, 304*(5679), 1926-1929. doi: 10.1126/science.1099745

Buzsáki, G., & Wang, X.-J. (2012). Mechanisms of gamma oscillations. *Annu Rev Neurosci, 35*, 203-225.

Calvin, W. H., & Stevens, C. F. (1967). Synaptic noise as a source of variability in the interval between action potentials. *Science, 155*(3764), 842-844.

Canolty, R. T., Edwards, E., Dalal, S. S., Soltani, M., Nagarajan, S. S., Kirsch, H. E., . . . Knight, R. T. (2006). High gamma power is phase-locked to theta oscillations in human neocortex. *Science, 313*(5793), 1626-1628. doi: 10.1126/science.1128115

Canolty, R. T., & Knight, R. T. (2010). The functional role of cross-frequency coupling. *Trends Cogn Sci, 14*(11), 506-515. doi: 10.1016/j.tics.2010.09.001

Carroll, J. W. (2012). Laws of Nature. Retrieved May 2014, from The Stanford Encyclopedia of Philosophy (Spring 2012 Edition) <http://plato.stanford.edu/archives/spr2012/entries/laws-of-nature/>

Carter, G. C. (1987). Coherence and time delay estimation. *Proceedings of the IEEE, 75*(2), 236-255.

Cartwright, D., & Festinger, L. (1943). A quantitative theory of decision. *Psychol Rev, 50*(6), 595.

Celesia, G., & Peachey, N. (1993). Visual evoked potentials and electroretinograms. *Electroencephalography: basic principles, clinical applications and related fields. Baltimore: Williams and Wilkins*, 911-936.

Chakravarthi, R., & Vanrullen, R. (2012). Conscious updating is a rhythmic process. *Proceedings of the National Academy of Sciences of the United States of America, 109*(26), 10599-10604. doi: 10.1073/pnas.1121622109

Cohen, M. X. (2008). Assessing transient cross-frequency coupling in EEG data. *J Neurosci Methods, 168*(2), 494-499. doi: 10.1016/j.jneumeth.2007.10.012

Cohen, M. X. (2011). It's about Time. *Frontiers in human neuroscience, 5*, 2. doi: 10.3389/fnhum.2011.00002

Cohen, M. X., & Cavanagh, J. F. (2011). Single-trial regression elucidates the role of prefrontal theta oscillations in response conflict. *Front Psychol, 2*, 30. doi: 10.3389/fpsyg.2011.00030

Cohen, M. X., & Gulbinaite, R. (2014). Five methodological challenges in cognitive electrophysiology. *Neuroimage, 85 Pt 2*, 702-710. doi: 10.1016/j.neuroimage.2013.08.010

Cohen, M. X., & Voytek, B. (2013). Linking nonlinear neural dynamics to single-trial human behavior. In M. M. Pesenson (Ed.), *Multiscale Analysis and Nonlinear Dynamics: From Genes to the Brain* (pp. 217-232): John Wiley & Sons.

Corbetta, M., & Shulman, G. L. (2002). Control of goal-directed and stimulus-driven attention in the brain. *Nat Rev Neurosci, 3*(3), 201-215. doi: 10.1038/nrn755

Cosandier-Rimele, D., Merlet, I., Badier, J. M., Chauvel, P., & Wendling, F. (2008). The neuronal sources of EEG: modeling of simultaneous scalp and intracerebral recordings in epilepsy. *Neuroimage, 42*(1), 135-146. doi: 10.1016/j.neuroimage.2008.04.185

Cressie, N., & Whitford, H. (1986). How to Use the Two Sample t-Test. *Biometrical Journal, 28*(2), 131-148.

Cumming, G. (2013). *Understanding the new statistics: Effect sizes, confidence intervals, and meta-analysis*: Routledge.

David, O., Cosmelli, D., & Friston, K. J. (2004). Evaluation of different measures of functional connectivity using a neural mass model. *Neuroimage, 21*(2), 659-673. doi: 10.1016/j.neuroimage.2003.10.006

David, O., Kilner, J. M., & Friston, K. J. (2006). Mechanisms of evoked and induced responses in MEG/EEG. *Neuroimage, 31*(4), 1580-1591. doi: 10.1016/j.neuroimage.2006.02.034

Delorme, A., & Makeig, S. (2004). EEGLAB: an open source toolbox for analysis of single-trial EEG dynamics including independent component analysis. *J Neurosci Methods, 134*(1), 9-21. doi: 10.1016/j.jneumeth.2003.10.009

Delorme, A., & Makeig, S. (2014). The EEGLAB Discussion List.

Doesburg, S. M., Green, J. J., McDonald, J. J., & Ward, L. M. (2009). Rhythms of consciousness: binocular rivalry reveals large-scale oscillatory network dynamics mediating visual perception. *PloS one, 4*(7), e6142. doi: 10.1371/journal.pone.0006142

Donkin, C., Brown, S. D., & Heathcote, A. (2009). The overconstraint of response time models: rethinking the scaling problem. *Psychon Bull Rev, 16*(6), 1129-1135. doi: 10.3758/PBR.16.6.1129

Drewes, J., & VanRullen, R. (2011). This is the rhythm of your eyes: the phase of ongoing electroencephalogram oscillations modulates saccadic reaction time. *J Neurosci, 31*(12), 4698-4708. doi: 10.1523/JNEUROSCI.4795-10.2011

Dugue, L., Marque, P., & VanRullen, R. (2011). The phase of ongoing oscillations mediates the causal relation between brain excitation and visual perception. *J Neurosci, 31*(33), 11889-11893. doi: 10.1523/JNEUROSCI.1161-11.2011

Engel, A. K., Fries, P., & Singer, W. (2001). Dynamic predictions: oscillations and synchrony in top-down processing. *Nat Rev Neurosci, 2*(10), 704-716. doi: 10.1038/35094565

Finnigan, S., Humphreys, M. S., Dennis, S., & Geffen, G. (2002). ERP 'old/new' effects: memory strength and decisional factor(s). *Neuropsychologia, 40*(13), 2288-2304.

Fitzgibbon, S. P., Pope, K. J., Mackenzie, L., Clark, C. R., & Willoughby, J. O. (2004). Cognitive tasks augment gamma EEG power. *Clin Neurophysiol, 115*(8), 1802-1809. doi: 10.1016/j.clinph.2004.03.009

Fodor, J. A. (2001). *The mind doesn't work that way: The scope and limits of computational psychology*: MIT press.

Foxe, J. J., & Simpson, G. V. (2002). Flow of activation from V1 to frontal cortex in humans. A framework for defining "early" visual processing. *Exp Brain Res, 142*(1), 139-150. doi: 10.1007/s00221-001-0906-7

Freedman, D., & Diaconis, P. (1981). On the histogram as a density estimator: L 2 theory. *Probability theory and related fields, 57*(4), 453-476.

Freeman, W. J. (2000). *Neurodynamics: an exploration in mesoscopic brain dynamics*: Springer.

Freeman, W. J. (2002). *The limbic action-perception cycle controlling goal-directed animal behavior.* Paper presented at the Neural Networks, 2002. IJCNN'02. Proceedings of the 2002 International Joint Conference on.

Friedman, D., & Johnson, R., Jr. (2000). Event-related potential (ERP) studies of memory encoding and retrieval: a selective review. *Microsc Res Tech, 51*(1), 6-28. doi: 10.1002/1097-0029(20001001)51:1<6::AID-JEMT2>3.0.CO;2-R

Friedman, D., & Trott, C. (2000). An event-related potential study of encoding in young and older adults. *Neuropsychologia, 38*(5), 542-557.

Fries, P. (2005). A mechanism for cognitive dynamics: neuronal communication through neuronal coherence. *Trends Cogn Sci, 9*(10), 474-480. doi: 10.1016/j.tics.2005.08.011

Fries, P. (2009). Neuronal gamma-band synchronization as a fundamental process in cortical computation. *Annu Rev Neurosci, 32*, 209-224. doi: 10.1146/annurev.neuro.051508.135603

Fries, P., Neuenschwander, S., Engel, A. K., Goebel, R., & Singer, W. (2001). Rapid feature selective neuronal synchronization through correlated latency shifting. *Nat Neurosci, 4*(2), 194-200. doi: 10.1038/84032

Fries, P., Reynolds, J. H., Rorie, A. E., & Desimone, R. (2001). Modulation of oscillatory neuronal synchronization by selective visual attention. *Science, 291*(5508), 1560-1563. doi: 10.1126/science.291.5508.1560

Friston, K. J. (1997). Another neural code? *Neuroimage, 5*(3), 213-220. doi: 10.1006/nimg.1997.0260

Fu, S., Fedota, J. R., Greenwood, P. M., & Parasuraman, R. (2010). Dissociation of visual C1 and P1 components as a function of attentional load: an event-related potential study. *Biol Psychol, 85*(1), 171-178. doi: 10.1016/j.biopsycho.2010.06.008

Gaspar, C. M., & Rousselet, G. A. (2009). How do amplitude spectra influence rapid animal detection? *Vision Res, 49*(24), 3001-3012. doi: 10.1016/j.visres.2009.09.021

Gaspar, C. M., Rousselet, G. A., & Pernet, C. R. (2011). Reliability of ERP and single-trial analyses. *Neuroimage, 58*(2), 620-629. doi: 10.1016/j.neuroimage.2011.06.052

Gazzaniga, M. S., Ivry, R. B., & Mangun, G. R. (2013). *Cognitive neuroscience : the biology of the mind* (Fourth edition. ed.). New York, N.Y.: W. W. Norton & Company, Inc.

Genovese, C. R., Lazar, N. A., & Nichols, T. (2002). Thresholding of statistical maps in functional neuroimaging using the false discovery rate. *Neuroimage, 15*(4), 870-878. doi: 10.1006/nimg.2001.1037

Gleich, D., & Zhukov, L. (2004). Soft clustering with projections: PCA, ICA and Laplacian. *New York Research Labs*.

Goffaux, V., Jemel, B., Jacques, C., Rossion, B., & Schyns, P. G. (2003). ERP evidence for task modulations on face perceptual processing at different spatial scales. *Cogn Sci, 27*(2), 313-325.

Gold, J. I., & Shadlen, M. N. (2007). The neural basis of decision making. *Annu Rev Neurosci, 30*, 535-574. doi: 10.1146/annurev.neuro.29.051605.113038

Grandchamp, R., & Delorme, A. (2011). Single-trial normalization for event-related spectral decomposition reduces sensitivity to noisy trials. *Front Psychol, 2*, 236. doi: 10.3389/fpsyg.2011.00236

Gray, C. M., Konig, P., Engel, A. K., & Singer, W. (1989). Oscillatory responses in cat visual cortex exhibit inter-columnar synchronization which reflects global stimulus properties. *Nature, 338*(6213), 334-337. doi: 10.1038/338334a0

Gregoriou, G. G., Gotts, S. J., Zhou, H., & Desimone, R. (2009a). High-frequency, long-range coupling between prefrontal and visual cortex during attention. *Science, 324*(5931), 1207-1210. doi: 10.1126/science.1171402

Gregoriou, G. G., Gotts, S. J., Zhou, H., & Desimone, R. (2009b). Long-range neural coupling through synchronization with attention. *Prog Brain Res, 176*, 35-45. doi: 10.1016/S0079-6123(09)17603-3

Grossberg, S. (1999). The link between brain learning, attention, and consciousness. *Consciousness and cognition, 8*(1), 1-44.

Grossman, M., Smith, E. E., Koenig, P., Glosser, G., DeVita, C., Moore, P., & McMillan, C. (2002). The neural basis for categorization in semantic memory. *Neuroimage, 17*(3), 1549-1561.

Gruber, T., & Muller, M. M. (2002). Effects of picture repetition on induced gamma band responses, evoked potentials, and phase synchrony in the human EEG. *Brain Res Cogn Brain Res, 13*(3), 377-392.

Gruber, T., Muller, M. M., & Keil, A. (2002). Modulation of induced gamma band responses in a perceptual learning task in the human EEG. *J Cogn Neurosci, 14*(5), 732-744. doi: 10.1162/08989290260138636

Gwin, J. T., Gramann, K., Makeig, S., & Ferris, D. P. (2010). Removal of movement artifact from high-density EEG recorded during walking and running. *Journal of neurophysiology, 103*(6), 3526-3534. doi: 10.1152/jn.00105.2010

Halgren, E., Boujon, C., Clarke, J., Wang, C., & Chauvel, P. (2002). Rapid distributed fronto-parieto-occipital processing stages during working memory in humans. *Cereb Cortex, 12*(7), 710-728.

Handel, B. F., Haarmeier, T., & Jensen, O. (2011). Alpha oscillations correlate with the successful inhibition of unattended stimuli. *J Cogn Neurosci, 23*(9), 2494-2502. doi: 10.1162/jocn.2010.21557

He, B. J., Zempel, J. M., Snyder, A. Z., & Raichle, M. E. (2010). The temporal structures and functional significance of scale-free brain activity. *Neuron, 66*(3), 353-369.

Hentschke, H., & Stüttgen, M. C. (2011). Computation of measures of effect size for neuroscience data sets. *European Journal of Neuroscience, 34*(12), 1887-1894.

Herrmann, C. S., Crigutsch, M., & Busch, N. A. (2005). EEG Oscillations and Wavelet Analysis. *Event-related potentials: A methods handbook*, 229.

Herrmann, C. S., Lenz, D., Junge, S., Busch, N. A., & Maess, B. (2004). Memory-matches evoke human gamma-responses. *BMC Neurosci, 5*, 13. doi: 10.1186/1471-2202-5-13

Herrmann, C. S., Munk, M. H., & Engel, A. K. (2004). Cognitive functions of gamma-band activity: memory match and utilization. *Trends Cogn Sci, 8*(8), 347-355. doi: 10.1016/j.tics.2004.06.006

Hopfield, J. J. (1982). Neural networks and physical systems with emergent collective computational abilities. *Proceedings of the national academy of sciences, 79*(8), 2554-2558.

Hopfield, J. J., & Tank, D. W. (1986). Computing with neural circuits- A model. *Science, 233*(4764), 625-633.

Hoppensteadt, F. C., & Izhikevich, E. M. (1998). Thalamo-cortical interactions modeled by weakly connected oscillators: could the brain use FM radio principles? *Biosystems, 48*(1-3), 85-94.

Hughes, S. W., Lorincz, M., Cope, D. W., Blethyn, K. L., Kekesi, K. A., Parri, H. R., . . . Crunelli, V. (2004). Synchronized oscillations at alpha and theta frequencies in the lateral geniculate nucleus. *Neuron, 42*(2), 253-268.

Ioannidis, J. P. (2005). Why most published research findings are false. *PLoS medicine, 2*(8), e124.

Jensen, O., Bonnefond, M., & VanRullen, R. (2012). An oscillatory mechanism for prioritizing salient unattended stimuli. *Trends Cogn Sci, 16*(4), 200-206. doi: 10.1016/j.tics.2012.03.002

Jensen, O., & Lisman, J. E. (1996). Hippocampal CA3 region predicts memory sequences: accounting for the phase precession of place cells. *Learn Mem, 3*(2-3), 279-287.

Jensen, O., & Lisman, J. E. (1996). Novel lists of 7+/-2 known items can be reliably stored in an oscillatory short-term memory network: interaction with long-term memory. *Learning & Memory, 3*(2-3), 257-263.

Jervis, B. W., Nichols, M. J., Johnson, T. E., Allen, E., & Hudson, N. R. (1983). A fundamental investigation of the composition of auditory evoked potentials. *IEEE Trans Biomed Eng, 30*(1), 43-50.

Johnson, R., Jr., Pfefferbaum, A., & Kopell, B. S. (1985). P300 and long-term memory: latency predicts recognition performance. *Psychophysiology, 22*(5), 497-507.

Jung, T.-P., Humphries, C., Lee, T.-W., Makeig, S., McKeown, M. J., Iragui, V., & Sejnowski, T. J. (1998). *Removing electroencephalographic artifacts: comparison between ICA and PCA*. Paper presented at the Neural Networks for Signal Processing VIII, 1998. Proceedings of the 1998 IEEE Signal Processing Society Workshop.

Kanwisher, N., & Wojciulik, E. (2000). Visual attention: insights from brain imaging. *Nat Rev Neurosci, 1*(2), 91-100. doi: 10.1038/35039043

Keightley, M. L., Winocur, G., Graham, S. J., Mayberg, H. S., Hevenor, S. J., & Grady, C. L. (2003). An fMRI study investigating cognitive modulation of brain regions associated with emotional processing of visual stimuli. *Neuropsychologia, 41*(5), 585-596.

Kelso, J. S. (1995). *Dynamic patterns: The self-organization of brain and behavior*: MIT press.

Kiebel, S. J., David, O., & Friston, K. J. (2006). Dynamic causal modelling of evoked responses in EEG/MEG with lead field parameterization. *Neuroimage, 30*(4), 1273-1284.

Kiebel, S. J., & Friston, K. J. (2004a). Statistical parametric mapping for event-related potentials (II): a hierarchical temporal model. *Neuroimage, 22*(2), 503-520. doi: 10.1016/j.neuroimage.2004.02.013

Kiebel, S. J., & Friston, K. J. (2004b). Statistical parametric mapping for event-related potentials: I. Generic considerations. *Neuroimage, 22*(2), 492-502. doi: 10.1016/j.neuroimage.2004.02.012

Kilner, J. M., Kiebel, S. J., & Friston, K. J. (2005). Applications of random field theory to electrophysiology. *Neurosci Lett, 374*(3), 174-178. doi: 10.1016/j.neulet.2004.10.052

Klimesch, W., Russegger, H., Doppelmayr, M., & Pachinger, T. (1998). A method for the calculation of induced band power: implications for the significance of brain oscillations. *Electroencephalogr Clin Neurophysiol, 108*(2), 123-130.

Klimesch, W., Sauseng, P., & Hanslmayr, S. (2007). EEG alpha oscillations: the inhibition-timing hypothesis. *Brain Res Rev, 53*(1), 63-88. doi: 10.1016/j.brainresrev.2006.06.003

Kok, A. (1997). Event-related-potential (ERP) reflections of mental resources: a review and synthesis. *Biol Psychol, 45*(1-3), 19-56.

Kriegeskorte, N., Simmons, W. K., Bellgowan, P. S., & Baker, C. I. (2009). Circular analysis in systems neuroscience: the dangers of double dipping. *Nat Neurosci, 12*(5), 535-540. doi: 10.1038/nn.2303

Kruschke, J. K. (2010). What to believe: Bayesian methods for data analysis. *Trends Cogn Sci, 14*(7), 293-300. doi: 10.1016/j.tics.2010.05.001

Kutas, M., & Federmeier, K. D. (2011). Thirty years and counting: finding meaning in the N400 component of the event-related brain potential (ERP). *Annual review of psychology, 62*, 621-647.

Lachaux, J.-P., Rodriguez, E., Le van Quyen, M., Lutz, A., Martinerie, J., & Varela, F. J. (2000). Studying single-trials of phase synchronous activity in the brain. *International Journal of Bifurcation and Chaos, 10*(10), 2429-2439.

Lachaux, J.-P., Rodriguez, E., Martinerie, J., & Varela, F. J. (1999). Measuring phase synchrony in brain signals. *Hum Brain Mapp, 8*(4), 194-208.

Lachaux, J. P., Rodriguez, E., Martinerie, J., & Varela, F. J. (1999). Measuring phase synchrony in brain signals. *Hum Brain Mapp, 8*(4), 194-208.

Lambdin, C. (2012). Significance tests as sorcery: Science is empirical—significance tests are not. *Theory & Psychology, 22*(1), 67-90.

Le Van Quyen, M., Foucher, J., Lachaux, J.-P., Rodriguez, E., Lutz, A., Martinerie, J., & Varela, F. J. (2001). Comparison of Hilbert transform and wavelet methods for the analysis of neuronal synchrony. *J Neurosci Methods, 111*(2), 83-98.

Lehmann, D. (1971). Multichannel topography of human alpha EEG fields. *Electroencephalogr Clin Neurophysiol, 31*(5), 439-449.

Lehmann, D., & Skrandies, W. (1980). Reference-free identification of components of checkerboard-evoked multichannel potential fields. *Electroencephalogr Clin Neurophysiol, 48*(6), 609-621.

Litvak, V., Mattout, J., Kiebel, S., Phillips, C., Henson, R., Kilner, J., . . . Friston, K. (2011). EEG and MEG data analysis in SPM8. *Comput Intell Neurosci, 2011*, 852961. doi: 10.1155/2011/852961

Liu, J., Harris, A., & Kanwisher, N. (2002). Stages of processing in face perception: an MEG study. *Nat Neurosci, 5*(9), 910-916. doi: 10.1038/nn909

Llinas, R., Ribary, U., Contreras, D., & Pedroarena, C. (1998). The neuronal basis for consciousness. *Philos Trans R Soc Lond B Biol Sci, 353*(1377), 1841-1849. doi: 10.1098/rstb.1998.0336

Lobier, M., Siebenhuhner, F., Palva, S., & Palva, J. M. (2014). Phase transfer entropy: a novel phase-based measure for directed connectivity in networks coupled by oscillatory interactions. *Neuroimage, 85 Pt 2*, 853-872. doi: 10.1016/j.neuroimage.2013.08.056

Logothetis, N. K., Pauls, J., Augath, M., Trinath, T., & Oeltermann, A. (2001). Neurophysiological investigation of the basis of the fMRI signal. *Nature, 412*(6843), 150-157. doi: 10.1038/35084005

Luck, S. J. (2005). *An introduction to the event-related potential technique*: MIT press Cambridge, MA:.

Makeig, S., Debener, S., Onton, J., & Delorme, A. (2004). Mining event-related brain dynamics. *Trends Cogn Sci, 8*(5), 204-210. doi: 10.1016/j.tics.2004.03.008

Makeig, S., Westerfield, M., Jung, T. P., Enghoff, S., Townsend, J., Courchesne, E., & Sejnowski, T. J. (2002). Dynamic brain sources of visual evoked responses. *Science, 295*(5555), 690-694. doi: 10.1126/science.1066168

Mantel, N., & Brown, C. (1974). Alternative tests for comparing normal distribution parameters based on logistic regression. *Biometrics, 30*(3), 485-497.

Maris, E., & Oostenveld, R. (2007). Nonparametric statistical testing of EEG- and MEG-data. *J Neurosci Methods, 164*(1), 177-190. doi: 10.1016/j.jneumeth.2007.03.024

Maris, E., van Vugt, M., & Kahana, M. (2011). Spatially distributed patterns of oscillatory coupling between high-frequency amplitudes and low-frequency phases in human iEEG. *Neuroimage, 54*(2), 836-850. doi: 10.1016/j.neuroimage.2010.09.029

Martinez, A., Anllo-Vento, L., Sereno, M. I., Frank, L. R., Buxton, R. B., Dubowitz, D. J., . . . Hillyard, S. A. (1999). Involvement of striate and extrastriate visual cortical areas in spatial attention. *Nat Neurosci, 2*(4), 364-369. doi: 10.1038/7274

Masicampo, E., & Lalande, D. R. (2012). A peculiar prevalence of p values just below. 05. *The Quarterly Journal of Experimental Psychology, 65*(11), 2271-2279.

Maturana, H. R., & Varela, F. J. (1984). *El árbol del conocimiento : las bases biológicas del entendimiento humano*. Santiago, Chile: Programa de Comunicación Transcultural, Organización de Estados Americanos.

Meltzer, J. A., Zaveri, H. P., Goncharova, II, Distasio, M. M., Papademetris, X., Spencer, S. S., . . . Constable, R. T. (2008). Effects of working memory load on oscillatory power in human intracranial EEG. *Cereb Cortex, 18*(8), 1843-1855. doi: 10.1093/cercor/bhm213

Merker, B. (2013). Cortical gamma oscillations: the functional key is activation, not cognition. *Neurosci Biobehav Rev, 37*(3), 401-417. doi: 10.1016/j.neubiorev.2013.01.013

Miller, E. K., & Cohen, J. D. (2001). An integrative theory of prefrontal cortex function. *Annu Rev Neurosci, 24*, 167-202. doi: 10.1146/annurev.neuro.24.1.167

Miller, J. (1988). Discrete and continuous models of human information processing: theoretical distinctions and empirical results. *Acta Psychol (Amst), 67*(3), 191-257.

Min, B. K., Busch, N. A., Debener, S., Kranczioch, C., Hanslmayr, S., Engel, A. K., & Herrmann, C. S. (2007). The best of both worlds: phase-reset of human EEG alpha activity and additive power contribute to ERP generation. *Int J Psychophysiol, 65*(1), 58-68. doi: 10.1016/j.ijpsycho.2007.03.002

Moran, M. D. (2003). Arguments for rejecting the sequential Bonferroni in ecological studies. *Oikos*, 403-405.

Mormann, F., Lehnertz, K., David, P., & E Elger, C. (2000). Mean phase coherence as a measure for phase synchronization and its application to the EEG of epilepsy patients. *Physica D: Nonlinear Phenomena, 144*(3), 358-369.

Morup, M., Hansen, L. K., & Arnfred, S. M. (2008). Algorithms for sparse nonnegative Tucker decompositions. *Neural Comput, 20*(8), 2112-2131. doi: 10.1162/neco.2008.11-06-407

Mulert, C., Leicht, G., Pogarell, O., Mergl, R., Karch, S., Juckel, G., . . . Hegerl, U. (2007). Auditory cortex and anterior cingulate cortex sources of the early evoked gamma-band response: relationship to task difficulty and mental effort. *Neuropsychologia, 45*(10), 2294-2306. doi: 10.1016/j.neuropsychologia.2007.02.020

Musall, S., von Pfostl, V., Rauch, A., Logothetis, N. K., & Whittingstall, K. (2014). Effects of neural synchrony on surface EEG. *Cereb Cortex, 24*(4), 1045-1053. doi: 10.1093/cercor/bhs389

Narum, S. R. (2006). Beyond Bonferroni: less conservative analyses for conservation genetics. *Conservation Genetics, 7*(5), 783-787.

Neville, H. J., Kutas, M., Chesney, G., & Schmidt, A. L. (1986). Event-related brain potentials during initial encoding and recognition memory of congruous and incongruous words. *Journal of Memory and Language, 25*(1), 75-92.

Nosek, B. A., Spies, J. R., & Motyl, M. (2012). Scientific utopia II. Restructuring incentives and practices to promote truth over publishability. *Perspectives on Psychological Science, 7*(6), 615-631.

Nunez, P. L., & Srinivasan, R. (2006). *Electric fields of the brain : the neurophysics of EEG* (2nd ed.). Oxford ; New York: Oxford University Press.

Nuzzo, R. (2014). Scientific method: statistical errors. *Nature, 506*(7487), 150-152. doi: 10.1038/506150a

Oliva, A., & Torralba, A. (2006). Building the gist of a scene: the role of global image features in recognition. *Prog Brain Res, 155*, 23-36. doi: 10.1016/S0079-6123(06)55002-2

Onton, J., Westerfield, M., Townsend, J., & Makeig, S. (2006). Imaging human EEG dynamics using independent component analysis. *Neurosci Biobehav Rev, 30*(6), 808-822. doi: 10.1016/j.neubiorev.2006.06.007

Oostenveld, R., Fries, P., Maris, E., & Schoffelen, J. M. (2011). FieldTrip: Open source software for advanced analysis of MEG, EEG, and invasive electrophysiological data. *Comput Intell Neurosci, 2011*, 156869. doi: 10.1155/2011/156869

Oppermann, F., Hassler, U., Jescheniak, J. D., & Gruber, T. (2012). The rapid extraction of gist-early neural correlates of high-level visual processing. *J Cogn Neurosci, 24*(2), 521-529. doi: 10.1162/jocn_a_00100

Osipova, D., Hermes, D., & Jensen, O. (2008). Gamma power is phase-locked to posterior alpha activity. *PloS one, 3*(12), e3990. doi: 10.1371/journal.pone.0003990

Palva, J. M., Palva, S., & Kaila, K. (2005). Phase synchrony among neuronal oscillations in the human cortex. *The Journal of neuroscience : the official journal of the Society for Neuroscience, 25*(15), 3962-3972. doi: 10.1523/JNEUROSCI.4250-04.2005

Palva, S., & Palva, J. M. (2007). New vistas for alpha-frequency band oscillations. *Trends Neurosci, 30*(4), 150-158. doi: 10.1016/j.tins.2007.02.001

Paninski, L. (2003). Estimation of entropy and mutual information. *Neural Comput, 15*(6), 1191-1253.

Pantazis, D., Nichols, T. E., Baillet, S., & Leahy, R. M. (2005). A comparison of random field theory and permutation methods for the statistical analysis of MEG data. *Neuroimage, 25*(2), 383-394. doi: 10.1016/j.neuroimage.2004.09.040

Parada, F. J., Moravec, L., Emerick, B., & Busey, T. A. (in preparation). *Independent roles of temporospatial alpha, beta, and gamma phase synchrony in the tilt illusion*.

Penny, W. D., Duzel, E., Miller, K. J., & Ojemann, J. G. (2008). Testing for nested oscillation. *J Neurosci Methods, 174*(1), 50-61. doi: 10.1016/j.jneumeth.2008.06.035

Pereda, E., Quiroga, R. Q., & Bhattacharya, J. (2005). Nonlinear multivariate analysis of neurophysiological signals. *Prog Neurobiol, 77*(1-2), 1-37. doi: 10.1016/j.pneurobio.2005.10.003

Pernet, C. R., Chauveau, N., Gaspar, C., & Rousselet, G. A. (2011). LIMO EEG: a toolbox for hierarchical LInear MOdeling of ElectroEncephaloGraphic data. *Comput Intell Neurosci, 2011*, 831409. doi: 10.1155/2011/831409

Philiastides, M. G., Ratcliff, R., & Sajda, P. (2006). Neural representation of task difficulty and decision making during perceptual categorization: a timing diagram. *The Journal of neuroscience : the official journal of the Society for Neuroscience, 26*(35), 8965-8975. doi: 10.1523/JNEUROSCI.1655-06.2006

Philiastides, M. G., & Sajda, P. (2007). EEG-informed fMRI reveals spatiotemporal characteristics of perceptual decision making. *The Journal of neuroscience : the official journal of the Society for Neuroscience, 27*(48), 13082-13091. doi: 10.1523/JNEUROSCI.3540-07.2007

Pouille, F., & Scanziani, M. (2001). Enforcement of temporal fidelity in pyramidal cells by somatic feed-forward inhibition. *Science, 293*(5532), 1159-1163. doi: 10.1126/science.1060342

Pulvermüller, F., Keil, A., & Elbert, T. (1999). High-frequency brain activity: perception or active memory? *Trends Cogn Sci, 3*(7), 250-252.

Rauss, K., Pourtois, G., Vuilleumier, P., & Schwartz, S. (2012). Voluntary attention reliably influences visual processing at the level of the C1 component: a commentary on Fu, Fedota, Greenwood, and Parasuram (2010). *Biol Psychol, 91*(2), 325-327; author reply 321-324. doi: 10.1016/j.biopsycho.2012.03.013

Rihs, T. A., Michel, C. M., & Thut, G. (2007). Mechanisms of selective inhibition in visual spatial attention are indexed by alpha-band EEG synchronization. *Eur J Neurosci, 25*(2), 603-610. doi: 10.1111/j.1460-9568.2007.05278.x

Rodriguez, E., George, N., Lachaux, J. P., Martinerie, J., Renault, B., & Varela, F. J. (1999). Perception's shadow: long-distance synchronization of human brain activity. *Nature, 397*(6718), 430-433.

Rossi, A., Parada, F. J., Kolchinsky, A., & Puce, A. (2014). Neural correlates of apparent motion perception of impoverished facial stimuli: A comparison of ERP and ERSP activity. *Neuroimage*. doi: 10.1016/j.neuroimage.2014.04.029

Rossi, V., & Pourtois, G. (2012). State-dependent attention modulation of human primary visual cortex: a high density ERP study. *Neuroimage, 60*(4), 2365-2378. doi: 10.1016/j.neuroimage.2012.02.007

Rousselet, G. A., Gaspar, C. M., Wieczorek, K. P., & Pernet, C. R. (2011). Modeling Single-Trial ERP Reveals Modulation of Bottom-Up Face Visual Processing by Top-Down Task Constraints (in Some Subjects). *Front Psychol, 2*, 137. doi: 10.3389/fpsyg.2011.00137

Rousselet, G. A., Husk, J. S., Bennett, P. J., & Sekuler, A. B. (2008). Time course and robustness of ERP object and face differences. *J Vis, 8*(12), 3 1-18. doi: 10.1167/8.12.3

Rousselet, G. A., & Pernet, C. R. (2011). Quantifying the Time Course of Visual Object Processing Using ERPs: It's Time to Up the Game. *Front Psychol, 2*, 107. doi: 10.3389/fpsyg.2011.00107

Rousselet, G. A., Pernet, C. R., Bennett, P. J., & Sekuler, A. B. (2008). Parametric study of EEG sensitivity to phase noise during face processing. *BMC Neurosci, 9*, 98. doi: 10.1186/1471-2202-9-98

Schadow, J., Lenz, D., Thaerig, S., Busch, N. A., Frund, I., Rieger, J. W., & Herrmann, C. S. (2007). Stimulus intensity affects early sensory processing: visual contrast modulates

evoked gamma-band activity in human EEG. *Int J Psychophysiol, 66*(1), 28-36. doi: 10.1016/j.ijpsycho.2007.05.010

Schneider, B. L., DeLong, J. E., & Busey, T. A. (2007). Added noise affects the neural correlates of upright and inverted faces differently. *J Vis, 7*(4), 4. doi: 10.1167/7.4.4

Schroeder, C. E., & Lakatos, P. (2009a). The gamma oscillation: master or slave? *Brain Topogr, 22*(1), 24-26. doi: 10.1007/s10548-009-0080-y

Schroeder, C. E., & Lakatos, P. (2009b). Low-frequency neuronal oscillations as instruments of sensory selection. *Trends Neurosci, 32*(1), 9-18. doi: 10.1016/j.tins.2008.09.012

Schyns, P. G. (2010). Grand challenges in perception science: modeling the future. *Front Psychol, 1*, 10. doi: 10.3389/fpsyg.2010.00010

Schyns, P. G., Gosselin, F., & Smith, M. L. (2009). Information processing algorithms in the brain. *Trends Cogn Sci, 13*(1), 20-26. doi: 10.1016/j.tics.2008.09.008

Schyns, P. G., Petro, L. S., & Smith, M. L. (2007). Dynamics of visual information integration in the brain for categorizing facial expressions. *Curr Biol, 17*(18), 1580-1585. doi: 10.1016/j.cub.2007.08.048

Schyns, P. G., Thut, G., & Gross, J. (2011). Cracking the code of oscillatory activity. *PLoS biology, 9*(5), e1001064. doi: 10.1371/journal.pbio.1001064

Seth, A. K. (2010). A MATLAB toolbox for Granger causal connectivity analysis. *J Neurosci Methods, 186*(2), 262-273. doi: 10.1016/j.jneumeth.2009.11.020

Singer, W. (1999). Neuronal synchrony: a versatile code for the definition of relations? *Neuron, 24*(1), 49-65, 111-125.

Smith, P. L., & Ratcliff, R. (2004). Psychology and neurobiology of simple decisions. *Trends Neurosci, 27*(3), 161-168. doi: 10.1016/j.tins.2004.01.006

Soltesz, I., & Deschenes, M. (1993). Low- and high-frequency membrane potential oscillations during theta activity in CA1 and CA3 pyramidal neurons of the rat hippocampus under ketamine-xylazine anesthesia. *Journal of neurophysiology, 70*(1), 97-116.

Sporns, O. (2011). *Networks of the Brain*: The MIT Press.

Sporns, O., Chialvo, D. R., Kaiser, M., & Hilgetag, C. C. (2004). Organization, development and function of complex brain networks. *Trends Cogn Sci, 8*(9), 418-425. doi: 10.1016/j.tics.2004.07.008

Stam, C. J., Nolte, G., & Daffertshofer, A. (2007). Phase lag index: assessment of functional connectivity from multi channel EEG and MEG with diminished bias from common sources. *Hum Brain Mapp, 28*(11), 1178-1193. doi: 10.1002/hbm.20346

Stam, C. J., & Reijneveld, J. C. (2007). Graph theoretical analysis of complex networks in the brain. *Nonlinear Biomed Phys, 1*(1), 3. doi: 10.1186/1753-4631-1-3

Suh, N. P. (2004). On functional periodicity as the basis for long-term stability of engineered and natural systems and its relationship to physical laws. *Research in Engineering Design, 15*(1), 72-75.

Suzuki, M., Fujii, T., Tsukiura, T., Okuda, J., Umetsu, A., Nagasaka, T., . . . Yamadori, A. (2002). Neural basis of temporal context memory: a functional MRI study. *Neuroimage, 17*(4), 1790-1796.

Tallon-Baudry, C., & Bertrand, O. (1999). Oscillatory gamma activity in humans and its role in object representation. *Trends Cogn Sci, 3*(4), 151-162.

Tallon-Baudry, C., Bertrand, O., Delpuech, C., & Pernier, J. (1996). Stimulus specificity of phase-locked and non-phase-locked 40 Hz visual responses in human. *The Journal of Neuroscience, 16*(13), 4240.

Tallon-Baudry, C., Bertrand, O., & Fischer, C. (2001). Oscillatory synchrony between human extrastriate areas during visual short-term memory maintenance. *The Journal of neuroscience : the official journal of the Society for Neuroscience, 21*(20), RC177.

Tallon-Baudry, C., Bertrand, O., Peronnet, F., & Pernier, J. (1998). Induced gamma-band activity during the delay of a visual short-term memory task in humans. *The Journal of neuroscience : the official journal of the Society for Neuroscience, 18*(11), 4244-4254.

Tallon-Baudry, C., Mandon, S., Freiwald, W. A., & Kreiter, A. K. (2004). Oscillatory synchrony in the monkey temporal lobe correlates with performance in a visual short-term memory task. *Cereb Cortex, 14*(7), 713-720. doi: 10.1093/cercor/bhh031

Tass, P., Rosenblum, M., Weule, J., Kurths, J., Pikovsky, A., Volkmann, J., . . . Freund, H.-J. (1998). Detection of n:m phase locking from noisy data: application to magnetoencephalography. *Phys Rev Lett, 81*, 3291–3294.

Tenke, C. E., Schroeder, C. E., Arezzo, J. C., & Vaughan, H. G., Jr. (1993). Interpretation of high-resolution current source density profiles: a simulation of sublaminar contributions to the visual evoked potential. *Exp Brain Res, 94*(2), 183-192.

Theiler, J., Eubank, S., Longtin, A., Galdrikian, B., & Doyne Farmer, J. (1992). Testing for nonlinearity in time series: the method of surrogate data. *Physica D: Nonlinear Phenomena, 58*(1), 77-94.

Thompson-Schill, S. L., D'Esposito, M., Aguirre, G. K., & Farah, M. J. (1997). Role of left inferior prefrontal cortex in retrieval of semantic knowledge: a reevaluation. *Proceedings of the National Academy of Sciences of the United States of America, 94*(26), 14792-14797.

Tiesinga, P., & Sejnowski, T. J. (2009). Cortical enlightenment: are attentional gamma oscillations driven by ING or PING? *Neuron, 63*(6), 727-732.

Tomarken, A. J., & Serlin, R. C. (1986). Comparison of ANOVA alternatives under variance heterogeneity and specific noncentrality structures. *Psychological Bulletin, 99*(1), 90.

Tononi, G., Edelman, G. M., & Sporns, O. (1998). Complexity and coherency: integrating information in the brain. *Trends Cogn Sci, 2*(12), 474-484.

Tort, A. B., Komorowski, R., Eichenbaum, H., & Kopell, N. (2010). Measuring phase-amplitude coupling between neuronal oscillations of different frequencies. *Journal of neurophysiology, 104*(2), 1195-1210. doi: 10.1152/jn.00106.2010

Uchida, N., Kepecs, A., & Mainen, Z. F. (2006). Seeing at a glance, smelling in a whiff: rapid forms of perceptual decision making. *Nat Rev Neurosci, 7*(6), 485-491. doi: 10.1038/nrn1933

Uhlhaas, P. J., Pipa, G., Lima, B., Melloni, L., Neuenschwander, S., Nikolic, D., & Singer, W. (2009). Neural synchrony in cortical networks: history, concept and current status. *Front Integr Neurosci, 3*, 17. doi: 10.3389/neuro.07.017.2009

Uhlhaas, P. J., Pipa, G., Neuenschwander, S., Wibral, M., & Singer, W. (2011). A new look at gamma? High- (>60 Hz) gamma-band activity in cortical networks: function, mechanisms and impairment. *Prog Biophys Mol Biol, 105*(1-2), 14-28. doi: 10.1016/j.pbiomolbio.2010.10.004

Ullman, S. (1995). Sequence seeking and counter streams: a computational model for bidirectional information flow in the visual cortex. *Cereb Cortex, 5*(1), 1-11.

van Rijsbergen, N. J., & Schyns, P. G. (2009). Dynamics of trimming the content of face representations for categorization in the brain. *PLoS Comput Biol, 5*(11), e1000561. doi: 10.1371/journal.pcbi.1000561

Vanrullen, R. (2011). Four common conceptual fallacies in mapping the time course of recognition. *Front Psychol, 2*, 365. doi: 10.3389/fpsyg.2011.00365

VanRullen, R., Busch, N. A., Drewes, J., & Dubois, J. (2011). Ongoing EEG Phase as a Trial-by-Trial Predictor of Perceptual and Attentional Variability. *Front Psychol, 2*, 60. doi: 10.3389/fpsyg.2011.00060

VanRullen, R., & Koch, C. (2003). Is perception discrete or continuous? *Trends Cogn Sci, 7*(5), 207-213.

VanRullen, R., & Thorpe, S. J. (2001). The time course of visual processing: from early perception to decision-making. *J Cogn Neurosci, 13*(4), 454-461.

Varela, F., Lachaux, J. P., Rodriguez, E., & Martinerie, J. (2001). The brainweb: phase synchronization and large-scale integration. *Nat Rev Neurosci, 2*(4), 229-239. doi: 10.1038/35067550

Varela, F. J., Thompson, E., & Rosch, E. (1991). *The embodied mind : cognitive science and human experience*. Cambridge, Mass.: MIT Press.

Vinck, M., Battaglia, F. P., Womelsdorf, T., & Pennartz, C. (2012). Improved measures of phase-coupling between spikes and the Local Field Potential. *J Comput Neurosci, 33*(1), 53-75. doi: 10.1007/s10827-011-0374-4

Vinck, M., Lima, B., Womelsdorf, T., Oostenveld, R., Singer, W., Neuenschwander, S., & Fries, P. (2010). Gamma-phase shifting in awake monkey visual cortex. *The Journal of neuroscience : the official journal of the Society for Neuroscience, 30*(4), 1250-1257. doi: 10.1523/JNEUROSCI.1623-09.2010

Vinck, M., Oostenveld, R., van Wingerden, M., Battaglia, F., & Pennartz, C. M. (2011). An improved index of phase-synchronization for electrophysiological data in the presence of volume-conduction, noise and sample-size bias. *Neuroimage, 55*(4), 1548-1565. doi: 10.1016/j.neuroimage.2011.01.055

Viola, F. C., Debener, S., Thorne, J., & Schneider, T. R. (2010). Using ICA for the Analysis of Multi-Channel EEG Data. *Simultaneous EEG and fMRI: Recording, Analysis, and Application: Recording, Analysis, and Application*, 121.

Voytek, B., Canolty, R. T., Shestyuk, A., Crone, N. E., Parvizi, J., & Knight, R. T. (2010). Shifts in gamma phase-amplitude coupling frequency from theta to alpha over posterior cortex during visual tasks. *Frontiers in human neuroscience, 4*, 191. doi: 10.3389/fnhum.2010.00191

Voytek, B., D'Esposito, M., Crone, N., & Knight, R. T. (2013). A method for event-related phase/amplitude coupling. *Neuroimage, 64*, 416-424. doi: 10.1016/j.neuroimage.2012.09.023

Wang, X. J. (2010). Neurophysiological and computational principles of cortical rhythms in cognition. *Physiol Rev, 90*(3), 1195-1268. doi: 10.1152/physrev.00035.2008

Weinstein, S., & Ebert, P. (1971). Data transmission by frequency-division multiplexing using the discrete Fourier transform. *Communication Technology, IEEE Transactions on, 19*(5), 628-634.

Weiss, P. H., Marshall, J. C., Zilles, K., & Fink, G. R. (2003). Are action and perception in near and far space additive or interactive factors? *Neuroimage, 18*(4), 837-846.

Wendling, F., Ansari-Asl, K., Bartolomei, F., & Senhadji, L. (2009). From EEG signals to brain connectivity: a model-based evaluation of interdependence measures. *J Neurosci Methods, 183*(1), 9-18. doi: 10.1016/j.jneumeth.2009.04.021

Whittingstall, K., & Logothetis, N. K. (2009). Frequency-band coupling in surface EEG reflects spiking activity in monkey visual cortex. *Neuron, 64*(2), 281-289. doi: 10.1016/j.neuron.2009.08.016

Wilcox, R. R. (2005a). *Introduction to robust estimation and testing*.

Wilcox, R. R. (2005b). New Methods for Comparing Groups Strategies for Increasing the Probability of Detecting True Differences. *Current Directions in Psychological Science, 14*(5), 272-275.

Wilcox, R. R., & Keselman, H. J. (2003). Modern robust data analysis methods: measures of central tendency. *Psychol Methods, 8*(3), 254-274. doi: 10.1037/1082-989X.8.3.254

Wilkinson, D. T., & Halligan, P. W. (2003). Stimulus symmetry affects the bisection of figures but not lines: evidence from event-related fMRI. *Neuroimage, 20*(3), 1756-1764.

Wolfe, J. M., Vo, M. L., Evans, K. K., & Greene, M. R. (2011). Visual search in scenes involves selective and nonselective pathways. *Trends Cogn Sci, 15*(2), 77-84. doi: 10.1016/j.tics.2010.12.001

Womelsdorf, T., & Fries, P. (2007). The role of neuronal synchronization in selective attention. *Curr Opin Neurobiol, 17*(2), 154-160. doi: 10.1016/j.conb.2007.02.002

Worsley, K. J., Marrett, S., Neelin, P., Vandal, A. C., Friston, K. J., & Evans, A. C. (1996). A unified statistical approach for determining significant signals in images of cerebral activation. *Hum Brain Mapp, 4*(1), 58-73. doi: 10.1002/(SICI)1097-0193(1996)4:1<58::AID-HBM4>3.0.CO;2-O
10.1002/(SICI)1097-0193(1996)4:1<58::AID-HBM4>3.0.CO;2-O

Wyart, V., de Gardelle, V., Scholl, J., & Summerfield, C. (2012). Rhythmic fluctuations in evidence accumulation during decision making in the human brain. *Neuron, 76*(4), 847-858. doi: 10.1016/j.neuron.2012.09.015

Xue, Z., Li, J., Li, S., & Wan, B. (2006). *Using ICA to remove eye blink and power line artifacts in EEG.* Paper presented at the Innovative Computing, Information and Control, 2006. ICICIC'06. First International Conference on.

Yu, S. S., & Rugg, M. D. (2010). Dissociation of the electrophysiological correlates of familiarity strength and item repetition. *Brain Res, 1320*, 74-84. doi: 10.1016/j.brainres.2009.12.071

10. Curriculum Vitae

Francisco J. Parada
Department of Psychological and Brain Sciences
Indiana University
fjparada@indiana.edu

Education:

Aug. 2009 – Sept. 2014
Indiana University, Bloomington. Psychological & Brain Sciences Department. Cognitive Psychology/Neuroscience PhD. (advisory committee: Drs. Tom Busey, Aina Puce, Olaf Sporns, and Bennett Berthental)

2007
Universidad de Chile, Santiago de Chile. Medical Sciences Department, Master degree in Neuroscience (Unfinished). (adviser: Dr. Pedro Maldonado)

2002 – 2006
Universidad de las Américas, Santiago de Chile. Psychology Department. (advisory committee: Profs. Oriana Vilches & Jorge Fernandez Tornini)

Publications:

Busey, T. & Parada F.J. (2010). The Nature of Expertise in Fingerprint Examiners. *Psychonomic Bulletin & Review*, 17.2 (2010): 155-160

Busey, T., Yu, C., Wyatte, D., Vanderkolk, J., Parada, F.J., & Akavipat, R. (2011). Consistency and Variability Among Latent Print Examiners as Revealed by EyeTracking Methodologies. *Journal of Forensic Identification*, 61(1), 60-91

Rossi, A., Parada, F.J., Haga, Z., Gooteboer, C., Lenoir, M., Wels, H., Savelsbergh, G.J., Bekoff, M., Allen, C. (2013). Eyes-tracking the gaze of dogs and humans in a pointing gesture study. *Journal of Veterinary Behavior: Clinical Applications and Research*, 8(4). doi: 10.1016/j.jveb.2013.04.049

Rossi, A., Smedema, D., Parada, F.J., & Allen, C. (2014). Visual attention in dogs and the evolution of non-verbal communication. In Dog Behavior and Cognition (133-154). Ed: Alexandra Horowitz. Springer. Berlin, Germany

Rossi, A.*, Parada, F. J.*, Kolchinsky, A., & Puce, A. (2014). Neural correlates of apparent motion perception of impoverished facial stimuli: A comparison of ERP and ERSP activity. *NeuroImage*.

Parada, F.J., Wyatte, D., Yu, C., Akavipat, R., Emerick, B., & Busey, T. (2014). ExpertEyes: Open-source, high-definition eyetracking. *Behavior research methods*, 1-12.

Rossi, A., Smedema, D., Parada, F.J., & Allen, C. (2014). Visual Attention in Dogs and the Evolution of Non-Verbal Communication. In Domestic Dog Cognition and Behavior (133-154). Springer. Berlin, Germany

Puce, A., Rossi, A., Parada, F.J. (in press). Biological Motion. In: Brain Mapping: An Encyclopedic Reference. Ed: Toga AW, M. M. Mesulam, & S. Kastner. Elsevier. Oxford, UK

[* = co-first authors]

Publications in progress:

Rossi, A.*, Parada, F.J.*, Latinus, M., Puce, A. (revised and resubmitted). Neural activity differences elicited to viewing gaze changes in real and line-drawn faces

Latinus, M., Love, S., Rossi, A., Parada, F.J., Huang, L., Conty, L., George, N., James, K., Puce, A. (in revision). Social decision affect neural activity to perceived dynamic gaze

Parada, F.J.*, Emerick, B.*, Moravec, L., Sporns, O., Busey, T. (in preparation). Independent roles of temporospatial alpha, beta, and gamma phase synchrony in the tilt illusion

Parada,F.J.*, Moravec, L.*, Emerick,B., Sporns, O.,Busey, T. (in preparation). Entropy-based temporo-spatial phase synchrony in the tilt illusion: The effects of context in perception

[* = co-first authors]

Teaching experience:

Summer 2014:
Associate instructor at Indiana University. Bloomington, IN. USA. Organization and Instruction of the "1st IRF Neural Time-Series Analysis Workshop"

Fall 2013 – Spring 2014:
Associate instructor at Indiana University. Bloomington, IN. USA. Teaching Cognitive Neuroscience (P349)

Spring 2012:
Associate instructor at Indiana University. Bloomington, IN. USA. Teaching Experimental Methods in Psychology (P211)

March 2006 – January 2008:
Lecturer at Universidad de Las Américas. Santiago, Chile. Teaching Neurophysiology and Psychophysiology

2003 – 2006:
Undergraduate Teaching Assistant at Universidad de Las Américas. Santiago, Chile. Assistant in Neurophysiology and Psychophysiology classes

Research & professional employment:

September 2014 – Present:
Postdoctoral Research Fellow. Department of Psychiatry. Harvard Medical School. Boston, MA. USA

August 2008 – Present:
Technical advisor/co-developer of eye-tracking technology for Cannis Lupus Familiaris. Collaboration with Dr. Colin Allen (Indiana University), PhD(c) Alejandra Rossi (Indiana University), Dr. Harry Wels (VU University of Amsterdam), and Dr. Geert Savelsbergh (VU University of Amsterdam)

August 2009 – August 2013:
Graduate Research Assistant for Dr. Aina Puce at the Psychological & Brain Sciences Department Imaging Research Facility. Indiana University, Bloomington, IN, USA. Involved in collecting and analyzing EEG data and supervision of undergraduate honor theses

April 2012:
EEG acquisition and analysis consultant. Department of Psychology. University of Wisconsin – Stout. Menomonie, WI. USA

July – August 2009:
Research Assistant for Dr. Aina Puce. Indiana University, Bloomington, IN, USA. Hardware and software set up for the EEG/TMS Laboratory at Imaging Research Facility.

February 2008 – August 2009:
Research Associate for Dr. Thomas Busey. Indiana University, Bloomington, IN, USA. Functions included experimental design, and data collection and analysis of Eye-Tracker and EEG. Supervision of undergraduate honor theses and managing laboratory data.

2007 – 2008:
Research Assistant (volunteer) for Dr. Francisco Ceric. Universidad Católica de Chile. Santiago, Chile. Involved in EEG projects. Research Assistant (volunteer) for Dr. Vladimir López. Universidad Diego Portales. Santiago, Chile. Involved in EEG projects.

2006:
Intership at Hospital de Urgencia Asistencia Pública (HUAP). Santiago, Chile.

Awards & Funding:

2013 – 2014:
Supported by Department of Psychological & Brain Sciences. Indiana University

2009 – 2013:
Supported by NIH grant NS-NS049436 and NS-049436 to Dr. Puce

December 2010:
Indiana University Graduate School Award

Summer 2010:
McFall Summer Research Award

2008 – 2010:
Supported by National Institute of Justice grants #2005-MU-BX-K076 and #2009-DN-BX-K226 to Dr. Busey

Selected oral presentations:

Parada F.J., Sporns, O., Busey, T.A. Decisiones Perceptuales: Estudios de EyeTracker y EEG. Cognitive Neuroscience Program Research Seminar. Pontificia Universidad Católica de Chile. August 2014. Santiago, Chile

Parada F.J. Pensamientos sobre Neurociencia y Educación: Construyendo Conexiones. Instituto Miguel León Prado (High school and Middle school). Santiago, Chile

Parada, F.J., Sporns, O., Busey, T.A. Mining Functional Temporal and Spatial Connectivity Dynamics in the Human EEG. Centre de Recherche Cerveau et Cognition (CerCo). November 2013. Toulouse, France

Parada, F.J., Sporns, O., Busey, T.A. Mining Functional Temporal and Spatial Connectivity Dynamics in the Human EEG. Spinoza Centre for Neuroimaging. November 2013. Amsterdam, The Netherlands

Parada, F.J. & Busey, TA. Open source Eye-Tracking: Software, Hardware, and Applications. 42nd Annual Meeting of the Society for Computers in Psychology. Minneapolis, MN. USA. 2012

Parada, F.J. Eye-Tracking as a Measure of Visual Attention. Fall 2012 Psychology Department Colloquium, Indiana University Northwest. Gary, IN. USA

Parada, F.J. Brain Machine Interfaces: A Focus on EEG and Eye-Tracking. Bloomington Science Café 2012, a space to bring together scientists and the public. Bloomington, IN. USA

Parada, F.J., Kolchinsky, A., Rossi, A., Busey, T., Sporns, O., Puce, A. Spatial organization of EEG cross- frequency coupling in a perceptual task. Society for Neuroscience Conference 2011 Meeting. Washington, DC. USA

Parada, F.J., Kolchinsky, A., Rossi, A., Busey, T., Sporns, O., Puce, A. Measuring event-related cross- frequency coupling in the human EEG. Fall 2011 Indiana University Neuroimaging Colloquium. Bloomington, IN. USA

Parada, F.J. & Busey, T. ExpertEyes: Open-source eye tracker. Workshop presented at Measuring Behavior 2010. Eindhoven, The NetherlandsParada, F.J. & Busey, T. ExpertEyes: Open-source eye tracker. Workshop presented at the Psychological and Brain Sciences Department. Bloomington, IN. USA. 2010

Parada, F.J. Psychology and Neuroscience: A necessary link. Psychology Students' National Conference. Santiago, Chile. 2007

Selected poster presentations:

Parada,F.J., Kolchinsky, A., Rossi, A., Puce, A. EEG phase-coupling dynamics in apparent motion perception. Organization for Human Brain Mapping 2013 Meeting. Seattle, WA. USA

Parada,F.J., Kolchinsky, A., Rossi, A., Busey, T., Sporns, O., Puce, A. From Visual Awareness to Perceptual Decision-Making: neural correlates of top-down and bottom-up dynamics. Rhythms and Oscillations Workshop at the Mathematical Biosciences Institute of Ohio. Columbus, OH. USA

Kolchinsky, A., Parada, F.J., Rossi, A., Busey, T., Sporns, O., Puce, A. Statistical methods for multiple comparison correction in event-related and resting-state EEG cross-frequency coupling dynamics. Rhythms and Oscillations Workshop at the Mathematical Biosciences Institute of Ohio. Columbus, OH. USA

Rossi, A., Parada, F.J., Kolchinsky, A., Puce, A. Neural responces to changes in social attention depicted by biological motion stimuli. Organization for Human Brain Mapping 2012 Meeting. Beijing, China

Kitchell, L.M., Parada, F.J., Emerick, B., Busey, T. Feature Selection Strategies and Perceptual Expertise in Configuration Search Tasks. 52nd Annual Meeting of The Psychonomic Society. Seattle, WA. USA

Parada, F.J., Busey, T., Puce, A. Eye-Tracking Guided EEG Analyses. Organization for Human Brain Mapping 2011 Meeting. Quebec City, Canada

Rossi, A., Parada, F.J., & Allen, C. Dogcam: A way to measure visual patterns in social interactions in dogs. 2009 Cognitive Science Society Conference. Amsterdam, The Netherlands

Contact for References:

1. Dr. Tom Busey (busey@indiana.edu)
Psychological & Brain Sciences Department. Indiana University. Bloomington, IN. USA

2. Dr. Aina Puce (ainapuce@indiana.edu)
Psychological & Brain Sciences Department. Indiana University. Bloomington, IN. USA

3. Dr. Olaf Sporns (osporns@indiana.edu)
Psychological & Brain Sciences Department. Indiana University. Bloomington, IN. USA